

UNIVERSIDADE DE LISBOA
FACULDADE DE CIÊNCIAS
DEPARTAMENTO DE FÍSICA



Quantifying the Ergonomic Risk and Biomechanical Exposure in Automotive Assembly Lines

Maria Lua de Coelho Nunes

Mestrado Integrado em Engenharia Biomédica e Biofísica
Perfil em Biofísica Médica e Fisiologia de Sistemas

Dissertação orientada por:
Prof. Dr. Sara Madeira
Dr. André Carreiro

Agradecimentos

O presente documento nasce ao fim de nove meses de trabalho, árduo e consistente, com a ambição de trazer ao mundo da investigação algo aplicável e que traduza valor para a sociedade. Por esta razão, agradeço ao leitor.

É incontestável a participação de várias entidades na elaboração e execução deste documento, que passarei a citar.

Agradeço aos colegas do AICOS Fraunhofer Portugal, particularizando o Duarte Folgado que traçou um percurso de supervisão exímio, com um dom nato para a crítica, sempre construtiva, e ao qual devo boa parte da minha linha de aprendizagem exponencial relativa aos últimos meses. Aos restantes colegas do projeto OPERATOR, em especial do Intelligent Systems, começando pelo André Carreiro, pela orientação, insistência e persistência no que toca à resolução de burocracias, ao Ricardo Leonardo e ao Pedro Matias, pelo apoio técnico nas aquisições na Autoeuropa, e à Marília Barandas, pelo seu espírito positivo. Aos colegas do escritório de Lisboa que aceitaram participar neste estudo. A estes e aos restantes, agradeço pelos momentos de partilha que foram motor de motivação para o trabalho espelhado neste documento.

À equipa de ergonomia da Volkswagen Autoeuropa, Carlos Fujão, Jacqueline Gaspar e Natércia Domingues, pela voto de confiança e por possibilitarem que esta dissertação apresente mais valor, constituindo um prorrogar de uma relação frutífera entre o AICOS e a Autoeuropa; e aos operadores que participaram no estudo.

À Sara Madeira pela orientação e por diligenciar a resolução de burocracias.

Aos amigos que a par e passo me acompanharam nesta jornada académica. Agradeço aos “Biomédicos” por partilharam comigo os momentos de maior desespero ao longo dos últimos cinco anos: Ema, Bia, Teresa, Cláudia, Sara, Marta, Pedro, Vasco, João e Dani. Que os nossos jantares e amizade perdurem no tempo! À Mónica e à Valentina por me terem acolhido em Enschede, pelo pesto caseiro e pela pizza de batata que foram para o coração. À Carol e à Margarida pelas vivências em Copenhaga, pelo companheirismo e pela partilha que deixam saudades.

Aos “Anébcicos” de um passado próximo, especialmente aos “rebentinhos”, à Glória, pela genuinidade e generosidade, e ao António, pelo dinamismo e proatividade; e à restante Direção, à Inês, pelas partilhas, ao Pedro, pela disponibilidade, à Tatiana, pelo sentido de missão, e à Ana, pela resiliência. Ao longo de um mandato trabalhoso e irrepreensível, o vosso suporte deu-me alento e força para a escrita deste documento. Um GIGANTE obrigada, de coração!

Aos amigos de longa data que perduram no tempo. Em especial à amiga mais querida, Mariana, ao amigo de sempre, JP, e ao grupo de amigas mais aventureiro e audaz, à Cata, à Madu, à Tata e à Anocas.

Foi ainda imprescindível o apoio da família e a genética incurável. À mãe, por ser o alicerce de todos os momentos e pela ambição hereditária, ao pai, pelo mimo incontestável e por uma boa dose de loucura, ao mano João, teimoso incurável, pelos beijos e abraços forçados em dias de menos bons, às “Kitty cats”, Pipoca e Pérola, pela companhia de quatro patas e lealdade, e aos avós pelo tamanho orgulho e força de transbordam.

Por fim, resta-me ao meu namorado, Duarte Saraiva, pela presença constante, embora por vezes distante, pelo carinho e compreensão. Obrigada pelo apoio incondicional.

Resumo

As Lesões Musculoesqueléticas Relacionadas com o Trabalho (LMERTs) representam 15% do número total de anos de vida perdidos por danos físicos ou doenças com a sua gênese no trabalho. De entre os fatores de risco para as LMERTs, no presente estudo, destacam-se as posturas corporais relacionadas com o trabalho. A exposição biomecânica a posturas consideradas prejudiciais tem um impacto negativo na saúde dos trabalhadores, na economia das empresas e na sociedade. A fim de aperceber a prática recorrente de posturas prejudiciais no local de trabalho, têm sido invocados métodos de autoavaliação ergonómica, nos quais o risco é percebido pelo próprio trabalhador; observacionais, conduzidos por peritos em ergonomia; e de medição direta, que recorrem ao emprego de soluções tecnológicas para a recolha e monitorização objetiva de variáveis pertinentes para a avaliação ergonómica. Porém, frequentemente e em contexto industrial, são apenas aplicados métodos de autoavaliação e observacionais, apesar da medição direta constituir uma solução mais notável.

O advento da *Internet* das Coisas vem revelar a oportunidade da utilização de *wearables* para uma recolha de dados omnipresente, amplificando a quantidade de dados disponível com o fim de uma avaliação ergonómica mais individual e imparcial. Deste modo, estudos relativos à avaliação ergonómica no local de trabalho têm primado pelo uso de *wearables* com vista a monitorização do movimento humano.

A presente dissertação respeita ao desenvolvimento de uma abordagem automática para a avaliação ergonómica em contexto industrial. As contribuições principais são o desenvolvimento de (1) uma rotina de captura de movimento, através da utilização de um sistema *wearable* com sensores inerciais; (2) uma *framework* computacional para a monitorização do movimento da parte superior do corpo humano, em termos dos ângulos relativos às articulações entre os segmentos anatómicos, estimados com recurso à cinemática inversa; e (3) implementações computacionais de especificações estabelecidas e relativas aos fatores de risco de postura para a quantificação da exposição biomecânica e consequente risco ergonómico em âmbito ocupacional. Subsequentemente, as implementações das especificações foram aplicadas por forma a prover constatações acerca de um caso de estudo das linhas de montagem de automóveis da Volkswagen Autoeuropa.

O estudo delineado foi dividido em dois cenários: validação e avaliação. A validação consistiu em comparar os dados provisionados por um sistema inercial de referência e determinados através dos métodos desenvolvidos. Para tal, usaram-se dados de sensores inerciais recolhidos em laboratório (N = 8 participantes) e nas linhas de montagem de automóveis (N = 9 participantes). A avaliação consistiu em quantificar a exposição biomecânica e consequente risco ergonómico respeitantes ao caso de estudo, empregando as estimativas angulares calculadas pela *framework* desenvolvida, e a partir dos dados recolhidos com o nosso sistema nas linhas de montagem de automóveis.

Os resultados revelaram que a *framework* proposta tem o potencial para ser aplicada na monitorização de tarefas industriais. A avaliação ergonómica é mais lata através da medição direta, desvendando diferenças de exposição biomecânica e consequente risco ergonómico entre operadores.

Palavras-chave: Ergonomia, Lesões musculoesqueléticas, Postura, Sensores inerciais, Cinemática inversa

Abstract

Work-related musculoskeletal disorders (WRMSDs) represent 15% of the total number of life-years lost due to work-related injuries and illness. Among WRMSDs' risk factors, work-related postures are underlined in this research. Biomechanical exposure to hazardous postures negatively impacts workers' health, enterprises' economy, and society. Toward the apperception about the recurrent practice of hazardous postures in the workplace, self-reported, observational, and directly measured ergonomic assessment methods have been established. However, only self-reported and observational approaches are enforced on a more frequent basis, besides directly measured is a more compelling choice.

The advent of the Internet of Things poses the opportunity of using wearables in the direction of ubiquitous data collection, increasing the amount of available data for a more personal and non-biased ergonomic evaluation. As follows, over workplace ergonomics research, wearables have been used to monitor human motion.

The dissertation developed an automatic approach to ergonomic evaluation in industrial contexts. Its main contributions are the development of (1) a motion capture routine using inertial sensors; (2) a computational framework to monitor human upper body motion, in terms of joints' angles, through inverse kinematics; and (3) computational implementations of posture risk factors specifications to quantify the biomechanical exposure and consequent ergonomic risk in occupational settings. Subsequently, specifications implementations were applied to provide insights in consideration of a case study from Volkswagen Autoeuropa automotive assembly lines.

The research was divided into two scenarios: validation and evaluation. Validation consisted of comparing data provided by a ground truth inertial motion capture system and computed throughout the developed methods. Hence, inertial sensors' data, collected in the laboratory (N = 8 participants) and automotive assembly lines (N = 9 participants) settings, were used. The evaluation consisted of quantifying the biomechanical exposure and consequent ergonomic risk concerning the case study, using angular estimates computed through the developed framework and about data collected in automotive assembly lines.

The results revealed that the proposed framework has the potential to be applied to monitor industrial tasks. The ergonomic evaluation is more comprehensive through direct measures, uncovering differences about biomechanical exposure and consequent ergonomic risk among operators.

Keywords: Ergonomics, Musculoskeletal disorders, Posture, Inertial sensors, Inverse Kinematics

Graphical Abstract

IA

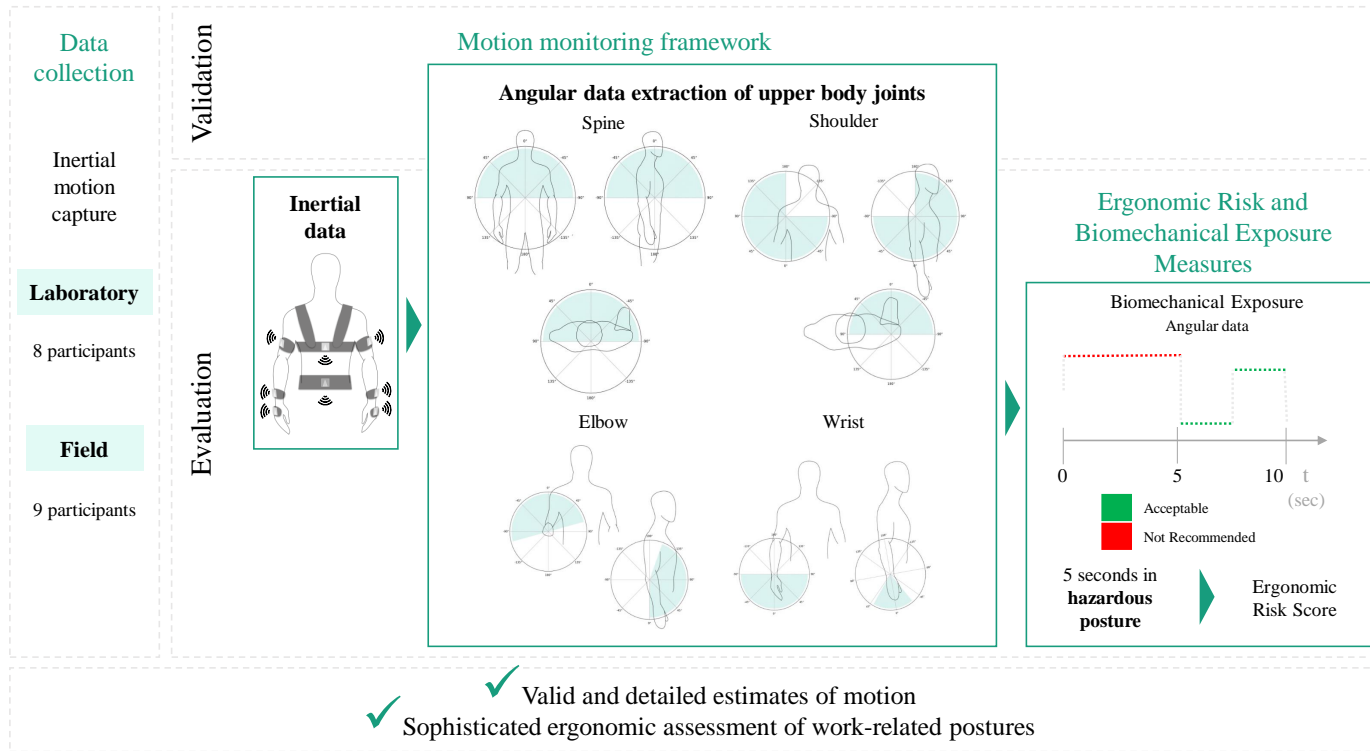


Figure 1: Graphical abstract of the dissertation.

Index

Agradecimientos	i
Resumo	iii
Abstract	v
Graphical Abstract	vi
List of Figures	x
List of Tables	xvi
Acronyms	xviii
1 Introduction	1
1.1 Problem	1
1.2 Motivation	2
1.3 Context	2
1.4 Objectives and Research Questions	3
1.5 Structure	3
1.6 Chapter Conclusions	4
2 State of the Art	5
2.1 Ergonomic Risk Assessment	5
2.1.1 Guidelines for Ergonomic Assessment	6
2.2 Current Available Commercial Solutions	6
2.3 Workplace Ergonomics Research	8
2.3.1 Motion Capture Technology in Industrial Contexts	8
2.3.2 Work-Method Characterisation	8
2.4 Chapter Conclusions	11
3 Theoretical Background	13
3.1 Model Human Motion	13
3.1.1 Musculoskeletal System	14
3.1.2 Musculoskeletal Disorders	17
3.1.3 Biomechanics	18
3.1.4 Kinematics	19
3.2 Sense Human Motion	25

INDEX

3.2.1	Inertial Measurement Unit Sensors	26
3.2.2	Devices Synchronisation	28
3.3	Monitor Human Motion	29
3.3.1	Strap-Down Integration	29
3.3.2	Vector Observation algorithms	30
3.3.3	Complementary Filters	30
3.3.4	Kalman Filters	31
3.3.5	Sensor Fusion Algorithms Conclusions	32
3.3.6	Orientation Estimation Issues	33
3.4	Characterise Human Motion	34
3.5	Chapter Conclusions	35
4	Materials and Methods	37
4.1	Study Design	37
4.1.1	Study Type	37
4.1.2	Study Scenarios	37
4.1.3	Case Study	37
4.1.4	Study Boundaries	38
4.1.5	Study Stop Criteria	38
4.1.6	Participants Recruitment	39
4.1.7	Study Specific Research Questions	39
4.2	Data Collection	39
4.2.1	Motion Capture Fundamentals	40
4.2.2	Setup	40
4.2.3	Protocol	41
4.3	Data Pre-processing	43
4.3.1	Correction	43
4.3.2	Resampling	43
4.3.3	Filtering	43
4.3.4	Synchronisation	44
4.4	Monitoring Motion	46
4.4.1	Data Preparation	46
4.4.2	Angular Extraction	47
4.5	Systems Comparison	50
4.5.1	Performance Metrics	51
4.6	Ergonomic Assessment	52
4.6.1	Work-Cycle Annotation	52
4.6.2	Angular Ranges Quantisation	53
4.6.3	Ergonomic Assessment Implementations	53
4.7	Chapter Conclusions	55
5	Results and Discussion	57
5.1	Design Recommendations	57
5.2	Population Characterisation	58
5.3	Orientation Errors	59

5.4	Validation	61
5.4.1	Root Mean Squared Error and Determination Coefficient	61
5.4.2	Cumulative Distribution Function	63
5.5	Evaluation	65
5.5.1	Workstation-Level	66
5.5.2	Operator-Level	69
5.6	Study Limitations	73
5.7	Chapter Conclusions	74
6	Conclusions and Future Work	75
6.1	Conclusions	75
6.2	Future Work	77
	Appendices	87
A	State of the Art	89
B	Theoretical Background	93
C	Materials and Methods	95
C.1	Motion Capture Systems	95
C.2	Laboratory Protocol	97
C.3	Laboratory Informed Consent	103
C.4	Signals Example	105
C.5	Computational Tools	106
C.5.1	Python Packages	106
C.6	Filtering Example	107
C.7	Synchronisation Method Algorithm	109
C.8	Synchronisation Example	110
C.9	OpenSim Files Format Examples	111
C.10	European Assembly Worksheet	113
C.11	Risk Assessment Guidelines Sheet	117
C.12	Individual Ergonomic Report Example	121
D	Results and Discussion	127
D.1	Self-Report Results	127
D.2	Dataset	128
D.2.1	Summary Statistics	129

List of Figures

1	Graphical abstract of the dissertation.	vi
1.1	Diagram of risk factors for the development of WRMSDs.	1
1.2	Dissertation’s document structure.	3
1.3	Block diagram about the chapters’ information linkage from chapter 1 to 3 (inclusive).	4
3.1	Anatomical planes (left) and axes (right).	13
3.2	Shoulder joint complex’s components: (1) sternoclavicular, (2) acromioclavicular, (3) scapulothoracic and (4) glenohumeral.	15
3.3	Shoulder motion: abduction/adduction (upper left), inward/outward rotation (bottom middle) and extension/flexion (upper right).	15
3.4	Elbow joint’s components: (1) humeroradial (spherical-shaped), (2) humeroulnar (trochlea-shaped) and (3) proximal radioulnar (cylindrical-shaped).	16
3.5	Elbow motion: pronation/supination (upper left) and extension/flexion (bottom right).	16
3.6	Wrist’s (1) radiocarpal joint.	16
3.7	Wrist motion: extension/flexion (left) and ulnar/radial deviation (right).	17
3.8	Spine motion: lateral bending (upper left), rotation (bottom middle) and extension/flexion (upper right).	17
3.9	3D space particle position changes along x , y and z -axis - 3-DoF position (only) problem (left). Rigid-body pose changes, position and orientation (i.e. rotation around x , y and z -axis) - 6-DoF position and orientation problem (right).	20
3.10	Generic coordinate frames used in rigid-body orientation representation: the Earth-fixed inertial coordinate frame - \mathbf{E} (left); and the body-fixed non-inertial coordinate frame - \mathbf{B} (right).	20
3.11	DCM as a representation of \mathbf{B} rotation relative to \mathbf{E} . Representation of v projections (v_i , v_j , v_k) in each axis of \mathbf{B} (x , y , z) (top left). Note that, each projection of v reflects the angle between each axis and the vector v v may represent \mathbf{B} orientation changes over time, but, in human motion tracking, it is usually required to represent \mathbf{B} changes relative to a reference coordinate frame, as \mathbf{E} (top right). The concept of projections can be applied in human motion tracking, constructing a <i>projection-matrix</i> , in which each column represents the projection of x , y , z – axis on x , y , z – axis (each row) . The <i>projection-matrix</i> is a rotation matrix, R , which describes how \mathbf{B} is rotated relative to \mathbf{E} . (bottom).	21
3.12	Euler Angles α , β and γ , where xyz is the reference coordinate frame, usually \mathbf{E} , XYZ is the rotated coordinate frame, \mathbf{B} , and \mathbf{N} the axis of the coordinate rotation (Wikipedia, n.a).	22

LIST OF FIGURES

3.13	Example of a v_0 posing, with respect to a (fixed) reference coordinate frame. The v_0 rotation is described by the unit quaternion $q = 6.123234e - 17 + 0i + 0j + k$ about the unit vector $\mathbf{u} = [00\ 1]$ (i.e. corresponding to the reference coordinate frame z -axis). Note that q rotates v_0 around a coordinate axis by 180° (i.e. π rad), which is consistent with equation 3.12. There is also a change in v_0 position along the reference coordinate frame axes, which is represented by $p = [-1\ -1\ -1]$. v_1 is the pose of v_0 after pose changing, depicted by q (i.e. orientation/rotation) and p (i.e. position).	24
3.14	Accelerometer (left), Gyroscope (middle) and Magnetometer (right) geometric representations.	26
3.15	Synchronised data streams (first row), with a time lag of 1s (second row), a linear drift (third row), a non-linear drift (fourth row) and presenting all the data desynchronisation problems, delay and drift (fifth row). A stands for “Amplitude” and a.u for “adimensional unit”.	29
3.16	Block diagram of the SFAs.	32
3.17	Magnetometer without magnetic interferences (top), with soft (middle) and hard (bottom) iron interferences (Teslabs, n.a).	34
3.18	Data Mining Taxonomy (based on Wang et al., 2012).	34
4.1	Volkswagen model with shadows above the car parts to be aligned in each fitting process type.	38
4.2	Inertial Motion Capture systems setup. MVN Awinda and Fraunhofer’s systems that consisted of 17 and 7/8 Inertial Measurement Units, respectively. Representation of standing in the N-Pose.	41
4.3	Fraunhofer system placement schema, showing each sensor orientation on its corresponding segment. Note that each sensor was placed with the x -axis of the sensor frame along the longitudinal axis of the respective body segment, pointing from distal to proximal extremity. Lumbar IMU was only assembled within the laboratory data collection.	42
4.4	Butterworth filter <i>cutoff</i> frequency and <i>order</i> effect - in purple color - and Savitzky-Golay filter <i>polyorder</i> and <i>window length</i> effect - in coral color.	44
4.5	Synchronisation Method Algorithm. Input parameters are: Master signal (Accelerometer, Gyroscope or Magnetometer), M_s , and axis (x , y or z), M_{ax} ; Peaks height minimal threshold, h , from which a peak is considered a synchronisation opportunity O ; Reference segment, S_r ; Interval maximal threshold, t_A , i.e. the maximal difference in time between an O in the reference segment data stream s_r and an O in another segment data stream s , defining if the O in s is or not an alignment point A ; Sampling frequency, f_s . The algorithm (1-7) steps description is provided in Table C.1.	45
4.6	Sensor fusion algorithms execution times, angular RMSE and R^2 . SFAs tested were Complementary, Madgwick and Mahony filters by Fraunhofer, and Kalman, Complementary, Madgwick and Mahony filters from AHRS.	47

4.7 An example of the OpenSense input parameters selection. Before (left) and after (right) sensor frames calibration. The selected input parameters to the initial angular offset calculation were: *pelvis* as base IMU with the heading axis *z*, and sensor to opensim rotations equal to $-\frac{\pi}{2}$ around the OpenSim *x*-axis, and 0 around the *y*- and the *z*-axis. The sensor to opensim rotations were selected by observing sensor orientation data, in which *pelvis* *x*-axis acceleration is identical to the gravitational acceleration in the initial calibration pose, so the sensors' *x*-axis should be pointing in the UP direction of the sensors' Earth frame, i.e. the direction of the gravitational force application. As follows, the sensors' frames were rotated by $-\frac{\pi}{2}$ around the OpenSim *x*-axis, and 0 around the *y*- and the *z*-axis, in order to achieve it. The pelvis acceleration *x*-axis component in the initial calibration pose is highlighted in the sensor orientation data *sto.* file (middle) - in coral color. 49

4.8 An example of the wrist flexion DoF angular data from Fraunhofer's - in turquoise color - and from Xsens' - in orange-red color - systems. 50

4.9 An example of the lag expression terms with respect to angular data in Figure 4.8. Cross-correlation values (left) and angular data streams from Fraunhofer's - in turquoise color - and from XSens' - in orange-red color - systems (right). In the cross-correlation plot, i_{max} and i_{max_r} are represented by the vertical lines in blue color and purple color, respectively. In the angular data plot, the points in the time-axis with the indexes of $|l_{x_{FHP}} - i_{max}|$ and $|l_{x_{FHP}} - i_{max_r}|$ are displayed by the vertical lines in blue color and purple color, respectively. Note that the maximum cross-correlation value was observed for i_{max} , so the index corresponding to the lag was $|l_{x_{FHP}} - i_{max}|$ 51

4.10 **Ergonomic Assessment Steps.** Work-cycles annotations were performed from the 1st to the *i*th cycle in data from an acquisition. Work-cycle angular data is a set of angular time series, one for each segment's S_N DoF θ_n , where *N* varies from 1-7 and *n* from 1-3. Angular ranges quantisation: a function *q* was implemented for each DoF. The angular ranges were taken as input to the ergonomic assessment. Biomechanical exposure assessment (ISO norm): each segment's condition was characterised over cycle time, as "Acceptable" or "Not Recommended"; Ergonomic risk determination (EAWS): each percentage of cycle time in an EAWS condition, and the respective risk score were computed. C_X or $C_Y|C_X$ and V_X or $V_Y|X$, denotes a single or a combined condition percentages and single or a combined risk score values, respectively. Single and combined condition concepts are explained in the risk assessment guidelines sheet in Appendix C.11. 54

4.11 Block diagram of the dissertation methods and their respective outputs. 55

5.1 Body measurements values distributions, concerning laboratory and field settings. Weight, height, shoulder width, arm span, hip height, knee height, ankle height and shoe size body measurements. 58

5.2 Orientation error data from laboratory data collection. 60

5.3 Orientation error data from field data collection. 60

5.4 RMSE (left) and R^2 (right) mean values and the respective standard deviation, depicted in the horizontal error bar, for each DoF and acquisition trial conducted in laboratory setting. 62

LIST OF FIGURES

5.5	RMSE (left) and R^2 (right) mean values and the respective standard deviation, depicted in the horizontal error bar, for each DoF and acquisition set conducted in field setting.	62
5.6	Relation plot of RMSE and R^2 values for each DoF and acquisition trial conducted in laboratory (left) and field (right) settings.	63
5.7	Mean error CDFs with respect to laboratory (left) and field acquisitions (right) results for each segment.	64
5.8	Block diagram about the risk assessment results analysis and the respective research questions.	65
5.9	Total risk score values for each workstation and operator.	65
5.10	Biomechanical exposure outputs with regard to postures described in the ISO norm 11226 for each workstation and operator. Percentage of the mean work-cycle time in a not recommended condition.	69
5.11	Ergonomic risk score outputs with regard to conditions described in the EAWS section "Standing (and Walking)" - Part a (corresponding to single conditions) - for each workstation and operator. Score with respect to each condition.	69
5.12	Ergonomic risk score outputs with regard to conditions described in the EAWS section "Standing (and Walking)" - Part b (corresponding to combined conditions) - for each workstation and operator. Score with respect to each condition.	70
5.13	Operator-level biomechanical exposure and ergonomic risk results.	72
6.1	The main research topics for future work.	77
A.1	Inertial Systems <i>Setups</i> used in Occupational Ergonomics (Lim et al., 2020).	91
B.1	The major branches of mechanics used in most biomechanical studies (Arus, 2018).	93
B.2	The nine principles of biomechanics (Arus, 2018).	93
C.1	MVN Awinda XSens system setup (source: <i>Cdn.bitrix24.ru</i> 2021).	95
C.2	An example of Fraunhofer's sensors signals' components - acceleration (upper right), angular velocity (upper left) and magnetic field (bottom) - for each IMU attached to a body segment.	105
C.3	An example of IMU sensors signals magnitude power spectrum for each body segment tracked before (left) and after (right) filtering. Hand, right and left, chest and arm right body segments.	107
C.4	An example of IMU sensors signals magnitude power spectrum for each body segment tracked before (left) and after (right) filtering. Arm right and forearm, right and left, body segments.	108
C.5	An example of usage of the synchronisation method for a long-term acquisition (of 2h). The input parameters chosen were: Accelerometer as M_s and z as M_{ax} , h of 16, "Server" as r , t_A of 0.2s and f_s of 100Hz. Zoom in into the first (top), a middle and the last (bottom) As in Accelerometer z data, from Server - in turquoise color - and Forearm right - in purple color.	110
C.6	APDM format file example.	111
C.7	settings/XML file example.	111
C.8	<i>sto.</i> format file example.	112

LIST OF FIGURES

D.1 Summary results of a self-reported ergonomic assessment, conducted by Volkswagen Autoeuropa.	127
--	-----

List of Tables

1.1	Study objectives and their respective research questions.	3
2.1	Criteria for system’s design complexity component’s level assignment. System’s design complexity components are: explainability, invasiveness and scalability. Each component can be classified as high, medium or low level.	7
2.2	Current available commercial solutions.	7
2.4	Human Activity Recognition through mining time series’ tasks (adapted from Lim et al., 2020).	10
4.1	Synchronisation Approaches: Basic, Delay and Drift.	45
4.2	SFAs by Fraunhofer and from Attitude and Heading Reference Systems library tested.	46
4.3	Upper body joints’ DoFs and their respective RoMs. Note that forearm supination/pronation RoM is from 0° - 180°, which is equivalent to -60° - 90°.	48
5.1	Ergonomic outputs mean values classification criteria. The biomechanical exposure refers to the percentage of the work-cycle time in a not recommended posture and the ergonomic risk is about the score units depicted in the EAWS.	66
5.2	Mean and standard deviation of the percentages of work-cycle times in not recommended conditions with regard to postures described in the ISO norm 11226 for each workstation. Values in bold present high biomechanical exposure. The list of abbreviations used is in the risk assessment guidelines sheet in Appendix C.11.	66
5.3	Mean and the standard deviation of the score for the mean work-cycle with regard to conditions described in the EAWS section ”Standing (and Walking)” for each workstation. Values in bold present high ergonomic risk. Note that conditions showing null values among workstations were excluded. The list of abbreviations used is in the risk assessment guidelines sheet in Appendix C.11.	67
A.1	Proforma sheets used whilst observational ergonomic risk assessment (based on OSH-wiki, 2020).	89
A.3	Examples of countries/entities codes, standards and guidelines primarily aimed to prevent WRMSDs. Table from Berlin et al., 2017 p. 152-153.	90
C.1	Synchronisation Method Algorithm.	109
D.1	Study participants’ characteristics values.	128
D.2	Study participants’ characteristics values summary statistics.	129

Acronyms

3D 3-Dimensional.

4D 4-Dimensional.

AAWS Automotive Assembly Worksheet.

AFS Swedish Work Environment Authority's Statute Book.

AHRS Attitude and Heading Reference Systems library.

API Application Programming Interface.

ART Assessment of Repetitive Tasks.

CDF Cumulative Distribution Function.

CF Complementary Filter.

CMC Coefficient of Multiple Correlation.

DCM Direction Cosine Matrix.

DoF Degrees of Freedom.

DT Decision Tree.

DTW Dynamic Time Warping.

EAWS European Assembly Worksheet.

EC European Community.

ED Euclidean Distance.

EEC European Economic Community.

EMG Electromyography.

EU European Union.

FDIS Final Draft International Standard.

FK Forward Kinematics.

Acronyms

FQA Factored Quaternion Algorithm.

GDA Gradient Descent Algorithm.

GIF Gravito-Inertial Force.

GUI Graphical User Interface.

HAL Hand Activity Level.

HAR Human Activity Recognition.

HMM Hidden Markov Model.

HSE Health and Safety Executive.

IAD Institute of Ergonomics of Darmstadt Technical University.

IDE Integrated Development Environment.

IEA International Ergonomics Association.

IHMT Inertial Human Motion Tracking.

IK Inverse Kinematics.

IMU Inertial Measurement Unit.

IoT Internet of Things.

ISB International Society of Biomechanics.

ISO International Organisation for Standardisation.

KF Kalman Filter.

KIM Key Indicator Methods.

k-NN k-Nearest Neighbour.

LDA Linear Discriminant Analysis.

LMERTs Lesões Musculoesqueléticas Relacionadas com o Trabalho.

MAC Manual handling Assessment Chart.

MEMS Micro-Electro-Mechanical Systems.

ML Machine Learning.

MoCap Motion Capture.

MP Matrix Profile.

MPF Mean Power Frequency.

MSAAI Modelling-Sensing-Analysis-Assessment-Intervention.

MSDs Musculoskeletal Disorders.

MSE Mean Squared Error.

MTw Wireless Motion Trackers.

NaN Not-A-Number.

NIOSH National Institute for Occupational Safety and Health.

NN Neural Network.

NOHCs Non-Operating Holding Companies.

N-Pose Neutral Pose.

OCRA Occupational Repetitive Action.

OOS Occupational Overuse Syndrome.

OSHA Occupational Safety and Health Administration.

OWAS Ovako Working posture Assessment System.

QUEST QUaternion ESTimator.

R² Determination Coefficient.

RAPP Risk Assessment of Pushing and Pulling.

RF Random Forest.

RMSE Root Mean Squared Error.

RoM Range of Motion.

RSI Repetitive Strain Injury.

RULA Rapid Upper Limb Assessment.

SDI Strap-Down Integration.

SEMG Surface Electromyography.

SFA Sensor Fusion Algorithm.

STA Soft Tissue Artifact.

STC Standard Terminology Committee.

SVM Support Vector Machine.

TAM Time Alignment Measurement.

Acronyms

TRIAD TRi-axial Attitude Determination.

UK United Kingdom.

USA United States of America.

VO Vector Observation.

WRMSDs Work-Related Musculoskeletal Disorders.

1. Introduction

This chapter introduces the purpose of the current dissertation. Firstly, it poses the problem (1.1) from which it arises, the motivation (1.2), and the context (1.3) in which the dissertation was developed. Afterward, the study’s objectives and research questions (1.4), and structure (1.5) are depicted.

1.1 Problem

According to Kok et al., 2019, Musculoskeletal Disorders (MSDs) are the most prevalent work-related health problem among European Union (EU) workers, three out of five reporting MSDs complaints. The prevalence of work-related MSDs (WRMSDs) varies between the Member States, sectors and occupations. The construction, water supply and agriculture, forestry and fishing sectors are the most affected ones. Additionally, sociodemographic factors play a differentiating role in WRMSDs prevalence, female and elder workers bearing the higher rates. Section 3.1.2 presents a brief description of a few WRMSDs.

There is a wide range of risk factors related to the development of these disorders, which can be divided into three main categories: related to work, individual (also known as *co-factors*), and organisational/psychosocial. Note that the exposure to the risk factors, just by itself, does not enforce the development of MSDs; it depends on three additional factors: intensity, repetition and duration of the exposure to the risk factor (Direção-Geral da Saúde, 2008) (Figure 1.1).

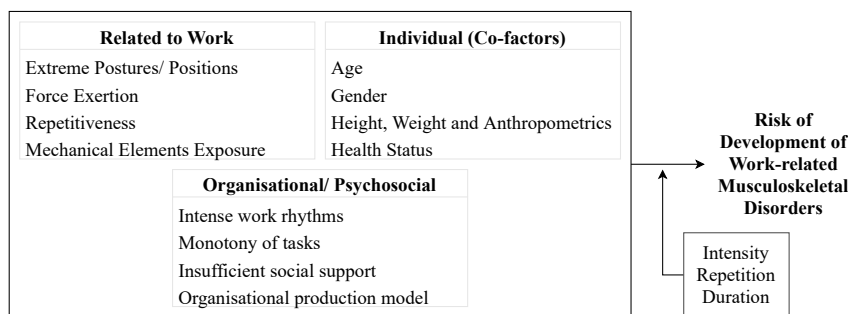


Figure 1.1: Diagram of risk factors for the development of WRMSDs.

Risk factors related to work are highly present in the automotive industry, and a considerable degree of their additional factors. The current dissertation tackles this problem, assessing the posture of operators with different individual characteristics during a work shift in automotive assembly lines and focusing on the *case study* of Volkswagen Portugal automotive industry.

1. INTRODUCTION

1.2 Motivation

Nowadays, WRMSDs have a huge impact on workers' health, representing 15% of the total number of (disability-adjusted) life years lost due to work-related injuries and illness, and enterprises' economy, being intimately related to higher rates of absenteeism and for more extended periods. Ultimately, WRMSDs affect EU countries, in terms of financial and social cost (i.e. loss of productivity and higher social expenses) (Kok et al., 2019).

Motivated by these consequences, German enterprises have been investing in the prevention of WRMSDs. In the Financial Times' article *Germany invests to prolong employees' working lives* (McGee, 2019), employers also justify their recent investments in ergonomic solutions explaining that experienced workers have the *know-how*, which makes them fundamental to productive and efficient processes. Likewise, as life expectancy has increased over the last years, workers' length of service will be extended over the next ones. Hence, there is a need to promote workers' health to ensure their well-being and performance.

1.3 Context

Towards WRMSDs prevention, several ergonomics approaches have been chased, and a few are described in section 2.1. Those approaches often involve an observer evaluating the performance of workers at the assembly line. They require a time-consuming manual data collection process, hindering the possibility of collecting individual data on a more frequent basis. In addition, they might require an observer to analyse the operator's motion, which often leads to biased results since the worker is aware that an external auditor is observing his work-method.

The advent of the Internet of Things (IoT) poses the opportunity of using wearables in the direction of ubiquitous data collection, increasing the amount of available data for a more personal and non-biased ergonomic evaluation. Along with these lines, the project OPERATOR (Fraunhofer Portugal, Center for Assistive Information and Communication Solutions – AICOS, 2020), which proposes a set of tools for risk exposure analysis in the workplace, sprang up.

This dissertation was developed in the context of the OPERATOR project. It follows the research of the authors of Santos et al., 2020, as it aims to solve their study limitations, validating an inertial sensing system setup for tracking wrist motion, refining the general upper body motion tracking algorithm, and upgrading the risk exposure analysis.

Presently and in line with Industry 4.0, the typology of the "Operator 4.0", established by the authors of Romero et al., 2016, has been developed about topics of motion capturing and analysis in industrial contexts, covered by research detailed in chapter 2. The current dissertation focuses on the Healthy type of the "Operator 4.0" (i.e. Operator + Wearable Tracker). It comprehends the development of methods using wearable trackers to monitor the motion of operators with different individual characteristics and in automotive assembly lines.

Ahead, as it is referred to in chapter 2, there is a considerable amount of solutions providers and research on the topic of risk assessment in the workplace. However, the solutions are often high-priced or do not provide any explanation about the ergonomic risk given, while research studies are usually conducted in controlled settings. Therefore, under the OPERATOR, this dissertation proposes to use *low-cost* wearable technology to track human motion and provide relevant insights of ergonomic risk assessment about a *case study* of Volkswagen Autoeuropa automotive assembly lines.

Furthermore, in the present future, we will assist the growth of Industry 5.0, which is a re-found and

widened purposefulness concept, going beyond producing goods and services for profit. This broader purpose constitutes three core elements: human-centricity, sustainability and resilience (De Nul et al., 2021). This perspective further motivated the work carried out in this dissertation.

1.4 Objectives and Research Questions

The main goal of this dissertation is to quantify the ergonomic risk and biomechanical exposure in automotive assembly lines, and its objectives and their respective research questions are depicted in Table 1.1.

Table 1.1: Study objectives and their respective research questions.

Objective	Research Question
1 Validation of an inertial sensing system setup to track upper body motion;	Which is the best placement of sensors on human body's segments to track the upper body motion?
2 Development of a methodology to synchronise the system over time;	How to synchronise system's sensors over time, and in what extend?
3 Application of kinematic/biomechanical constraints to the body segments' motion estimates;	How to estimate body segment's orientation and movement from wearable sensors' data, and using a model that describes the human upper body motion?
4 Definition of biomechanical exposure measures for ergonomic risk assessment;	What should be the criterion used to assess operators' posture and position?
5 Characterisation of the motion from different workers in automotive assembly lines;	How the operator's profile affects the his/her work-method while operating in the automotive assembly lines?
6 Design of an ergonomics report.	How to report ergonomic risk in order to support ergonomists' intervention?

1.5 Structure

The present document is divided into six main chapters (Figure 1.2).

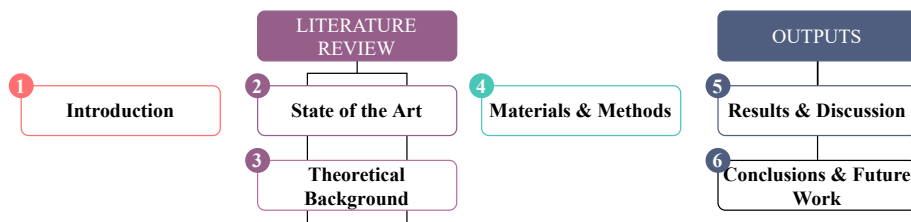


Figure 1.2: Dissertation's document structure.

1. Introduction - regards the root cause of this dissertation project and its end goal;
2. State of the Art - reviews current commercial solutions and latest research studies to assess ergonomic risk in occupational settings;
3. Theoretical Background - describes knowledge base theory, considered to be crucial to the dissertation development and comprehension;
4. Materials and Methods - details materials deployed and methods implemented and developed during the dissertation's project;
5. Results and Discussion - exhibits and interprets dissertation's outputs;

1. INTRODUCTION

- 6. Conclusions and Future Work - provides final resolution of this dissertation and the future steps in the research topic.

Note that every chapter ends up with a summary of its information, as conclusions, excluding chapter 6.

1.6 Chapter Conclusions

WRMSDs are a big problem with negative impact on individuals’ health, enterprises’ economy, and countries’ social and financial costs. Also, these disorders are increasing in modern societies. The current dissertation, developed within the Fraunhofer’s OPERATOR project and toward Industry 4.0 view, proposes a framework using wearable sensors’ data to monitor the motion of operators in automotive assembly lines and, subsequently, to evaluate the movements through ergonomic risk assessment and relate it to the work method conducted by each operator.

As it is indicated in Figure 1.3, the next chapter is the state of the art (2), supporting the topics explored in the theoretical background chapter (3). It follows the introduction provided, presenting “What?” has been done to accomplish the dissertation’s main goal, and precedes theoretical background, posing the challenge of “How?” to sense and monitor human motion.

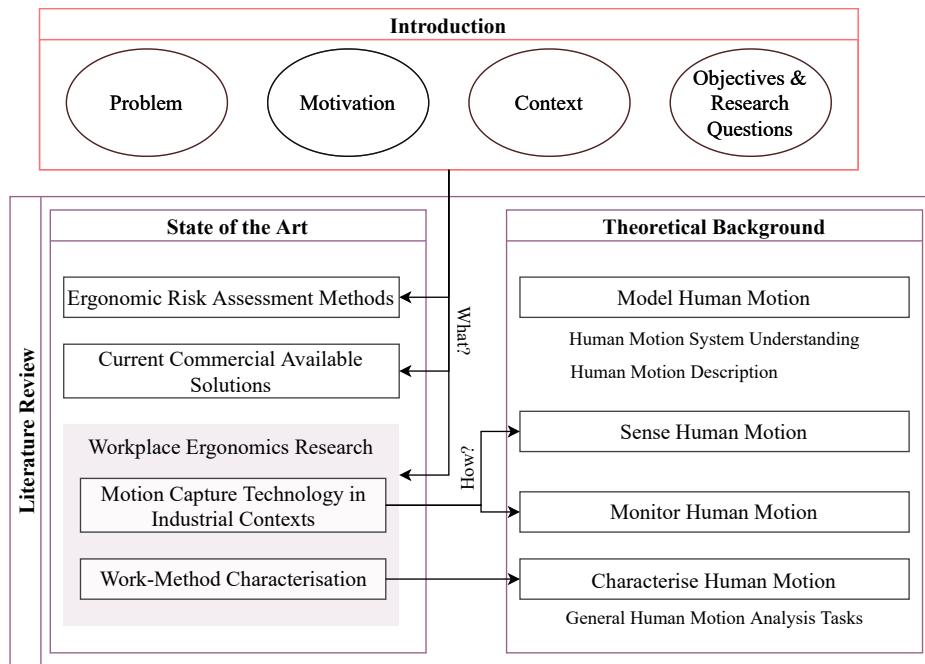


Figure 1.3: Block diagram about the chapters’ information linkage from chapter 1 to 3 (inclusive).

2. State of the Art

Berlin et al., 2017, explain the etymology of the word “ergonomics” which comes from the Greek roots *ergon* (work) and *nomos* (laws), being roughly translated as “the science of work”.

According to International Ergonomics Association (IEA) (The International Ergonomics Association, 2000), ergonomics (or human factors) is defined as a *scientific discipline concerned with the understanding of interactions among humans and other elements of a system, and the profession that applies theory, principles, data, and methods to design in order to optimise human well-being and overall system performance*. Also, IEA recognises the physical, cognitive and organisational branches of ergonomics as the three main “domains of specialisation”. It should be noted that this dissertation focuses solely on the ergonomics’ physical branch.

In this chapter, ergonomic tools are introduced, from generic ergonomic risk assessment methods (2.1) to particular current available commercial solutions (2.2). The latter are the main competitors of the solution developed in the OPERATOR. Additionally, a few research studies (2.3), that have been pursued to improve ergonomic risk assessment, are presented.

2.1 Ergonomic Risk Assessment

An ergonomic risk assessment method can be classified as:

- Self-reported, involving the interpretation of worker’s diaries, interviews and questionnaires;
- Observational, in which worker’s behaviour is evaluated by ergonomic teams experts, e.g. on proforma sheets. A proforma sheet is a checklist with domains related to workers’ exposure to ergonomic risk factors. After an ergonomist fills it out, it provides a score or a judgment about the workstation/task risk rating;
- Directly measured, which measures the exposure to the ergonomic risk using sensors to quantify workers’ motion effectively.

Concerning the self-report method, its outcome can result in the unreliability of the worker’s exposure perception, as the risk is discerned by himself/herself, and its comprehension or interpretation depends on the worker’s literacy, which hinders the possibility to compare different workers’ outcomes. In order to overcome these limitations, observational methods have been developed, and, in Table A.1, a few proforma sheets that are used during observational ergonomic risk assessment are indicated.

Nevertheless, the scoring system used in ergonomic assessment sheets may be questionable, and filling them out can be time-consuming for ergonomic teams, leading to biased conclusions. In order to cope with observational methods’ drawbacks, direct measuring has been used to record human motion

2. STATE OF THE ART

continuously, at the workplace or under standardised experimental conditions. Its goal is to accurately characterise human motion (Menolotto et al., 2020, OSHwiki, 2020). Next, in sections 2.2 and 2.3, approaches used to directly characterise human motion in industrial contexts are outlined.

However, a directly measured method also has disadvantages; it is usually more expensive and challenging to analyse and interpret the recorded data in real time.

2.1.1 Guidelines for Ergonomic Assessment

Ergonomics guidelines have been developed in different countries and by various entities. Those guidelines may have a powerful impact on achieving the implementation of good workplace standards, as the legal status and recognition of the guidelines may be the only thing that will persuade the management to take action in benefit of the workers' well-being (Berlin et al., 2017). Table A.3 from the authors of Berlin et al., 2017, was reproduced, as it enumerates some of the standards, guidelines and legal status primarily aimed to prevent WRMSDs.

2.2 Current Available Commercial Solutions

A considerable number of solution providers offer the ability to monitor human motion automatically and assess one or more risk factors in occupational settings. Table 2.2 shows a comparison between some of the available commercial solutions in terms of the system's design complexity.

Each solution was evaluated according to the criteria proposed by Santos et al., 2020:

- Explainability, i.e. the degree of information that the system can report;
- Invasiveness, i.e. the user discomfort levels and also the impact of the system's setup on his/her motion due to physical restrictions;
- Scalability, i.e. related to the number of subjects that can, simultaneously, use the setup. It depends on the system's invasiveness and cost.

Table 2.1 explains the criteria for high, medium and low level assignment to each system's design complexity component. If the system provides high level movement data, it means the system outputs more generalised metrics (e.g., it counts the number of bad lifting instances). Otherwise, if low level movement data is provided, the system outputs more detailed metrics (e.g., it calculates the angles from anatomical joints during bad lifting instances).

Most of the solutions focus on providing high-level movement data to supply indicators for assessing the ergonomic risk exposure. Nevertheless, not all featured it, such as Reactec Ltd., which focuses on reporting vibration tools usage, and WakeCap Technologies Inc., which mainly meet construction industry requirements, focusing on outdoor location and fall detection.

Every system in Table 2.2 relied on wearable (superficial) sensing technology. However, invasiveness was considered medium level for highly compound systems, i.e. systems that require the placement of a high number of sensors in the user's body, which suggests physical restrictions on the user's motion. For example, ViveLab Ergo and Scalefit solutions make use of XSens full-body system to capture their user's motion. Additionally, AXS Motion System Ltd. presents a full-body motion capture system with wires connecting its sensors, which may limit even more its user's motion.

2.2 Current Available Commercial Solutions

Table 2.1: Criteria for system’s design complexity component’s level assignment. System’s design complexity components are: explainability, invasiveness and scalability. Each component can be classified as high, medium or low level.

Component	Low	Medium	High
Explainability	If neither high nor low level movement data is provided	If only high or low level movement data is provided	If both high and low level movement data are provided
Invasiveness	If the setup is comfortable and it does not limit user’s motion	If the setup is uncomfortable or it limits user’s motion	If the setup is both uncomfortable and it limits user’s motion
Scalability	If the setup has many pieces and it is high-priced	If the setup has many pieces or it is high-priced	If the setup has a few pieces and it is not high-priced

Table 2.2: Current available commercial solutions.

Commercial solution	Explainability	Invasiveness	Scalability
WearHealth (WearHealth, n.a)	High	Medium	Medium
AXS Motion System Ltd. (AXS, n.a)	High	Medium	Medium
Modjoul (Smartbelt) (Modjoul, n.a)	medium (activities recognised from the waist down)	Low/Medium (depends on what indicators the user desires to track)	High/Medium (depends on what indicators the user desires to track)
VIT (VIT, n.a)	Medium (only detects lifts – back injuries)	Low	High
Reactec Ltd. (Reatec, n.a)	Low	Low	High
Wearable Technologies Limited (Eleksen, n.a)	Medium	Low	High
WakeCap Technologies Inc. (Reporting et al., n.a)	Low (although it detects falls, trips, etc.)	Low	High
Soter Analytics (SoterAnalytics, n.a)	Medium	Low	Medium
ViveLab Ergo (ViveLab, n.a)	High	Medium	Medium
Romware (Rombit, n.a)	Medium (detects falls, stillness)	Low	High
Kinetic (WearKinetic, n.a)	Medium (detects posture)	Low	High
Equival’s Life Monitor (Equival, n.a)	High (motion and fall detection)	Low	High
Scalefit (Scalefit, n.a)	High	Medium	Medium
XSens (Xsens, n.a)	High	Medium	Medium

Concerning scalability, some examples used a small number of sensors which increases their scalability to a high level (e.g. WearHealth, VIT, Wearable Technologies Limited, WakeCap Technologies Inc.). However, usually, those solutions were/are being developed to track particular indicators.

In addition, Soter Analytics solution uses artificial intelligence to compute ergonomic risk indicators.

Overall, high explainability systems depend on many sensors to monitor human motion, which increases systems’ cost and may have a negative impact on user’s motion, that downgrades systems’ invasiveness and scalability. Conversely, low to medium level explainability systems display a few sensors, decreasing invasiveness and increasing scalability. Note that, besides Equival’s Life Monitor solution has a nice trade-off between the three components; it mainly provides physiological data, e.g. Electromyography (EMG) data.

2. STATE OF THE ART

The framework developed within this dissertation provides low and high level data using *low-cost* inertial sensors that will be mounted on workers' apparel in the near future. The OPERATOR project proposes a solution with high level explainability and scalability and low to medium level invasiveness.

2.3 Workplace Ergonomics Research

This section addresses topics of research about workplace ergonomics. It starts with Motion Capture (MoCap) technology in industrial contexts (2.3.1) and, then, points out methods used to characterise individuals' work-method through motion data analysis (2.3.2).

2.3.1 Motion Capture Technology in Industrial Contexts

In the current revolution of the Industry 4.0 (Romero et al., 2016), MoCap solutions have been incorporated in order to improve the workers' health and safety, increase productivity, and improve industrial processes. The majority of the MoCap systems that were employed in industry were Inertial Measurement Unit-based (IMU-based) (Menolotto et al., 2020). For a more detailed description of MoCap systems and IMUs, refer to section 3.2.

There are several advantages of inertial sensing usage concerning occupational settings, as the reduced hardware dimensions and weight, inertial systems are cheaper than visual systems, recent advances in wireless connectivity and data processing, longer life battery, and larger bandwidth. Nonetheless, inertial sensing technique lags in compliance, sensor durability, information validity, and technique efficacy (Lim et al., 2020).

In Inertial Human Motion Tracking (IHMT), and with the aim of estimating multiple body segments' pose, more than one IMU has been deployed (Menolotto et al., 2020, Filippeschi et al., 2017), as it can be consulted in Figure A.1, which displays different inertial systems *setups* used in occupational ergonomics research (Lim et al., 2020).

However, note that a larger number of sensors involves higher frequency measurements and greater power consumption. So, it is crucial to consider the minimum set of sensors that solves a task satisfactorily (W3, 2017).

Moreover, to assess human motion data given by a MoCap, usually a comparison with human motion data from a ground truth MoCap is pursued, using e.g. Root Mean Squared Error (RMSE), correlation coefficients and Cumulative Distribution Function (CDF) as metrics, and drift and accuracy as performance measures (Santos et al., 2020, Filippeschi et al., 2017).

2.3.2 Work-Method Characterisation

In the present section, methods used to analyse time series from human motion data, i.e. ordered sequences of body segments angular data typically sampled at equal intervals in time, such as the ones in Figure 4.8, are introduced, from statistics (section 2.3.2.1), to more sophisticated approaches for Human Activity Recognition (HAR) (2.3.2.2).

In recent years, directly measuring methods have been developed and deployed to complement the self-reported and observational ones. Likewise, measures to quantify the biomechanical exposure have been designed, based on ergonomic risk factors specifications, and calculated from body segments angular data (Santos et al., 2020, Vignais et al., 2013, Malaise et al., 2019).

2.3 Workplace Ergonomics Research

Ergonomic risk factors related to work specifications (for WRMSDs of the upper limb) have been identified (Seidel et al., 2019, Keir et al., 2021) and evaluated using proforma sheets. The authors of Lim et al., 2020 suggest quantifying the intensity, repetition and duration in extreme postures and motions to measure the biomechanical exposure within workplace ergonomics.

In occupational ergonomics, measuring the biomechanical exposure has been taking part, as an input, on algorithm-based and automatic ergonomic risk assessment, and, subsequently, on intervention (Santos et al., 2020, Lim et al., 2020, Vignais et al., 2013, Malaise et al., 2019).

2.3.2.1 Descriptive and Inferential Statistics

Several studies used descriptive statistics to analyse time series from human motion data. In general, these studies contemplate measurements of median, mean, standard deviation, range and percentiles, among others, calculated either for the entire data collection duration or stratified by condition for comparison (e.g. by job category, task types) (Lim et al., 2020). Additionally, inferential statistics, such as ANOVA or mixed effects analyses, have been undertaken in order to establish relationships between upper limb ergonomics risk and biomechanical exposure variables (Álvarez et al., 2016, Brandt et al., 2015, Acuna et al., 2012, Möller et al., 2004).

The authors of Hansson et al., 2010 evaluated the physical workload in 43 types of work, using inclinometry for the head and upper arms, and EMG for the trapezius muscles. The researchers implemented meta-analysis techniques using aggregated group-level data (i.e. separating the combined data into females' and males' data). Then, the group mean values, the corresponding standard deviations, and correlations between motion from different body segments were used throughout the analysis. Similarly, in Hodder et al., 2010, they used inclinometry data to monitor nurses posture throughout their shift, including calculation of percentage time in high ergonomic risk postures and repetition.

Douphrate et al., 2012 analysed dairy parlour workers' ergonomics, extracting selected percentiles (10th, 50th, and 90th) from the cumulative distribution of postures, variables describing extreme postures and variables assumed to describe the occurrence of rest and recovery. As an index of repetitiveness, Mean Power Frequency (MPF) percentiles of the power spectra were calculated.

Vignais et al., 2013 computed task execution time and the percentage of time spent at each Range of Motion (RoM) defined in RULA. The authors of Vignais et al., 2013 also analysed each joint described in RULA and its limits, generating a *local* score, if the joint RoM values are higher than its limits, and calculating the total time and the frequency of appearance.

Recently, the authors of Santos et al., 2020 constructed an ergonomic risk score based on RULA, the Adjusted RULA (AdRULA). These used pie charts to display AdRULA score associated with each workstation in an automotive assembly line and violin plots to characterise the orientation of body segments in terms of the joint angular data distribution for each workstation and worker.

The authors of Maurer-Grubinger et al., 2021 constructed five new levels of complexity of RULA, i.e., from lowest complexity to highest. According to Maurer-Grubinger et al., 2021, an objective and detailed ergonomic analysis was possible using that method, which evaluates the entire task cycle and allows different levels of analysis.

Álvarez et al., 2016 provided a quantitative assessment of the ergonomic risk for the motion of the upper limbs, such as of the time in awkward postures, repetition percentages of time in which joints are unexpected angular ranges, motion frequency, and mean angular velocity. Repetition was computed using a Fourier analysis of the signals. In addition, the authors of Álvarez et al., 2016 displayed the measured angles in both angle–time and velocity–angle graphs. Angle–time graphs allow the detection

2. STATE OF THE ART

of joint angle values exceeding the recommended limits. Note that the percentage of time out of these bounds can be computed and used as a health risk evaluation tool. Differently, velocity–angle graphs allow the evaluation of the joint angle limitations and can be used to evaluate motion repeatability.

2.3.2.2 Human Activity Recognition in Occupational Settings

Over the years, several methods have been used in HAR within occupational settings, through mining time series’ tasks (Scheurer et al., 2020). In Table 2.4, a few of these are briefly depicted.

Table 2.4: Human Activity Recognition through mining time series’ tasks (adapted from Lim et al., 2020).

Study	Task	Method
Anderson et al., 2019	To classify activities: sitting, standing, weight-shifting, shuffling, and walking	Supervised learning based on Decision Tree (DT) algorithm, using mean and standard deviation values of human motion data, derived from inertial sensing, as features
Brandt et al., 2018	To classify the low and high-risk lifting based on the guidelines of the Danish Working Environment Authority	Supervised learning based on Linear Discriminant Analysis (LDA), using human motion data, derived from EMG and inclinometry, as features
Hosseinian et al., 2019	To classify manual material handling activities: four static and seven dynamic activities	Supervised learning based on Random Forest (RF) and Support Vector Machine (SVM) algorithms, using medians of postural angles and the area under the curve of transformed triaxial accelerometer data as features
Kim et al., 2014	To classify manual material handling task types: walking, carrying, lifting, lowering, pushing and pulling	Supervised learning based on Linear Discriminant Analysis (LDA), k-Nearest Neighbour (k-NN) and Multilayer Feedforward Neural Network (NN) algorithms. The authors used an unsupervised clustering algorithm to explore hidden structures in initial data and then clustered them. For each cluster, descriptive statistics and fast Fourier transform components were calculated and used as features
Peppoloni et al., 2016	To identify task types: neutral pose, reach, grasp, and move	Automatic segmentation based on State Machine, using posture estimates and muscle effort compared to the maximal voluntary contraction values to infer the current phase (i.e. state) within the work-cycle over time
Folgado et al., 2018	Classify the speed of predefined motions using inertial data	Supervised learning based on k-NN algorithm (k=1), using time series similarity measurements as features
Malaise et al., 2019	To classify tasks using the taxonomy proposed by the authors (constructed based on EAWS and later on upgraded by Maurice et al., 2019)	Supervised learning based on Hidden Markov Model (HMM) algorithm, using human motion data, derived from inertial sensing, as features
Varandas et al., 2019	To detect anomalies in generic, repetitive time series from human motion acquired in industrial contexts	Unsupervised learning based on Density-Based Spatial Clustering Algorithm for applications with noise, using statistical features extracted from cycles of repetitive time series (segmented through an unsupervised algorithm proposed by the authors), their representation transformations and similarity measurements

2.4 Chapter Conclusions

Toward ergonomic risk assessment, self-reported, observational and directly measured methods have been used. However, directly measured are not being used daily, because current commercial solutions do not provide an adequate trade-off between their systems' design complexity components. This requires the need to develop an accesible and intuitive solution that delivers a comprehensive and interpretable data to ergonomic assessment.

Concerning workplace ergonomics research, IHMT usage is preferable than other MoCap technologies. Moreover, implementations of guidelines/standards based on ergonomic risk factors related to work specifications have been settled to quantify the biomechanical exposure and the consequent ergonomic risk, associated with workers' work-method in terms of motion.

3. Theoretical Background

This chapter covers topics considered fundamental to the present dissertation development and comprehension. It introduces general knowledge about human motion description (3.1), describes the technology used to sense human motion (3.2), and depicts the computational methods implemented to monitor human motion (3.3) from sensed data. At the end of the chapter, a brief review of the existing approaches undertaken to characterise human motion (3.4) is provided.

3.1 Model Human Motion

Firstly, to study human motion, it is crucial to understand human anatomical description. Anatomy is the study of the structure of the human body, and it defines the human body relative to the *anatomical position* (Arus, 2018).

Figure 3.1 shows an approximation of the *anatomical position* and represents the three main spatial dimensions of the human body, the *anatomical planes* - frontal, sagittal and transverse -, and their associated *anatomical axes* - longitudinal, anteroposterior and mediolateral, respectively.

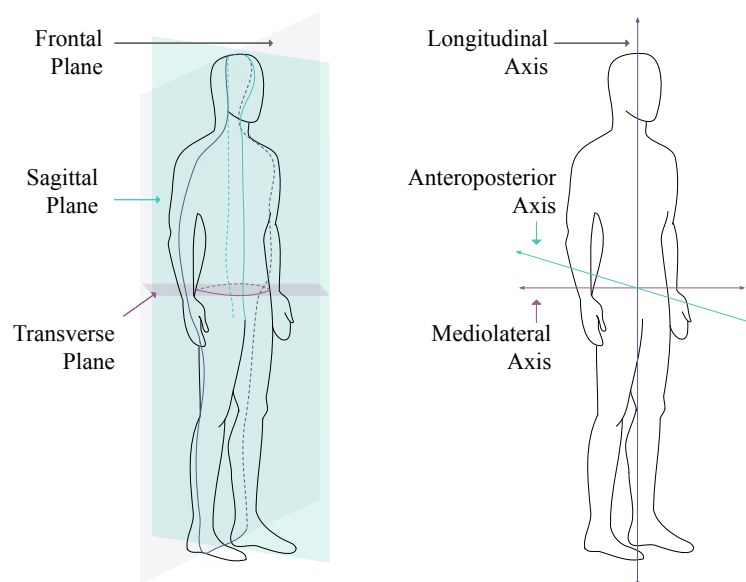


Figure 3.1: Anatomical planes (left) and axes (right).

Anatomical planes and axes are used to describe the human body's motion, as they will be presented in the following section 3.1.1, which briefly describes the main elements of the human body's musculoskeletal system, focusing on the upper body's joints description. From there on, the definition of MSDs is detailed and a few WRMSDs of the upper body's limbs and spine (3.1.2) are pointed out. Further, biomechanics (3.1.3) and human motion modelling approaches (3.1.4), using mathematical kinematics

3. THEORETICAL BACKGROUND

formulations, are introduced.

3.1.1 Musculoskeletal System

The musculoskeletal system is composed of passive and active elements (Nedoma et al., 2011), but only the study of the passive elements is in the scope of this dissertation.

Passive tissues, e.g. bones and joints, transfer originated and acting forces, while active tissues, e.g. muscles, can change the energy of biomechanical reactions into work and develop some power for achieving movement. Note that bones define body segments that are linked through joints.

Mobility of the human body's joints can be described as a combination of movements around the three anatomical axes (Nedoma et al., 2011, Arus, 2018):

1. Around the mediolateral axis, in the sagittal plane, the flexion (i.e. the decrease of the angle between two body segments in the sagittal plane) and the extension (i.e. the increase of the angle between two body segments in the sagittal plane). Note that extreme flexion/extension movement is called hyperflexion/hyperextension;
2. Around the anteriorposterior axis, in the frontal plane, the abduction (i.e. away from the midline in the frontal plane) and the adduction (i.e. back toward the midline in the frontal plane);
3. Around a longitudinal axis of the bone, in the transverse plane, the rotation can be inward or outward.

Depending on joint's type, it can be depicted by movements around one, two or the three anatomical axes. As this dissertation focuses on upper body movement study, the motions from joints of the upper limb (shoulder, elbow and wrist) and spine are explained. Ahead, Figures 3.3, 3.5, 3.7 and 3.8 picture joints' Degrees of Freedom (DoF) and their RoM. DoF and RoM are two fundamental concepts to keep in mind, derived from kinematics and biomechanics, which will be clarified in sections 3.1.4 and 3.1.3, respectively.

3.1.1.1 Shoulder joint

The shoulder consists of the glenohumeral, acromioclavicular, sternoclavicular, and scapulothoracic joints (Figure 3.2). It also has musculature structures that support these joints. Its motion includes flexion/extension, abduction/adduction, and inward/outward rotation (Figure 3.3). According to the shape of the contact surface, the shoulder joint is a ball-and-socket joint type. It can rotate about the mediolateral, the anteriorposterior, and the humerus' longitudinal axes. In addition, it can perform a shift movement, which occurs only in the luxation case (Nedoma et al., 2011).

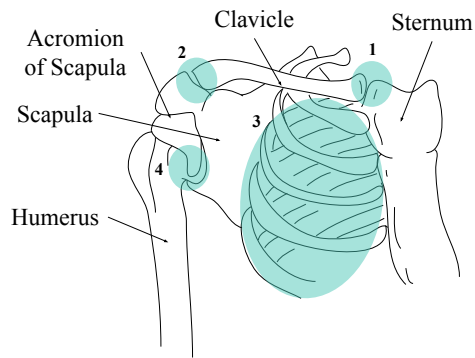


Figure 3.2: Shoulder joint complex's components: (1) sternoclavicular, (2) acromioclavicular, (3) scapulothoracic and (4) glenohumeral.

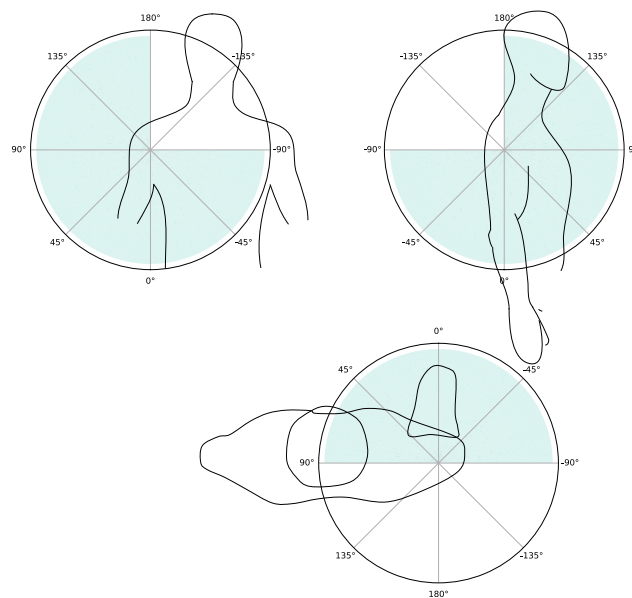


Figure 3.3: Shoulder motion: abduction/adduction (upper left), inward/outward rotation (bottom middle) and extension/flexion (upper right).

3.1.1.2 Elbow joint

The elbow joint is a compound joint that allows two types of motion: flexion/extension, related to the upper arm, and forearm's pronation/supination (Figure 3.5). The joint has three parts: trochlea-shaped, situated between the humerus and the ulna; spherical-shaped, placed between the humerus and the radius; cylindrical-shaped, located between the ulna and the radius (Nedoma et al., 2011) (Figure 3.4).

3. THEORETICAL BACKGROUND

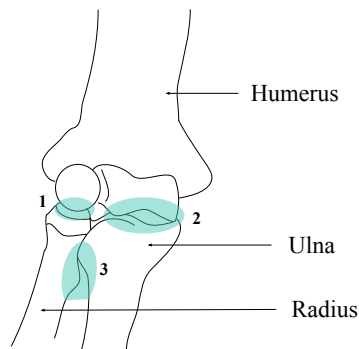


Figure 3.4: Elbow joint's components: (1) humeroradial (spherical-shaped), (2) humeroulnar (trochlea-shaped) and (3) proximal radioulnar (cylindrical-shaped).

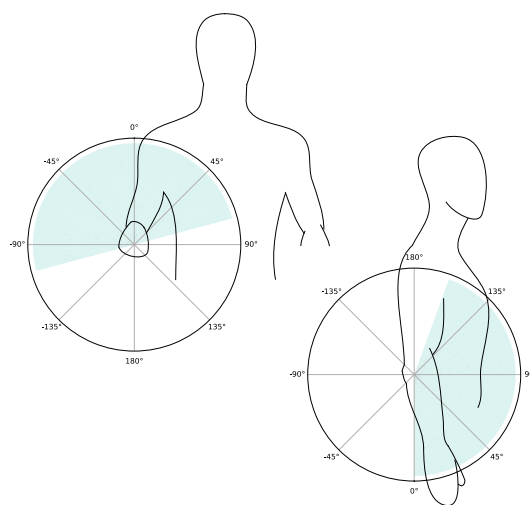


Figure 3.5: Elbow motion: pronation/supination (upper left) and extension/flexion (bottom right).

3.1.1.3 Wrist joint

The wrist is a compound joint named radiocarpal joint, which lies between the radius, its articular disc and three proximal carpal bones (the scaphoid, lunate and triquetral bones) (Figure 3.6). It enables two types of hand motion, related to the forearm: dorsal/palmar flexion (i.e. wrist extension/flexion, respectively) and ulnar/radial deviation (Nedoma et al., 2011) (Figure 3.7).

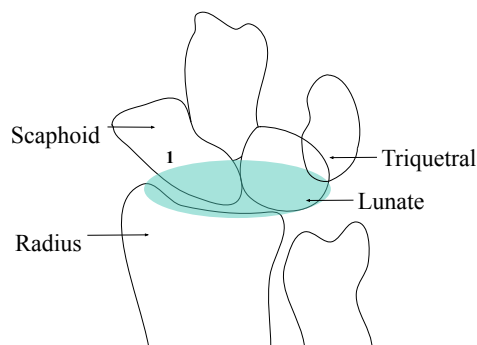


Figure 3.6: Wrist's (1) radiocarpal joint.

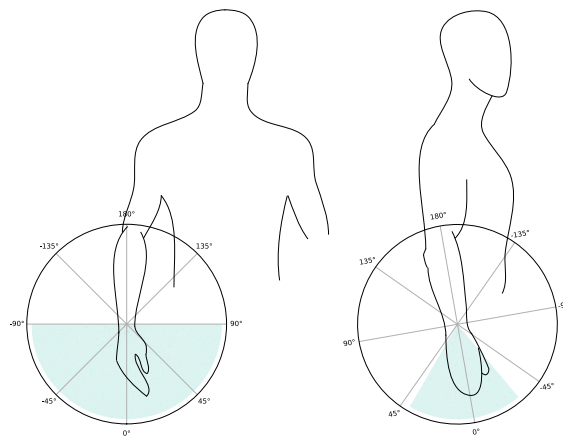


Figure 3.7: Wrist motion: extension/flexion (left) and ulnar/radial deviation (right).

3.1.1.4 Spine

The human spine is a complex structure created from 33 vertebrae, whose principal functions are to protect the spinal cord and transfer loads from the head and trunk to the pelvis and the lower limbs. The 33 vertebrae of the spinal column are divided into five regions: cervical (7), thoracic (12), lumbar (5), sacral (5), and coccygeal (4) (Nedoma et al., 2011). This complex structure enables trunk flexion/extension, lateral bending and rotation (Figure 3.8).

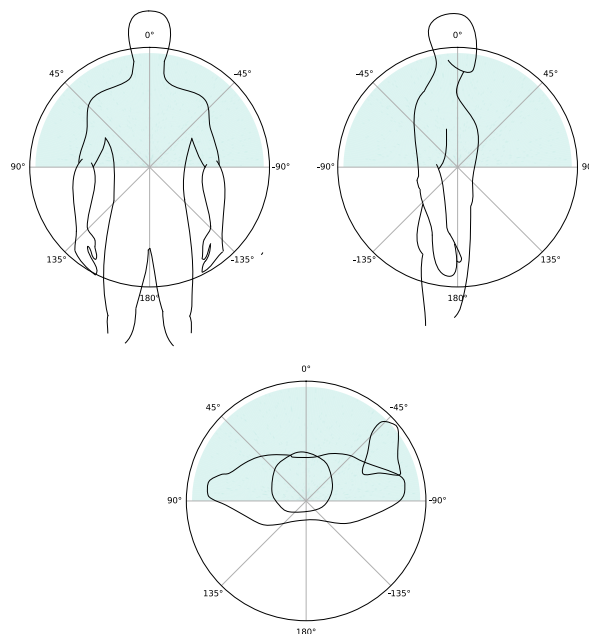


Figure 3.8: Spine motion: lateral bending (upper left), rotation (bottom middle) and extension/flexion (upper right).

3.1.2 Musculoskeletal Disorders

MSDs are defined as impairments of body structures such as muscles, joints, tendons, ligaments, nerves, cartilage, bones and the localised blood circulation system. If MSDs are caused or aggravated

3. THEORETICAL BACKGROUND

primarily by work and by the effects of the immediate environment in which work is carried out, they are known as WRMSDs (Kok et al., 2019). A few WRMSDs are listed as follows.

3.1.2.1 Work-Related Musculoskeletal Disorders

Rotator Cuff Tears Tendinitis One of the most frequent shoulder's WRMSDs. It is related to tasks consisting of sustained or repetitive elevation of the upper limbs at the shoulder's level or above it, or to the execution of circular movements with elevated arms (Direção-Geral da Saúde, 2008).

Carpal Tunnel Syndrome A neuropathy (i.e. pathology related to a peripheral nerve) due to compression of the median nerve within a limited space, i.e. the carpal tunnel, which is located in the fist. Excessive wrist extension or hyperflexion postures may lead to carpal tunnel syndrome (Direção-Geral da Saúde, 2008).

Wrist Tendonitis or Tenosynovitis It is triggered by the execution of repetitive movements of flexion/extension of the wrist and fingers or holding a load in an inadequate posture (Direção-Geral da Saúde, 2008).

Epicondylitis These are the lateral/tennis elbow and the medial/golfer's elbow epicondylitis. These are tendinopathies related to elbow's overload due to repetitive gestures or to manual handling of excessive or badly distributed loads (Direção-Geral da Saúde, 2008).

Rachialgias These WRMSDs are the most common ones. Symptoms vary according to the affected region(s) in the spine (cervical, thoracic and lumbar), back (lumbar) and neck (cervical) pain being frequently reported. Upright postures for long periods, frequent spine flexion/extension movements, manual handling and transportation of loads, and computer work (seated) for long periods are risk factors of rachialgias (Direção-Geral da Saúde, 2008).

3.1.3 Biomechanics

Biomechanics is described as an area of kinesiology, i.e. the whole scholarly area of human movement study, that focuses on *the study of the movement of living things using the science of mechanics*. Mechanics is the branch of physics that studies the motion of objects and the forces that cause that motion; it is divided into many areas, but the three main areas of biomechanics are: rigid-body, deformable-body, and fluids (Arus, 2018). In Figure B.1, are displayed the major branches of mechanics used in most biomechanical studies. This dissertation only concerns rigid body's and, particularly, dynamic motion's kinematics.

Likewise, biomechanics have been applied to improve performance and to prevent and treat injuries, using qualitative and quantitative measurements to analyse human motion (Arus, 2018). Respecting ergonomic risk assessment approaches, presented in chapter 2, these take part in injury prevention, especially respecting WRMSDs.

Before going through kinematics (3.1.4), the nine principles for application of biomechanics, according to Arus, 2018 (Figure B.2), are listed.

1. Force-Motion: Unbalanced forces act on our bodies or objects when we create or modify movement.

2. Force-Time: The amount of time over which a force is applied affects the resulting motion.
3. Inertia: The property of all objects to resist changes in their state of motion.
4. Range of Motion: The overall motion used in a movement which can be specified by linear or angular motion of the body segments.
5. Balance: Person's ability to control their body position relative to some base of support.
6. Coordination Continuum: How the muscle actions and body segment motions are timed in a human movement.
7. Segmental Interaction: The forces acting in a system of linked rigid bodies can be transferred through the links and joints.
8. Optimal Projection: There is an optimal range of projection angles for a specific goal for most human movements involving projectiles.
9. Spin: Rotations imparted to projectiles.

3.1.4 Kinematics

Kinematics is defined as *a branch of mechanics which describes the geometrically possible motions of objects (i.e. particles and rigid bodies) without regard to the forces that cause those motions*. In human movement study, each body segment is seen as a rigid-body, i.e. a set of many particles constrained to maintain constant distances between one another (Foxlin, 2002).

Next, kinematics representations (3.1.4.1) for posing body segments and human motion modelling approaches (3.1.4.3), using kinematics formulations, are introduced.

3.1.4.1 Kinematics Representations

Firstly, a particle in 3-Dimensional (3D) space is represented as a point, and defined by its mass, time-varying position $\mathbf{r}(t)$ and velocity $\mathbf{v}(t)$. Tracking an unconstrained particle in a 3D space consists of reporting the then-current three DoF of $\mathbf{r}(t)$, considering $\mathbf{v}(t)$, at any point in time (i.e. 3-DoF position (only) problem). On the other hand, a rigid-body requires 6-DoF to specify its pose, 3-DoF for position and 3-DoF for orientation (i.e. rotation) (Foxlin, 2002), as it is shown in Figure 3.9.

In order to describe the pose (position and orientation/rotation) of a rigid-body, two cartesian coordinate frames, both specified by a right-hand orthonormal basis, have been deployed: the Earth-fixed inertial (reference) coordinate frame, \mathbf{E} , and the body-fixed non-inertial coordinate frame, \mathbf{B} , represented in Figure 3.10 (Sabatini, 2011, Diebel, 2006).

Three translations can characterise a change in the rigid-body position, each one along a coordinate axis of \mathbf{E} , in other words, the rigid-body position is encoded by the position of the origin of \mathbf{B} in \mathbf{E} (Filippeschi et al., 2017, Diebel, 2006). Regard that translations are commutative (Haslwanter, 2018).

Concerning the rigid-body orientation, a change can be described by three rotations, each one about a coordinate axis of \mathbf{E} . Note that the rotations can be described in cartesian or in polar coordinates (Haslwanter, 2018).

3. THEORETICAL BACKGROUND

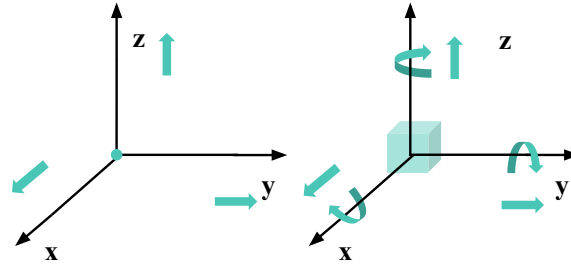


Figure 3.9: 3D space particle position changes along x , y and z -axis - 3-DoF position (only) problem (left). Rigid-body pose changes, position and orientation (i.e. rotation around x , y and z -axis) - 6-DoF position and orientation problem (right).

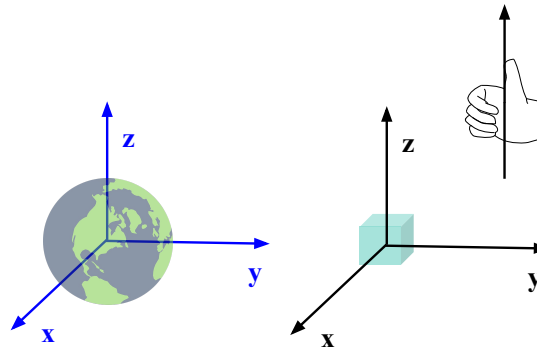


Figure 3.10: Generic coordinate frames used in rigid-body orientation representation: the Earth-fixed inertial coordinate frame - \mathbf{E} (left); and the body-fixed non-inertial coordinate frame - \mathbf{B} (right).

There are a few possibilities to represent rigid-body orientation over time, which are explained in the next sections.

Rotation Matrix A rotation matrix is defined as a matrix whose multiplication with a vector v rotates the v while preserving its length (Diebel, 2006). Therefore, it can describe the rotation of a rigid-body represented by v (Haslwanter, 2018).

There is a representation of v with respect to \mathbf{E} and to \mathbf{B} , v' and v , and these representations are related to each other through a rotation matrix, the Direction Cosine Matrix (DCM) R (Figure 3.11), as follows

$$v = Rv' \quad (3.1)$$

A DCM is a 3×3 orthogonal matrix with unit determinant and it belongs to the 3D *special orthogonal group of rotation matrices*, denoted by $SO(3)$, satisfying

$$R^T R = I = R R^T, \det(R) = 1, \quad (3.2)$$

Where I denotes the 3×3 identity matrix, the identity element of the $SO(3)$ group.

Its transpose R^T allows moving v representation from the body-fixed frame to the Earth-fixed frame,

as

$$v' = R^T v \tag{3.3}$$

Please note that DCM's column (row) vectors orthogonality requirement forces six constraints on its nine elements, thus only three elements of it are actually needed to uniquely characterise the rotation of v (Sabatini, 2011, Diebel, 2006).

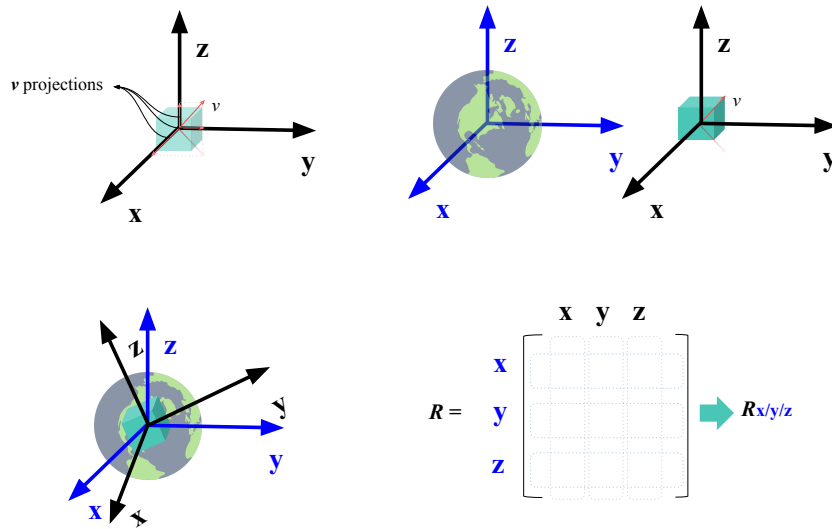


Figure 3.11: DCM as a representation of \mathbf{B} rotation relative to \mathbf{E} . Representation of v projections (v_i, v_j, v_k) in each axis of \mathbf{B} (x, y, z) (top left). Note that, each projection of v reflects the angle between each axis and the vector v v may represent \mathbf{B} orientation changes over time, but, in human motion tracking, it is usually required to represent \mathbf{B} changes relative to a reference coordinate frame, as \mathbf{E} (top right). The concept of projections can be applied in human motion tracking, constructing a *projection-matrix*, in which each column represents the projection of x, y, z -axis on x, y, z -axis (each row) . The *projection-matrix* is a rotation matrix, R , which describes how \mathbf{B} is rotated relative to \mathbf{E} . (bottom).

The rotation matrices that describe a rotation θ of \mathbf{B} relative to an axis of \mathbf{E} are

$$R_x = \begin{bmatrix} 1 & 0 & 0 \\ 0 & \cos \theta & -\sin \theta \\ 0 & \sin \theta & \cos \theta \end{bmatrix}, R_y = \begin{bmatrix} \cos \theta & 0 & \sin \theta \\ 0 & 1 & 0 \\ \sin \theta & 0 & -\cos \theta \end{bmatrix}, R_z = \begin{bmatrix} \cos \theta & -\sin \theta & 0 \\ \sin \theta & \cos \theta & 0 \\ 0 & 0 & 1 \end{bmatrix},$$

About \mathbf{E} 's x -, y -, and z -axis, respectively.

Often, a \mathbf{B} rotation relative to \mathbf{E} does not occur just about one single axis of \mathbf{E} , thus more compound approaches have been defined, such as Euler's theorem and angles and quaternion.

Euler's Theorem and Angles Euler's theorem states that the most general motion of a rigid-body with one fixed point is a coordinate rotation, which is a rotation about a single coordinate axis, and, also, that the composition of two rotations is again a rotation (Diebel, 2006, Haslwanter, 2018).

The orientation over time of \mathbf{B} relative to \mathbf{E} can be described using Euler's theorem in terms of three consecutive coordinate rotations, expressed by three body- or Earth-referenced Euler angles, α, β and γ , about the x -, y - and z -axis, respectively (Sabatini, 2011, Filippeschi et al., 2017, Diebel, 2006) (in Figure 3.12).

3. THEORETICAL BACKGROUND

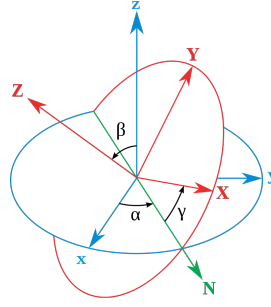


Figure 3.12: Euler Angles α , β and γ , where xyz is the reference coordinate frame, usually \mathbf{E} , XYZ is the rotated coordinate frame, \mathbf{B} , and \mathbf{N} the axis of the coordinate rotation (Wikipedia, n.a).

These angles can be arranged in a 3D-vector, parallel to the axis of the rotation and with a length proportional to the magnitude of the rotation in radians, the Euler vector:

$$u := [\alpha, \beta, \gamma]^T \quad (3.4)$$

With the corresponding rotation matrix (Diebel, 2006, Haslwanter, 2018):

$$R_{x,y,z}(\alpha, \beta, \gamma) := R_x(\alpha) R_y(\beta) R_z(\gamma) \quad (3.5)$$

In many applications, Euler angles time derivatives using finite difference approximations are necessary. Also, the usage of the linearised versions of primitive functions that generally describe Euler angles may be required (Diebel, 2006).

There are diverse configurations of the three consecutive Euler angles' rotations sequence. Diebel, 2006, summarises the most commonly used ones and their expressions for orientation representation.

Euler angles representation is easy to interpret, but it can suffer from singularities, referred to as *gimbal lock*. These are characterised by the indistinguishability of changes in the first and third angles when the second angle is at some critical value (Sabatini, 2011, Diebel, 2006). To overcome this limitation, one can alternatively use the quaternion kinematic representation to describe a rigid-body orientation over time.

Quaternion A quaternion is a 4-Dimensional (4D) complex number defined as the sum of a scalar q_0 and a vector $\mathbf{q} = (q_1, q_2, q_3)$ (Diebel, 2006, KUIPERS, 2020, Haslwanter, 2018) as it follows:

$$q = q_0 + \mathbf{q} = q_0 + q_1i + q_2j + q_3k \quad (3.6)$$

Where, according to Hamilton's expression $i^2 = j^2 = k^2 = ijk = -1$, the Hamilton's rules are:

$$ij = k \quad jk = i \quad ki = j \quad ji = -k \quad kj = -i \quad ik = -j \quad (3.7)$$

Quaternion Algebra Its conjugate, norm and inverse are given by (Haslwanter, 2018):

$$q^* = q_0 - q_1i - q_2j - q_3k \quad (3.8)$$

$$\|\mathbf{q}\| = \sqrt{q_0^2 + q_1^2 + q_2^2 + q_3^2} = \sqrt{\mathbf{q} \otimes \mathbf{q}^*} = \sqrt{\mathbf{q}^* \otimes \mathbf{q}} \quad (3.9)$$

$$q^{-1} = \frac{q^*}{\|q\|} \quad (3.10)$$

The multiplication of two quaternions, q and p , is not commutative and is given by (Haslwanter, 2018):

$$q \otimes p = (q_0 p_0 - \mathbf{q} \cdot \mathbf{p}) + (q_0 \mathbf{p} + p_0 \mathbf{q} + \mathbf{q} \times \mathbf{p}) \cdot (i, j, k) \quad (3.11)$$

Interpretation of Quaternions A quaternion can be named as (Haslwanter, 2018):

- *Pure* quaternion - its scalar component equals to 0;
- Scalar quaternion - its vector component is equivalent to $\mathbf{0}$;
- Unit quaternion - its norm verifies $\|q\| = \|q^*\| = 1$, so it belongs to $SO(3)$, being also known as rotation quaternion.

There are also quaternions that do not satisfy any of the conditions to be a *pure*, scalar or unit quaternion.

Quaternion Rotation Operator A unit quaternion describes a pure rotation in a 3D space, i.e. a rotation of an object about a fixed non-moving axis (Haslwanter, 2018). Remember that v can define a rigid-body orientation and is a pure quaternion ($v \in R^3$). Furthermore, KUIPERS, 2020, proves that the quaternion rotation (linear) operator $L_q(v)$ acts on v like a rotation about q and states it as follows:

Theorem 1 For any *unit quaternion*

$$q = q_0 + \mathbf{q} = \cos \frac{\theta}{2} + \mathbf{u} \sin \frac{\theta}{2} \quad (3.12)$$

and for any vector $v \in R^3$ the action of the operator

$$L_q(v) = qvq^* \quad (3.13)$$

on v is equivalent to a rotation of the vector through an angle θ about \mathbf{u} as the axis of rotation. Note that \mathbf{u} is a unit-norm vector along q .

Moreover, while the quaternion operator $L_q(v)$ may be interpreted as a point or vector rotation with respect to the (fixed) coordinate frame, its conjugate quaternion operator $L_{q^*}(v)$ may be interpreted as a coordinate frame rotation with respect to the (fixed) space of points, and it is stated as follows (KUIPERS, 2020):

Theorem 2 For any *unit quaternion*

$$q = q_0 + \mathbf{q} = \cos \frac{\theta}{2} + \mathbf{u} \sin \frac{\theta}{2} \quad (3.14)$$

and for any vector $v \in R^3$ the action of the operator

$$L_{q^*}(v) = q^*v(q^*)^* = q^*vq \quad (3.15)$$

is a rotation of the coordinate frame about the axis \mathbf{u} through an angle θ while v is not rotated. Equivalently, the operator $L_{q^*}(v)$ rotates the vector v with respect to the coordinate frame through an

3. THEORETICAL BACKGROUND

angle $-\theta$ about q .

According to these **Theorems**, if $L_q(v)$ describes a rotation of v in the body coordinate frame \mathbf{B} , about an axis in a (fixed) coordinate frame \mathbf{E} , then $L_q^*(v)$ describes it as a rotation of \mathbf{E} in \mathbf{B} .

A composition rotation is the product of quaternions (equation 3.11) which can be represented by the composite rotation operator $L_{qp}(v)$, equivalent to Euler angles rotation matrix in equation 3.5 (Diebel, 2006, KUIPERS, 2020). Additionally, as equation 3.13 equals equation 3.1 (Diebel, 2006, KUIPERS, 2020), then,

$$R = \begin{bmatrix} 1 - 2(q_3^2 - q_4^2) & 2(q_2q_3 - q_1q_4) & 2(q_2q_4 + q_1q_3) \\ 2(q_2q_3 + q_1q_4) & 1 - 2(q_2^2 - q_4^2) & 2(q_3q_4 + q_1q_2) \\ 2(q_2q_4 - q_1q_3) & 2(q_3q_4 + q_1q_2) & 1 - 2(q_2^2 - q_3^2) \end{bmatrix}$$

In Figure 3.13, an example of the rotation vector v_0 , using unit quaternion description is shown.

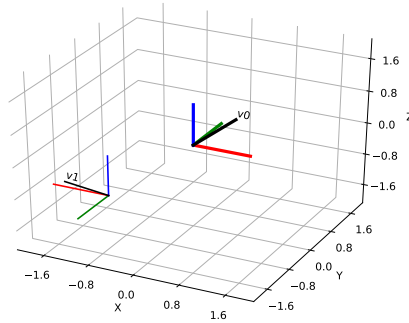


Figure 3.13: Example of a v_0 posing, with respect to a (fixed) reference coordinate frame. The v_0 rotation is described by the unit quaternion $q = 6.123234e-17 + 0i + 0j + k$ about the unit vector $\mathbf{u} = [0\ 0\ 1]$ (i.e. corresponding to the reference coordinate frame z -axis). Note that q rotates v_0 around a coordinate axis by 180° (i.e. π rad), which is consistent with equation 3.12. There is also a change in v_0 position along the reference coordinate frame axes, which is represented by $p = [-1\ -1\ -1]$. v_1 is the pose of v_0 after pose changing, depicted by q (i.e. orientation/rotation) and p (i.e. position).

3.1.4.2 Kinematics Representations Conclusions

According to the literature, unit quaternion representation has been extensively used in human motion tracking, as it overcomes Euler angles drawbacks: the presence of singularities (i.e. *gimbal lock*); less accurate than unit quaternion, when used to integrate incremental changes in orientation over time (i.e. higher error occurrence); and lower computational speed, due to the computation of trigonometric functions.

Unit quaternion representation also has disadvantages, i.e. less intuitive physical interpretation, and it may lead to complex optimisation problems due to the restriction of the unit norm to represent a pure rotation. Nonetheless, its mathematical elegance and lack of singularities make it a very popular representation for encoding the orientation of a rigid-body.

3.1.4.3 Human Motion Constraints

In human motion tracking, constraints equations define multiple body segments interactions (Foxlin, 2002). In section 3.1.1, it was noted that the human body is a high linkage system, e.g. through joints.

In order to track human body constrained motion, imposed by joints DoFs and respective RoMs, different methods have been applied as a part of Forward Kinematics (FK), i.e. generates simulation of movement, or Inverse Kinematics (IK), i.e. provides insight into observed/measured movement

(Carmichael et al., n.a). These two major techniques are based on transformations from(to) joint angles to(from) coordinates while considering body segments constant geometric parameters.

Moreover, a kinematics chain can be established. It encodes the motion of a body segment as a function of the previous segment's motion in the chain (Foxlin, 2002, Filippeschi et al., 2017). Alternatively, a free segment model that keeps some constraints as hard ones, while others are relaxed, can be implemented (Filippeschi et al., 2017). Therefore, kinematics chain and free segment are the most common types of kinematical models established based on the joints' biomechanics.

Setting human motion constraints is crucial because it can prevent the relative displacement of the body segments due to sensors' signals and computations *inaccuracies* over time (Filippeschi et al., 2017). These issues are explained in the following sections, 3.2 and 3.3.

Joints DoF constraints and body segments RoM limitations have been implemented by considering the orientation estimation as an optimisation problem, whose objectives are to respect the motion constraints and limitations and to optimise the consistency of the estimated orientations (Filippeschi et al., 2017).

About human motion tracking, IK has been deployed to solve kinematic chain global optimisation problems (Lim et al., 2020). To that end, biomechanical models have been constructed throughout kinematic and kinetic modelling. Biomechanical models can describe the motion of upper body joints (Sybele et al., 2006, Holzbaaur et al., 2005) or detail the motion of a specific compound joint, such as the scapulothoracic (Seth et al., 2016). Note that a few of these use the guidelines provided by the Standard Terminology Committee (STC) of the International Society of Biomechanics (ISB) (Wu et al., 2005, Lipton et al., 2002).

3.2 Sense Human Motion

Motion Capture (MoCap) is *the process of digitally tracking and recording the movements of objects or living beings in space*. To estimate the motion of body segments, MoCap systems comprise diverse tools and techniques (Yahya et al., 2019, Menolotto et al., 2020).

There are two main categories of MoCap systems, the visual and the non-visual (Yahya et al., 2019, Menolotto et al., 2020).

- Visual, or optical, MoCap systems comprise of depth camera, single camera and/or multiple cameras, and can be classified as marker-based (i.e. markers are attached to the body segments to track their motion, and they can be active or passive, e.g. Vicon (Vicon Motion Systems, n.a)) or as markerless (i.e. make use of images' features for detection of body segments motion, e.g. OpenPose (Cao et al., 2021));
- Non-visual MoCap systems are inertial which comprise the usage of IMUs, e.g. XSens (Xsens, n.a).

There are also hybrid solutions, combining both visual and non-visual technologies. Additionally, Surface Electromyography based sensors, which use surface electrodes that capture the myoelectric signal containing the muscles activation information, have been used alongside with MoCap systems.

From now on, this dissertation mainly focuses on Inertial Human Motion Tracking (IHMT), since IMUs are the elected technology in industrial contexts. As the goal is to obtain motion estimates from diverse body segments, the usage of diverse IMUs is needed and their signals have to be synchronised. Thus, devices synchronisation is outlined in the section 3.2.2.

3. THEORETICAL BACKGROUND

3.2.1 Inertial Measurement Unit Sensors

The most common type of IMUs used in biomedical applications consists of strap-down systems (i.e. systems wherein sensors are firmly fixed to the rigid-body being measured, and there are no “gimbals” or moving parts (Haslwanter, 2018)). Plus, in recent years, a new generation of IMUs based on Micro-Electro-Mechanical Systems (MEMS) technology supported the growth IHMT research (Filippeschi et al., 2017).

An IMU consists of a set of triaxial low-level sensors that measure 3D quantities in order to estimate the pose, or at least either the position or the orientation/rotation, of the body segment to which it is attached (W3, 2017, Lim et al., 2020, Filippeschi et al., 2017). Generally, it is composed of an accelerometer and gyroscope, and, many times, it is also equipped with a magnetometer. The naive use of an IMU is the integration of the sensors’ signals over time to estimate velocity, position and orientation (Filippeschi et al., 2017). Next, IMU’s low-level triaxial sensors are described. These are geometrically represented as in Figure 3.14.

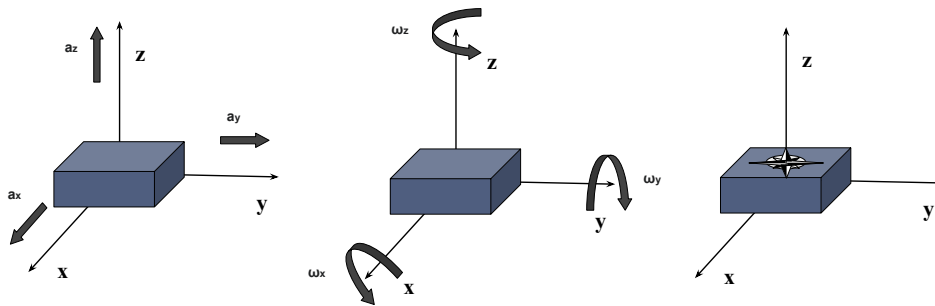


Figure 3.14: Accelerometer (left), Gyroscope (middle) and Magnetometer (right) geometric representations.

3.2.1.1 Accelerometer

Accelerometers are used to determine the direction of the local vertical (Roetenberg et al., 2009), also known as Gravito-Inertial Force (GIF), which is the sum of gravity and the inertial forces caused by linear accelerations. Note that accelerometers cannot distinguish between inertial and gravitational forces, as these sense all accelerations in one (Haslwanter, 2018).

An accelerometer is an inertial sensor. Thus, the directions of the force causing the motion and the associated sensed acceleration have opposite directions (Haslwanter, 2018). As follows, when the device is in free fall, the acceleration is 0 m/s^2 in the falling direction. Otherwise, when the device is laying flat on the table, its acceleration in the upwards direction will be equal to the Earth’s gravity (9.8 m/s^2), as it is measuring the force of the table pushing the device upwards (W3, 2017).

Accelerometers can provide the linear acceleration, the acceleration without gravity, or the gravitational acceleration, used to obtain the gravity vector that can be useful for some kinds of sensor fusion, such as creating a magnetic compass.

In acceleration measurements, there is interest in relevant variations and avoiding noise, which is given by acceleration’s low frequency component occurrences due to the slow changing force, the gravity. Therefore, a high-pass filter can help isolate the linear acceleration(s), while a low-pass filter can help to isolate the gravitational acceleration.

As accelerometers report acceleration, integration is needed to get velocity and double integration is required to obtain position. An integral creates drift and a double integral amplifies it. Hence, the position from an accelerometer’s data is very imprecise and not very useful.

According to Nazarahari et al., 2021, the accelerometer readings can be modeled as:

$$y_A = K_A[a + g] + b_A + v_A \quad (3.16)$$

Where y_A is the accelerometer readout, K_A is the scale factor matrix, a and g are the linear and gravitational accelerations, respectively, b_A is the bias, and v_A is a white noise term. In addition, the b_A term is obtained through a calibration procedure or estimated during orientation tracking.

3.2.1.2 Gyroscope

A gyroscope senses angular velocity relative to the inertial space (i.e. its reference frame). Particularly, a MEMS gyroscope measures its own rotation, making use of the *Coriolis effect*, which states that *in a reference frame rotating at a certain angular velocity, a given mass moving with a resultant velocity experiences a (fictitious) (inertial) force, the Coriolis force* (W3, 2017, Haslwanter, 2018).

This triaxial sensor consists of a (proof) mass, which is made to oscillate at a reasonably high frequency and a pickoff that is provided to measure the secondary vibration mode caused by the *Coriolis force*, which pushes the mass to vibrate in a direction perpendicular to the primarily driven vibration (Foxlin, 2002).

Gyroscopes sense high frequency oscillations, which make these inertial sensors the most power hungry and mean that they can easily be affected by other vibrations, like a vibration (rumble) motor or speaker in the same device (W3, 2017). Conversely, this characteristic makes gyroscopes helpful in achieving accurate orientation estimates for highly dynamic motions (Sabatini, 2011).

In order to get the rotation (angle) from the gyroscope's angular velocity data, there is a need to perform an integration that will turn noise into drift over time (i.e. low-frequency bias).

According to Nazarahari et al., 2021, the gyroscope readings can be modeled as:

$$y_G = K_G\omega_k + b_G + v_G \quad (3.17)$$

Where y_G is the gyroscope readout, K_G is the scale factor matrix, ω_k is the true angular velocity, b_G is the bias, and v_G is a white noise term.

3.2.1.3 Magnetometer

A magnetometer senses the magnetic field, meaning that it will only sense the Earth's magnetic field without any strong magnetic influence close by. Using that, one can obtain the *absolute* orientation (i.e. with respect to Earth's reference frame) of the sensor (Haslwanter, 2018). Magnetometers give a 3D vector pointing to the strongest magnetic field and do not enforce a specific device orientation in order to work. Notice that these sensors are susceptible to outside influence (W3, 2017).

As mentioned before, these devices can be used *in tandem with* accelerometers to isolate the gravitational acceleration; magnetometers need the gravity vector, provided by a low-pass filtered accelerometer's signal, in order to determine how the device is being held. Plus, more precise pose estimates can be achieved with an additional gyroscope, because its orientation computation update is faster than the combination of magnetometer and accelerometer. This combination of the sensors' signals is called *tilt compensation* (W3, 2017).

Static magnetic fields (e.g. Earth's magnetic field) in a conductor can be measured using the *Hall effect*, which results from *Lorentz force* (i.e. the combination of the electric and magnetic forces on a moving point charged due to electromagnetic fields). In IHMT, magnetometers sense an oscillating

3. THEORETICAL BACKGROUND

(dynamic) magnetic field as a result of the sensor's motion. Dynamic magnetic fields are described by the *induction effect* (Haslwanter, 2018).

According to Nazarahari et al., 2021, the magnetometer readings can be modeled as:

$$y_M = K_M m + d + v_M \quad (3.18)$$

Where y_M is the magnetometer readout, K_M is the scale factor matrix, m is the true geomagnetic field, d is the magnetic distortion, and v_M is a white noise term.

3.2.2 Devices Synchronisation

For most of the physical information sources (e.g. sensors), the acquired data is naturally ordered in time, so the information assigned to virtual objects (e.g. servers) must be ordered in time with respect to the (real) information chronology (Badihi, 2020).

Regarding devices (e.g. IMUs) synchronisation, there are three steps to take into account:

1. Querying the global time at which a specific event happened and is observed by an object;
2. Measuring the time difference between two events that are observed by different objects;
3. Relatively ordering the events that are observed by different objects.

Accordingly, if multiple sensors record or measure the same event, their data streams are coupled at a global time. Nevertheless, data streams from different sensors set up on a system (e.g. human body) are usually not correctly coupled. In other words, they are not synchronised.

Many of the synchronisation techniques currently used are based on wireless communication between sensors. These require: all the sensors in the network follow the same communication and synchronisation protocols; often, high-power sensors, which shorten sensors' battery life and usefulness; or incorporation of an accurate internal real-time clock, which may not be a feasible design decision due to the added cost and power consumption (Bennett, 2017).

In addition, there are datasets that have been collected without proper synchronisation, thus post-hoc and data-driven synchronisation methods have been developed (Shaabana et al., 2019).

Synchronisation issues arise due to clock oscillators inaccuracies (i.e. lack of stability).

The most common data desynchronisation problems, instigated in Figure 3.15, are:

- **Drift:** if the coupled sensors times are not the same, then there is some drift (i.e. error) in one or both sensors clocks oscillators, which needs to be corrected. One essential step in the correction is realigning or shifting the data in time to ensure the two data streams are aligned when the shared measurements are acquired and the coupling occurs;
- **Delay:** if acquisition initial time is different among data streams of the coupled sensors, then there is an initial lag of one stream relative to another.

The clock stability is affected by the oscillator type, the operating temperature and frequency shifts (i.e. jitter). Jitter is the deviation from the true periodicity of a presumably periodic signal, often about a reference clock oscillator signal (Bennett, 2017).

The clock stability is defined as follows:

$$ppm = \frac{\Delta t}{T} \times 1,000,000 \quad (3.19)$$

3.3 Monitor Human Motion

Where Δt is the difference between the actual time passed and the measured time passed, i.e. delay and drift, and T is the total time passed.

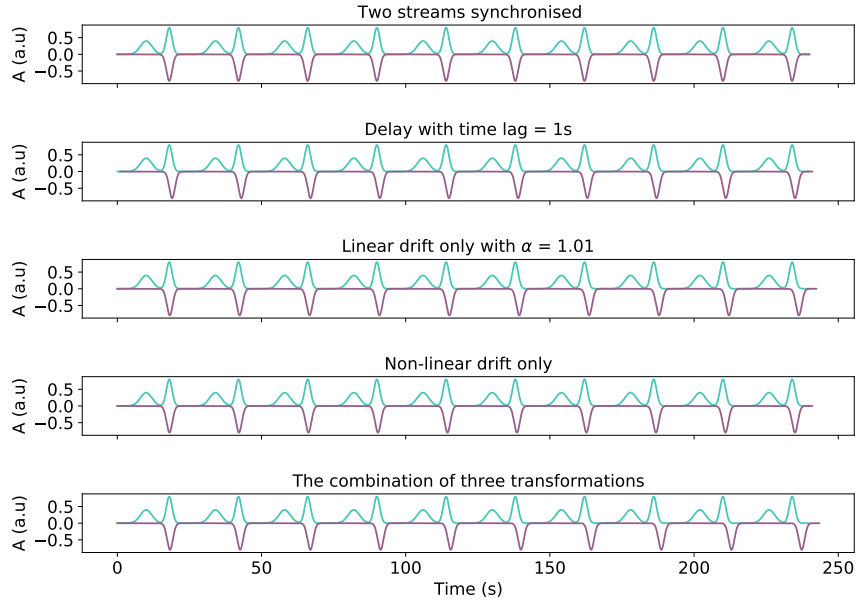


Figure 3.15: Synchronised data streams (first row), with a time lag of 1s (second row), a linear drift (third row), a non-linear drift (fourth row) and presenting all the data desynchronisation problems, delay and drift (fifth row). A stands for “Amplitude” and a.u for “adimensional unit”.

3.3 Monitor Human Motion

This section explains how to implement various Sensor Fusion Algorithms (SFAs), in order to obtain accurate and robust estimates of body segments 3D orientation.

3.3.1 Strap-Down Integration

Strap-Down Integration (SDI) is the basis of some SFAs. Remember that the term *strap-down* indicates the sensor is strapped onto the rigid-body, in opposition to gimbals.

Gyroscope readout SDI is used to update the orientation of an object at $t + 1$, taking into account a known orientation at t (Nazarahari et al., 2021), according to:

$$q_{t+1} = \exp(\Omega(y_G) T_s) q_t \quad (3.20)$$

$$q_0 = q(0) \quad (3.21)$$

Where q indicates a quaternion parametrization of orientation, $\Omega(y_G)$ is a 4×4 skew-symmetric matrix

which equals to $\frac{1}{2} \begin{bmatrix} 0 & -y_{G,x} & -y_{G,y} & -y_{G,z} \\ -y_{G,x} & 0 & -y_{G,z} & -y_{G,y} \\ -y_{G,y} & -y_{G,z} & 0 & -y_{G,x} \\ -y_{G,z} & -y_{G,y} & -y_{G,x} & 0 \end{bmatrix}$, T_s is the sampling rate of the IMU, $\exp(\bullet)$ is the

matrix exponential operator and $q(0)$ is the known initial orientation. Note that the $\exp(\Omega(y_G) T_s)$ term is the result from the integration of the angular velocity data $\Omega(y_G)$.

3. THEORETICAL BACKGROUND

3.3.2 Vector Observation algorithms

Vector Observation (VO) algorithms are SFAs that focus in minimising the cost function in equation 3.22, the Wahba's problem (Nazarahari et al., 2021). The solution of the Wahba's problem is the rotation matrix R , that is, subsequently, used to estimate an absolute orientation of the rigid-body with respect to \mathbf{E} , the Earth-fixed reference frame.

$$\mathbf{J} = \frac{1}{2} \sum_i a_i |b_i - Rr_i|^2 \quad (3.22)$$

Where a_i is the weight related to each VO (i.e. a VO is a vector in \mathbf{B} , the body-fixed reference frame), b_i is the unit vector measured in \mathbf{B} , R is the DCM that represents the rigid-body rotation (to be estimated), and r_i is the unit vector which corresponds to b_i in \mathbf{E} (Nazarahari et al., 2021).

VO algorithms are applied to IMU accelerometer and magnetometer readouts, wherein y_A and y_M are the b_i s (VOs), and the gravitational acceleration and the Earth geomagnetic field vectors are the r_i s (Nazarahari et al., 2021).

TRI-axial Attitude Determination (TRIAD) and QUaternion ESTimator (QUEST) are VO algorithms. These differ from each other as, contrarily to TRIAD, QUEST may accomodate more than two VOs. Moreover, Factored Quaternions Algorithm (FQA) is used to decouple y_A and y_M and cancel the effect of the magnetic disturbances on orientation calculation, returning a quaternion as a solution of the Wahba's problem (Nazarahari et al., 2021).

3.3.3 Complementary Filters

A Complementary Filter (CF) proposes an engagement between accelerometer, gyroscope and magnetometer properties. It involves low pass filtering of accelerometer and magnetometer data that isolates their low-frequency components, the gravitational acceleration and the Earth geomagnetic field, respectively, and high pass filtering of gyroscope data, to remove gyroscope's low frequency component, the bias.

Note that the filters optimal cut-off frequency k_P depends on motion dynamics. Thus, a higher k_P is preferred for relatively slow motions, while for high dynamics, a smaller k_P is required. In many cases, an integrator with gain k_I is added. It is relevant for the CF performance, along with the choice of k_P . While gyroscopes readings should be fairly considered in highly dynamic motion tracking, accelerometers and magnetometers can provide stable estimates under less dynamic movement. There are a few Modified CFs, proposed in the literature, which implement techniques in order to support gain's choice, as CF performance highly depends on it (Nazarahari et al., 2021).

Thus, rigid-body orientation is estimated from gyroscope, accelerometer and magnetometer data, using the SDI (3.3.1) and VO (3.3.2) algorithms, respectively, and then fused using CF SFA (Garcia, n.d.) as follows:

$$q = (1 - k_I)q_G + k_I q_{AM} \quad (3.23)$$

Where q_G is the orientation estimated from the gyroscope, q_{AM} is the orientation estimated from the accelerometer and the magnetometer.

3.3.3.1 Mahony filter

Proposed by the authors of Mahony et al., 2008, this filter is a non-linear CF that considers the decoupling between the estimated orientation from the gyroscope and the estimated orientation from the magnetometer and accelerometer and weights them according to its gain. This filter uses quaternion representation in rigid-body orientation estimation. Likewise, it is characterised by two parameters that control the algorithm performance: the weighting process directly on the quaternions and the filter proportional gain k_I .

3.3.3.2 Madgwick Filter

Freed by the authors of Madgwick, 2010 (Garcia, n.a[c]), the Madgwick filter algorithm is an innovative CF. This filter uses a VO algorithm, based on the Gradient Descent Algorithm (GDA) to compute the rotation matrix R . Thus, Madgwick filter is an analytically derived and optimised GDA. The algorithm enables a fair orientation estimation performance at low sampling rated data and (online) compensation of magnetometer magnetic distortion (detailed in section 3.3.6). Additionally, it ensures an optimal value of k_I , controlled by a single adjustable parameter (defined by observable system's characteristics), which compensates gyroscope low-frequency bias (i.e. drift). Madgwick filter uses a quaternion to represent the rigid-body orientation.

3.3.4 Kalman Filters

Kalman Filter (KF) SFA, at first proposed by Kalman, 1960, intends to estimate a state vector x , which represents the orientation of the rigid-body, based on the knowledge of:

- System model;
- System noise input u (usually y_G);
- System measurements z (usually y_A and y_M);
- White Gaussian noise processes (w and v) related to the system and their measurement models covariances;
- State transition matrix and equation (\mathcal{F} and f);
- Measurement prediction matrix and equation (\mathcal{H} and h).

x can be estimated by solving a linear discrete-time system as follows:

$$\begin{cases} x_{t+1} = \mathcal{F}_t + \mathcal{B}_t u_t + w_t \\ z_{t+1} = \mathcal{H}_{t+1} x_{t+1} + v_{t+1} \end{cases}, \quad (3.24)$$

Or a non-linear discrete-time system,

$$\begin{cases} x_{t+1} = f_t(x_t, u_t, w_t) \\ z_{t+1} = h_{t+1}(x_{t+1}, v_{t+1}) \end{cases}. \quad (3.25)$$

The solution of one of these systems is the state of the rigid-body in $t + 1$, in terms of orientation. Thus, KF computation basically comprehends two steps (Garcia, n.a[b]):

3. THEORETICAL BACKGROUND

1. The prediction step - estimates the next state of the system and its covariance, at time $t + 1$, given the previous state, at time t ;
2. The correction step - rectifies the estimation with a set of measurements z , at time t .

The system to be solved, i.e. system 3.24 or 3.25, is chosen accordingly to noise processes distribution and in order to minimise the error between the true state and an estimated state. In systems, SDI of the gyroscope is used to model \mathcal{F} or f in the prediction step. Moreover, the differences between the measured and the estimated accelerations and geomagnetic fields are used to model \mathcal{H} or h in the correction step (Nazarahari et al., 2021).

In the literature, a few variations of KFs have been described: the linear (i.e. linear system solution), the extended (i.e. non-linear system solution), the complementary (i.e. considers estimates of primary states' errors), and the modified KFs.

Furthermore, as KF performance highly depends on an accurate definition of the system's and measurement's models and noise covariance matrices, adaptive KFs which tune models' gain over time have been used (Nazarahari et al., 2021).

3.3.5 Sensor Fusion Algorithms Conclusions

SDI and VO algorithms have several drawbacks. The first requires knowing the initial orientation, and the gyroscope bias results in an increasing cumulative error in the orientation estimation due to the numerical integration. The latter is unsuitable for indoor orientation tracking while performing highly dynamic tasks, as algorithms can be affected by a and d (external non-gravitational acceleration and magnetic distortion, respectively).

CF and KF SFAs are used to compensate SDI and VO algorithms' disadvantages. Remember that, usually, both CF and KF algorithms use SDI of y_G to propagate the orientation in time and correct the propagated orientation with the estimated orientation by a VO algorithm, or by a corrective term obtained with an optimisation rule (Nazarahari et al., 2021). In Figure 3.16, SFAs are briefly illustrated.

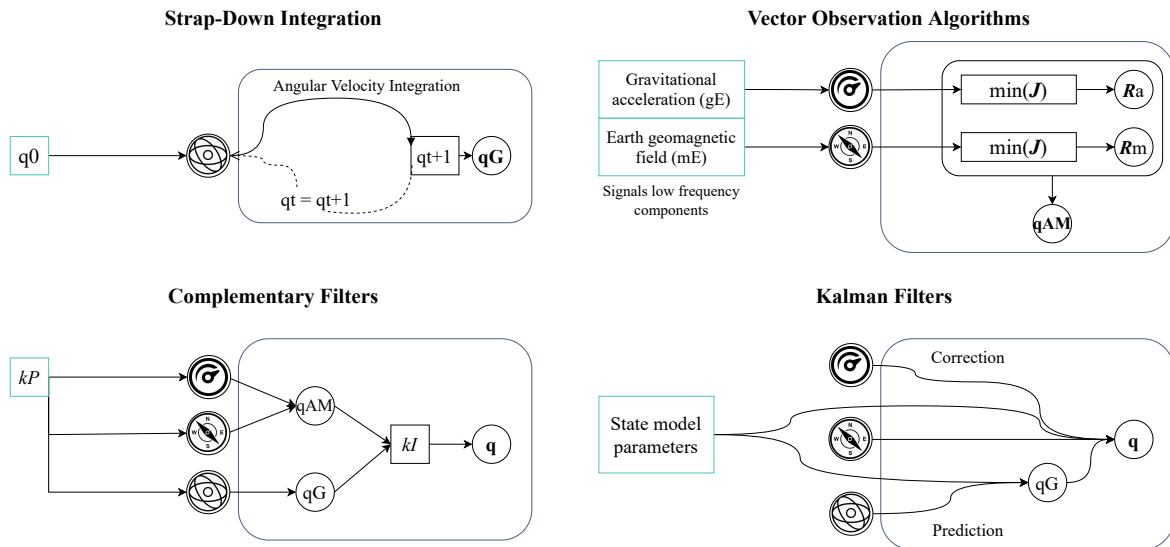


Figure 3.16: Block diagram of the SFAs.

Moreover, in order to improve the accuracy of the SDI, authors of Nazarahari et al., 2021, suggest the usage of a gyroscope with low bias, correction of the gyroscope's static bias and scale factor through

gyroscope's offline calibration, usage of stochastic models or heuristics to estimate the time-varying b_G in real-time and use of an accurate estimation of $\exp(\bullet)$ for the SDI.

Concerning accelerometer and magnetometer data in VO algorithms, authors of Nazarahari et al., 2021, propose the evaluation of sensors' calibration and usage of online stochastic models to estimate a and d , correcting y_A and y_M , respectively.

Ultimately, as it was already mentioned, gain is a key component in the performance of CF and KF SFAs. In order to better choose the gain, the same authors of Nazarahari et al., 2021, commend the usage of an online gain tuning strategy to adaptively put more weight on the most reliable source of information; decoupling of the gains associated with gyroscope, accelerometer and magnetometer; and selection of the filter gain(s) rigorously by evaluating these to diverse motion patterns, intensities, and durations.

3.3.6 Orientation Estimation Issues

In IHMT, drift, calibration and magnetic disturbances are frequent issues. Therefore, procedures have been carried out to handle these.

In order to deal with gyroscope's drift (i.e. to correct the cumulative error of the SDI), the fusion of y_G 's SDI with a quasi-static one, the inclusion of b_G in the y_G estimate, and exploitation of constraints from the kinematics chain to avoid drift in the orientation estimates of one body segment with respect to the others have been enforced (Filippeschi et al., 2017). Furthermore, Ribeiro et al., 2020, applied Machine Learning (ML) techniques in order to correct accelerometer's drift in position tracking. For that, the author used classifiers to identify the periods in which IMUs were stopped (i.e. zero-velocity detection) and combined these with ML regression models, capable of estimating the displacement of the sensors during periods of movement.

For long-term acquisitions, it is crucial to consider measurements from aiding sensors (i.e. accelerometer and magnetometer) to correct the gyroscope's drift (W3, 2017, Nazarahari et al., 2021).

Calibration is usually performed at the beginning of the session for data collection, defining the parameters used in motion reconstruction algorithms. Parameters can be related to the pose of IMU frames with respect to \mathbf{B} or anthropometric measures. Usually, initial calibration consists of resting in Neutral Pose (N-Pose) or standing in T-pose. Aside from these static poses, dynamic calibration may be required, i.e. to perform rotations around different joint axes to better align the IMU frames with the anatomical axes (Filippeschi et al., 2017). In addition, authors have been proposing the usage of MoCap visual systems *in tandem with* inertial MoCap in order to calibrate the IMU sensors over time (Santos et al., 2020), or to compensate magnetic disturbances (Bleser et al., 2011). Practical descriptions of calibration procedures are provided in section 4.2.1.

Magnetic disturbances can be classified as hard or soft iron interferences, which are related to permanently magnetised objects or objects that are magnetised only when an external field is applied. Hard iron's effects cause an offset of the Earth magnetic field, whereas soft iron's effects cause a distortion (i.e. the change in the intensity and direction of the sensed field). In Figure 3.17, the effects of magnetic interferences on the coordinate sensor frame are shown. When the magnetic environment does not change, magnetic disturbances can be corrected through internal sensor calibration. Otherwise, when the magnetic environment changes, a policy that decides if the y_M is reliable can be established, using a

3. THEORETICAL BACKGROUND

vector selection (also used to select y_A reliable estimations) and/or limiting the contribution of y_M , e.g. using a CF/ KF algorithm to weigh magnetometer's VO estimate (Filippeschi et al., 2017, Nazarahari et al., 2021).

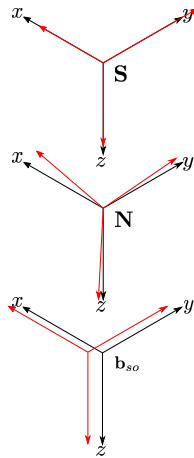


Figure 3.17: Magnetometer without magnetic interferences (top), with soft (middle) and hard (bottom) iron interferences (Teslabs, n.a).

3.4 Characterise Human Motion

Mining time series data, which is *the process that involves inferring of an algorithm to explore data, develop a model and discover previously unknown patterns*, has been pursued to analyse human motion (Wang et al., 2012). Data mining taxonomy is shown in Figure 3.18.

Mining tasks compromise a *query* time series Q and a measurement function, D , that provides similarity information between two time series, Q and C , $D(Q, C)$ in order to compare both for sequence matching, subsequence searching and motif detection/discovery (Wang et al., 2012). Note that there are distance measurements used to compute time series *shape similarity*, and probabilistic measurements, used to determine time series *structural similarity* (Keogh, 2006).

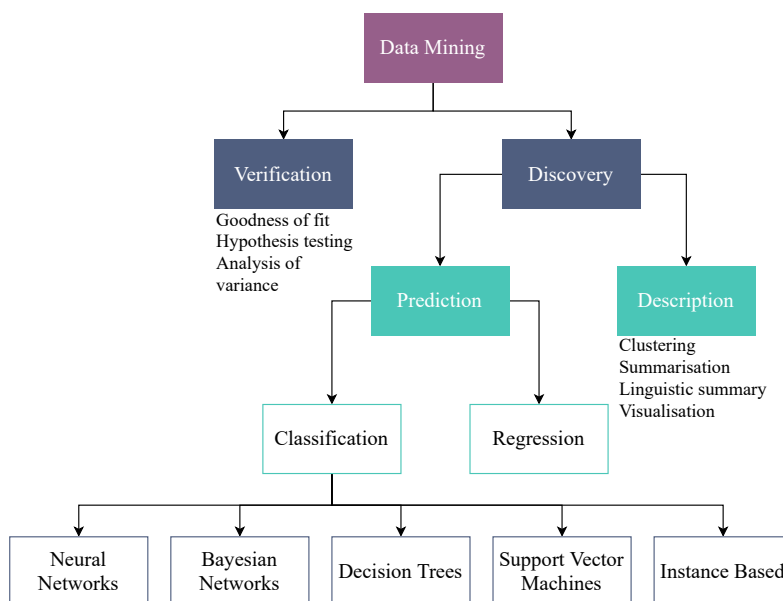


Figure 3.18: Data Mining Taxonomy (based on Wang et al., 2012).

3.5 Chapter Conclusions

Commonly used distance measurements are the Euclidean Distance (ED) and the Dynamic Time Warping (DTW) (Wang et al., 2012). Motivated by distance measurement algorithms difficulty of scaling search to large datasets, Rakthanmanon et al., 2012, depicted and introduced a few optimisation methods for subsequences of time series under DTW. In recent years, time series similarity distance measurements have been developed to account for amplitude differences (Brankovic et al., 2020, Gamboa, 2013, Chen et al., 2013, Wang et al., 2012, Marteau, 2009).

The authors of Folgado et al., 2018, developed Time Alignment Measurement (TAM) which describes the behaviour in time between two signals by measuring the fraction of time distortion between them. TAM is a distance measurement of time series similarity in the time domain and can be very useful to measure human motion performed during repetitive work-cycles. In particular, TAM can be useful to evaluate the temporal dissimilarity between operators that might be executing the same work process (i.e. which enforces identical time series' amplitude and shape) but at different working speeds.

On the other hand, towards mining time series using probabilistic measurements, a Q over uncertain dataset assigns to each uncertain data C a probability p , indicating the likelihood that C meets the Q predicate, $p = D(Q, C)$ (ABfalg et al., 2009).

Eamonn Keogh and his team Keogh, n.a, have been significant contributors to mining time series data, particularly motif discovery. Time series motif discovery can be defined as *the unearthing of locally conserved behaviour in a long time series*. Note that almost every motif discovery algorithm has been using ED. Alaei et al., 2020, present the Scalable Warping Aware Matrix Profile algorithm, which is an efficient, scalable and exact method to find time series motifs under Subsequences DTW. It uses the Matrix Profile (MP) representation of distances between all subsequences and their nearest neighbours.

Additionally, Yoshimura, 2019, proposes a hub motif (a type of motif) and an algorithm for finding hub motifs, based on the MP and presented an exciting application to task classification regarding human motion ergonomics.

3.5 Chapter Conclusions

Human body segments are linked through joints, which enable segments' motion within a set of DoFs and their respective RoMs. Upper body joints are shoulder, elbow, wrist and spine. In order to track the upper body motion, MoCap systems have been deployed. As the inertial MoCap system option is the more feasible alternative in industrial contexts, its usage was explored. In IHMT, IMUs are rigidly attached to segments to get acceleration, angular velocity and magnetic field measurements associated with the motion conducted by their user. These measures can be combined through SFAs to estimate segments' orientation over time. The reference frame relative to which each segment motion is described can be changed using rotation matrix algebra and throughout kinematics representations. Quaternions are the most common kinematics representation in human motion monitoring applications. Stem from orientation quaternion representation, joints' angular data can be determined using complex numbers mathematics. In addition, biomechanical models and, particularly, kinematics models that describe joints' real movements can be implemented to correct orientation data by applying human motion real constraints to monitor human motion accurately. Ultimately, acceleration, angular velocity, magnetic field, and orientation quantities can be brought together to characterise human motion by conducting mining time series tasks.

4. Materials and Methods

In this chapter, the materials used and methods deployed and developed during the dissertation project are described.

Using the framework Modelling-Sensing-Analysis-Assessment-Intervention (MSAAI), developed by the authors of Lim et al., 2020, to assess similar research, the following sections, data collection (4.2), data pre-processing (4.3) and monitoring motion (4.4), systems comparison metrics (4.5) and ergonomic assessment (4.6), can be addressed to sensing, modelling, analysis and assessment frames from MSAAI, respectively. The frames from MSAAI respect to human motion modelling (M) techniques, inertial sensing (S) usage, motion analysis (A) and ergonomic assessment (A) methods, and intervention (I) approaches in occupational settings. Note that this dissertation project did not include the design of an intervention approach.

Detailed descriptions about the MoCaps used and related to the computational tools deployed are provided in appendices C.1 and C.5, respectively.

4.1 Study Design

4.1.1 Study Type

The study conducted during the dissertation was explorative, i.e. established and validated the motion tracking system, and transversal, i.e. assessed measures at a selected time for each subject, not compromising *follow-up* measurements for the same subject.

4.1.2 Study Scenarios

The study can be divided in two scenarios:

- **Validation:** whose results validated the motion tracking system within controlled (i.e. laboratory) and uncontrolled (i.e. automotive assembly lines/field) settings;
- **Evaluation:** intended to assess the biomechanical exposure and ergonomic risk related to diverse processes carried out in an automotive assembly line and different operators' work-methods performed.

4.1.3 Case Study

The study aimed attention at an ergonomic assessment of automotive assembly lines' operators, specifically, those working at fitting processes. Clarifying, automotive assembly lines are divided into diverse processes, from parts production and rendering to their assemblage. Each set of processes constitutes a group of workstations.

4. MATERIALS AND METHODS

Fitting processes were selected, as they were being analysed by a plant project team that aimed to improve the working conditions under which they are performed.

There are three groups of workstations associated with automotive assembly lines' fit shop (Figure 4.1):

- **Group A:** Rear and Front End, consisting in the line up of the tailgate and the hood, respectively;
- **Group B:** Prefit and SBBR (right and left), that is an initial alignment of the tailgate and the fitting of the brake lights (right and left), respectively;
- **Group C:** Doors (right and left), which is the adjustment of both side doors, front and rear (right and left).

For each type of alignment, different processes are established. After checking the need for fitting on each car, the workers will perform processes of adjustments until the reference condition is achieved. In some workplaces, on top of fitting processes, workers are also responsible for performing other processes, such as screwing/assembling parts. The work cycle is constant within the same fitting processes type but different between the types studied. Note that a work cycle consists of carrying a vehicle fitting process and the worker's transition to the next vehicle.



Figure 4.1: Volkswagen model with shadows above the car parts to be aligned in each fitting process type.

4.1.4 Study Boundaries

The population of the study was purposive, i.e. volunteer participants within the scope of the study. Moreover, and related to the study boundaries, the population comprised Portuguese citizens; thus, the sample is geographically and culturally limited. Concerning public health boundaries, volunteers were healthy, as no disorders were indicated. There were also industry intern policy boundaries, as the requirement of the execution of security and safety protocol (e.g. usage of individual protective gear, fulfilment of surveillance sheets and requisitions), and research department investigation boundaries, as the compliance with the responsibility and confidentiality terms. Ethical/data protection boundaries were also imposed, as each participant's name, birthdate and body measurements were collected. Hence, informed consents were signed in order to respect each participant's privacy and inform them of precisely what is going to be done with their data (Appendix C.3).

4.1.5 Study Stop Criteria

The stop criteria, i.e. the study stage in which enough data has been collected, depended on the scenario of the data collection:

- **Validation:** record at least eight participants;

- **Evaluation:** record at least three operators, with different body profiles (i.e. body measurements), doing the same fitting process; for each operator, record three to six work cycles of the fitting process performed during the work shift.

4.1.6 Participants Recruitment

Participants recruitment was a time-consuming process since participation must be voluntary. Participants were informed of the purpose of the study, about their part in it, and how the collected data will be handled. To boost participation, recruiting can often involve incentives (e.g. snacks and beverages, tokens of appreciation, such as gift vouchers or movie tickets). Particularly, homemade cookies were given to participants in controlled settings (i.e. laboratory) as incentives.

Remark that it was desired that participants, who formed (laboratory and field) population (i.e. a group of people of interest who have been selected due to a particular characteristic, e.g. age, nationality or gender), had different body measurements among each other.

4.1.7 Study Specific Research Questions

Next sections, target materials and methods applied to answer specific research questions of those introduced in section 1.4:

1. Where to place sensors on the human upper body's segments (pelvis, chest, upper arms, forearms and hands) to avoid Soft Tissue Artifact (STA)? Is there a need to align sensors' axes according to specific criteria?
2. How to correct sensors data delay and drift over time?
3. How to accurately compute the upper body motion over time through IK? Which tools and input parameters should be used in order to conduct IK?
4. What are the standards/guidelines used by Volkswagen Portugal ergonomic team to evaluate the biomechanical exposure and consequent ergonomic risk? How can those be automatically calculated using motion sensing in order to extract relevant measures to evaluate the biomechanical exposure and consequent ergonomic risk?
5. For each workstation, is there any risk factor with greater biomechanical exposure than others? If yes, which is it? Is there any workstation of fit shop that can be associated with an overall high ergonomic risk? For each workstation, which is/are the operator(s) body profile(s) that is/are associated with the lowest biomechanical exposure to risk factors and consequent ergonomic risk?
6. How to present quantitative ergonomic risk assessment results?

4.2 Data Collection

The present section addresses topics related to data collection, starting by explaining concepts related to every MoCap routine (4.2.1), followed by the description of the setup used (4.2.2) and protocol designed (4.2.3) for data collection in laboratory and in automotive assembly lines. The design of a motion capture routine, described within the current section, was one of the main contributions of the dissertation to the OPERATOR.

4. MATERIALS AND METHODS

4.2.1 Motion Capture Fundamentals

Calibration is commonly conducted before a MoCap session, and it consists of establishing a relation between the sensor frame and the segment frame representing the underlying bone. In order to establish the relationship between each sensor frame and the corresponding segment, on which it is attached (i.e. segment frame), calibration could be accomplished by three different methods (Zabat et al., 2019):

- **Technical Calibration:** Rigorous positioning of the sensor on the human body segment, basically achieved by aligning the sensor edges about the anatomical segment;
- **Static Calibration:** By asking the subject to maintain a specific static pose. Then, all the segment frames can be generated and aligned altogether;
- **Dynamic Calibration:** By asking the subject to perform a series of specific functional movements during which each segment's axes can be estimated.

Remember that, in IHMT, each IMU should be firmly attached to the body it represents. However, in “real” applications, this is not always possible, which can lead to STAs, i.e. the skin motion relative to the underlying bone. STA is regarded as a major source of error that disrupts the estimation of joint angles when non-invasive measurement systems are used. In other words, the alignment difference between the sensor frame and the segment frame (i.e. sensor misalignment calculated during calibration) is supposed to be constant in time, a classical assumption made, but the sensor misalignment changes during the movement due to STAs.

4.2.2 Setup

During the upper body motion tracking, two inertial MoCaps, described in Appendix C.1, were used together with their recording systems.

First, the MVN Awinda system (Figure C.1) that was developed by XSens was set up and used as a ground truth system, as it has been extensively validated with visual MoCaps (XSens, n.a). In order to record data, during a MoCap session with the XSens' system, there was a need to have a computer installed with the software MVN Analyze. The software was also necessary for further reprocessing of data.

Moreover, the XSens' pack included a segmometer used to take each user body segment's measurements.

Second, the system *in development* by Fraunhofer was deployed in parallel (Figure 4.2) in order to compare the MoCaps outputs. It requires the connection to a server (i.e. smartphone), via Bluetooth, which is used to control the acquisition. There was a need to use two smartphones connected to Fraunhofer's sensors per tracked person. The communication was established via Bluetooth, depending on the devices bandwidth, which resulted in server saturation whenever more than four sensors were connected to a smartphone. In addition, to calibrate the Fraunhofer's sensors, also known as Kallistos, and to record data, the smartphones had to have the Kallisto ToolBox (available in App Store (Sensry, n.a[b])) and the Recorder (internal to Fraunhofer) applications installed, beforehand.

Note that there was a need to use a camera to record the acquisitions to have a visual reference for additional post-acquisition inspection.



Figure 4.2: Inertial Motion Capture systems setup. MVN Awinda and Fraunhofer's systems that consisted of 17 and 7/8 Inertial Measurement Units, respectively. Representation of standing in the N-Pose.

4.2.3 Protocol

Recall that acquisitions were conducted in the laboratory (i.e. controlled settings), at Fraunhofer Portugal Lisbon office, and in the field (i.e. uncontrolled settings), in Volkswagen Autoeuropa automotive assembly lines. However, laboratory data was only used in validation, while field data was handled within validation and evaluation scenarios.

Laboratory protocol can be consulted in Appendix C.2. The protocol sections are the objectives and the local where the data collection was performed, the materials deployed, and the adopted procedure. Notably, the procedure displays the five main sections, which are summarised next.

4.2.3.1 Preparation

The participant's information about the objectives of the conducted study and how his/her data was going to be handled subsequently. The informed consent (in the Appendix C.3) was signed. Next, the participant's name and birthdate were asked and his/her body segments' measurements were taken using the segmometer.

4.2.3.2 Devices Placement

The longest part of the data collection, in which both the MoCaps were attached to the user's body segments, as can be noted in Figure 4.2. The step by step for the MVN Awinda system attachment can be consulted in this page (XSens, 2021). About Fraunhofer's sensors placement, Figure 4.3 shows a schema of their correct placement, in terms of each sensor orientation on the corresponding body segment to which it was attached and of the alignment between the sensors composing the system. Note that, in the laboratory, an extra IMU was used in the lumbar that represented the pelvis segment.

4. MATERIALS AND METHODS

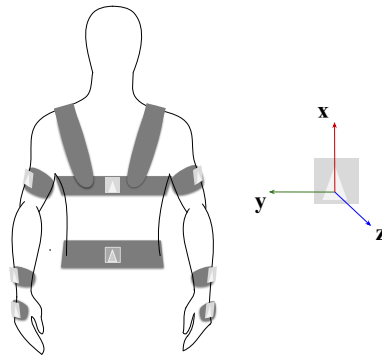


Figure 4.3: Fraunhofer system placement schema, showing each sensor orientation on its corresponding segment. Note that each sensor was placed with the x -axis of the sensor frame along the longitudinal axis of the respective body segment, pointing from distal to proximal extremity. Lumbar IMU was only assembled within the laboratory data collection.

4.2.3.3 Pairing

The connection between the sensors (i.e. MVN Awinda Wireless Motion Trackers (MTw) or Kallistos) and the respective MVN Analyze/Recorder App in order to start a new acquisition. First, the steps to pair of MTw to MVN Analyze software and, next, to start a new recording session are depicted in this page (XSens, 2021). Second, to connect Kallistos (previously charged and then calibrated using Kallisto ToolBox) to a server, the Recorder application was used to register the user and acquisition, name each sensor as the body segment it tracked, and start a new acquisition.

4.2.3.4 Calibration

Calibration methods were different for the two MoCap systems deployed. The MVN Awinda system calibration (for full-body tracking) was dynamic, while the Fraunhofer's system calibration (for only upper body tracking) was static. The MVN Awinda system calibration is also described on **AwindaStarting**. The Fraunhofer's system calibration consisted in standing in the N-Pose for 10 seconds at the beginning of each acquisition. The N-Pose is the body position pictured in Figure 4.2.

4.2.3.5 Acquisition

The acquisition is the process of conducting a new recording session, i.e. tracking the user's body segments motion with both MoCaps in a period.

For the XSens system tracking, after calibration, it is only necessary to start the new recording session in the MVN Analyze software. XSens system provides the acceleration, angular velocity, magnetic field, orientation as quaternions and segments' DoFs angular data.

On the other hand, for Fraunhofer's system tracking, after starting the new acquisition, there is a need to perform the static calibration, a synchronisation sequence and, subsequently, the trial motion itself. Fraunhofer's system provides the acceleration, angular velocity and magnetic field signals' components (x , y , z) relative to the user's body segments motion. An example of sensors' signals from a laboratory trial in which dynamic movements were performed is displayed in Figure C.2.

The static calibration was already described. The synchronisation sequence was designed to be detected in a selected component of a signal of every IMU. It consisted in performing a vertical jump plus the right arm flexion up to 90° , in case of the laboratory acquisitions.

About the motion tracked, this was the differentiating part between laboratory and field routines. In the laboratory, five diverse trials were idealised:

- Two **functional trials**, where upper limbs' and trunk's joints DoFs were mobilised within their respective RoMs;
- Three goal-oriented trials where a specific task was given to the participant, and he/she performed it in his/her way. These were named as **simulation sequences** as they were based on fitting processes and required the usage of additional materials as a few "work" tools.

In automotive assembly lines, the workers' movements were not controlled, as in laboratory settings. Each worker fit method was tracked regarding the fitting processes being conducted. During the acquisition, for every 30 minutes, it was requested that the worker perform the synchronisation sequence.

Furthermore, at the end of each acquisition, the participant was asked to perform the synchronisation sequence in both laboratory and field settings.

4.3 Data Pre-processing

Regarding Fraunhofer's system data pre-processing: correction (4.3.1), resampling (4.3.2), filtering (4.3.3) and synchronisation (4.3.4) between the IMUs sensors' signals, were performed. These are common practice in IHMT.

4.3.1 Correction

Data correction consisted in removing samples with Not-A-Number (NaN) values and sorting the data by timestamps. The root cause of the disordered timestamps is unknown. However, the NaN values, if observed, were at the last sample of the sensor data, which may be related to a incompleted sensor reporting or server updating.

4.3.2 Resampling

Real acquisition systems do not collect experimental data at a constant sampling rate. Sensor signals were resampled at 100Hz to obtain equally sampled signals in time. At this stage, a linear interpolation was deployed.

4.3.3 Filtering

In order to reduce sensors signals' noise, they were filtered. Sensors signals detailed descriptions were provided in section 3.2. With respect to accelerometer and magnetometer signals, a 4th order Butterworth low-pass filter (*Butterworth Filter - an overview — ScienceDirect Topics* n.a), from novainstrumentation Python package (Gamboa, n.a), was implemented with a cutoff frequency of 10Hz, similarly to the authors of Zhou et al., 2007 and of Hassan et al., 2018. As regard to gyroscope signal, a 4th order Savitzky-Golay polynomial filter (Schafer, 2011, He et al., 2019), from Scipy signal (Bell, 2021), was used with a window size of 11 samples. Note that filter type choices were based in the literature, but filters' parameters were selected according to the filter effect in the frequency domain (in Hz) (Figure 4.4) and with regard to the effect in the signals' magnitude power spectrum (Figures C.3-C.4).

In Figure 4.4, it can be observed that, concerning the low pass Butterworth (digital) filter, higher order increases the slope's depth for a selected *cutoff* frequency. About the Savitzky-Golay polynomial filter, whose effect is identical to a smooth filter, higher *polyorder* increases the *cutoff* frequency, and

4. MATERIALS AND METHODS

changes on it have little effect on the slope. Contrarily, higher *window length* decreases the *cutoff* frequency and changes on it have a significant effect on the slope (i.e. higher *window length* increases the slope's depth).

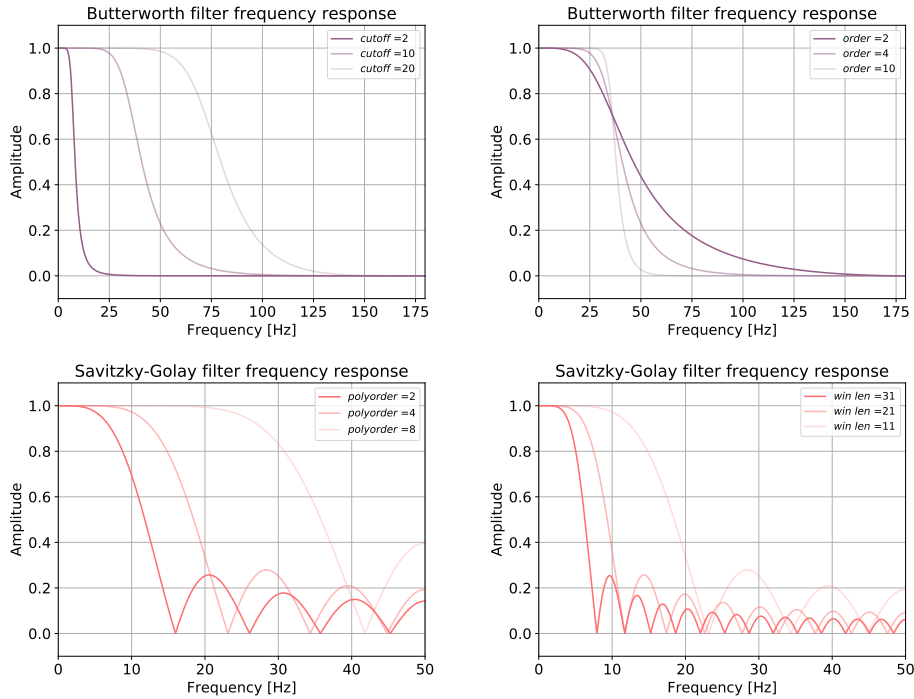


Figure 4.4: Butterworth filter *cutoff* frequency and *order* effect - in purple color - and Savitzky-Golay filter *polyorder* and *window length* effect - in coral color.

Plus, in Figures C.3 and C.4, an example of the power spectrums of sensors' signals magnitude for each segment is shown. The data in the example is from a laboratory trial in which dynamic movements were performed. It can be seen that the selected parameters had the expected effect: cutting off accelerometer and magnetometer data higher frequency components (i.e. the linear acceleration and the non-gravitational magnetic field, respectively), which are not interesting for the orientation estimation, introducing noise into it. Regarding the gyroscope, its signal low frequency component was attenuated to avoid the gyroscope's orientation estimates low frequency bias.

4.3.4 Synchronisation

To synchronisation, data-driven method was developed. Nonetheless, before going through its mathematical description, please note the theory presented in the section 3.2.2. So, in order to synchronise data from IMUs placed in different segments, the synchronisation sequence was designed and performed by the user in data collection. It was designed to be observed in (at least) one component of one signal of each IMU, enabling IMUs' signals coupling, initially and over the acquisition time.

Each structure in the selected signal and axis that represents a synchronisation sequence was named as alignment point A. Clarifying, an alignment point is a representation of a physical event in a sensor data stream that can be accurately distinguished and directly related to the same event in the data stream of another sensor (i.e. coupling) (Bennett, 2017).

The developed method consisted of steps depicted in Table C.1 and illustrated in Figure 4.5. The algorithm was not always entirely applied to synchronise various IMUs data. Thus, in Table 4.1, three different synchronisation approaches, which derived from the whole algorithm, are compared.

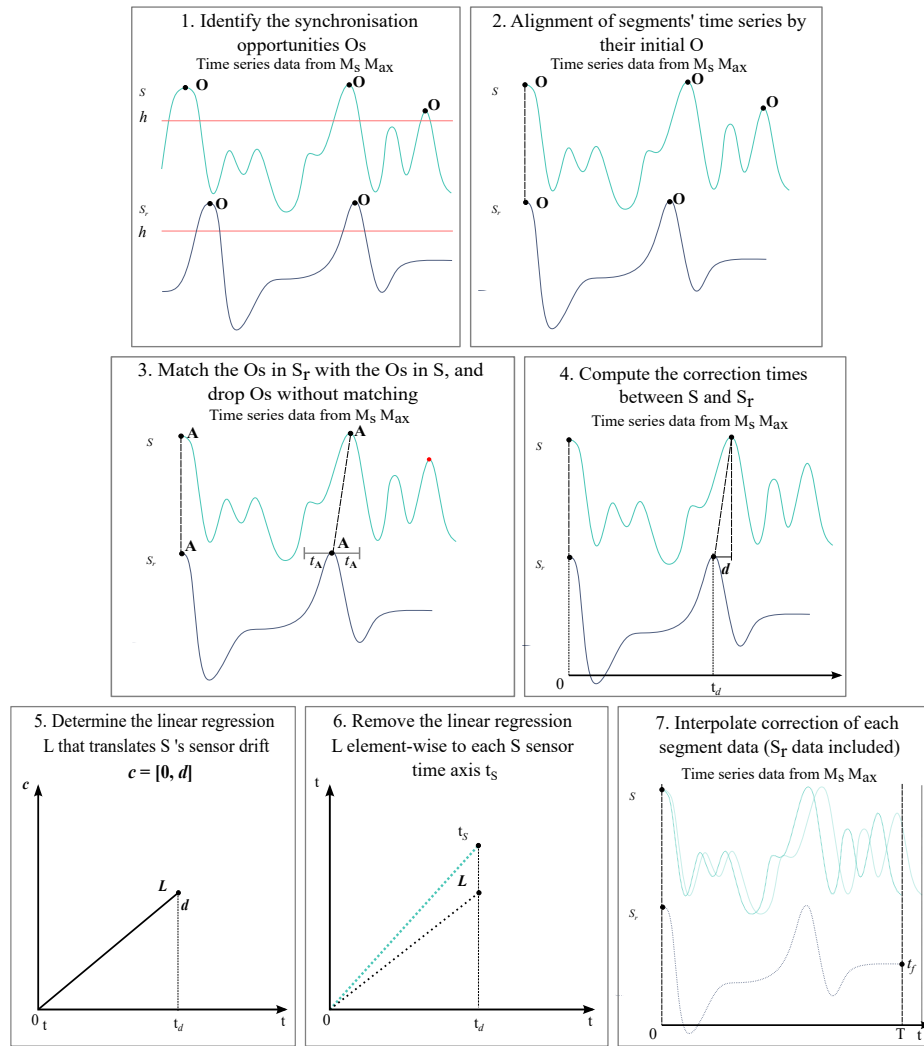


Figure 4.5: **Synchronisation Method Algorithm**. Input parameters are: Master signal (Accelerometer, Gyroscope or Magnetometer), M_s , and axis (x , y or z), M_{ax} ; Peaks height minimal threshold, h , from which a peak is considered a synchronisation opportunity O ; Reference segment, S_r ; Interval maximal threshold, t_A , i.e. the maximal difference in time between an O in the reference segment data stream s_r and an O in another segment data stream s , defining if the O in s is or not an alignment point A ; Sampling frequency, f_s . The algorithm (1-7) steps description is provided in Table C.1.

Table 4.1: **Synchronisation Approaches: Basic, Delay and Drift.**

Approach	Inputs	Steps	Use conditions
Basic	Filtered signals; Sampling frequency, f_s .	7	No synchronisation sequence was performed; Static acquisitions.
Delay	Filtered signals; Master signal (Accelerometer, Gyroscope or Magnetometer), M_s , and axis (x , y or z), M_{ax} ; Peaks height, h ; Sampling frequency, f_s .	1-2, 7	Synchronisation sequence was only performed in the beginning of the acquisition; The acquisition had less than 30 minutes (i.e. little drift effect).
Drift	Filtered signals; Master signal (Accelerometer, Gyroscope or Magnetometer), M_s , and axis (x , y or z), M_{ax} ; Peaks height, h ; Reference segment, S_r ; Interval maximal threshold, t_A ; Sampling frequency, f_s .	1-7	Synchronisation sequence was performed in the beginning of the acquisition and during the acquisition; The acquisition had more than 30 minutes (i.e. significant drift effect).

In Figure C.5, an example of usage of the complete synchronisation method (i.e. the drift approach) is shown, for a long-term acquisition (of 2h) conducted in the office in the course of initial test acquisitions.

4. MATERIALS AND METHODS

4.4 Monitoring Motion

At this stage, data collected by Fraunhofer’s system and further preprocessed were used to estimate each upper body segment orientation over time, as quaternions, followed by the calculus of the angles between body segments. The current section is divided into two sections: data preparation (4.4.1) to angular extraction and angular extraction (4.4.2). The development of a motion monitoring computational framework, described within the current section, was one of the main contributions of the dissertation to the OPERATOR.

4.4.1 Data Preparation

Firstly, inertial data sensor fusion and orientation estimation were undertaken. Thus and so, different algorithms implementations, by Fraunhofer and from Attitude and Heading Reference Systems library (AHRS) (Garcia, n.a[a]), were tested and are enumerated in Table 4.2. DoF column concerns the data used on the estimation, six DoF or nine DoF corresponding to the usage of accelerometer and gyroscope data or accelerometer, gyroscope and magnetometer data, respectively.

Toward SFAs results comparison, execution times and a few angular estimates performance metrics (described in section 4.5.1) were calculated. The comparison results are displayed in Figure 4.6, which concerns about data collected in the laboratory during a dynamic trial.

According to Figure 4.6, the algorithm with the best trade-off among the measurements was the Madgwick filter with nine DoF from the AHRS. So, this filter was used to estimate the upper body segments’ orientation over time, as quaternions.

Secondly, as every SFA has a convergence period related to data integration, the removal of this period was performed in order to obtain reliable motion data estimates.

Table 4.2: SFAs by Fraunhofer and from Attitude and Heading Reference Systems library tested.

Filter	DoF	Source
Madgwick	6	AHRS
Madgwick	9	AHRS
Madgwick	6	Fraunhofer
Madgwick	9	Fraunhofer
Mahony	6	AHRS
Mahony	9	AHRS
Mahony	6	Fraunhofer
Mahony	9	Fraunhofer
Complementary	6	AHRS
Complementary	9	AHRS
Complementary	6	Fraunhofer
Complementary	9	Fraunhofer
Extended Kalman	6	AHRS
Extended Kalman	9	AHRS

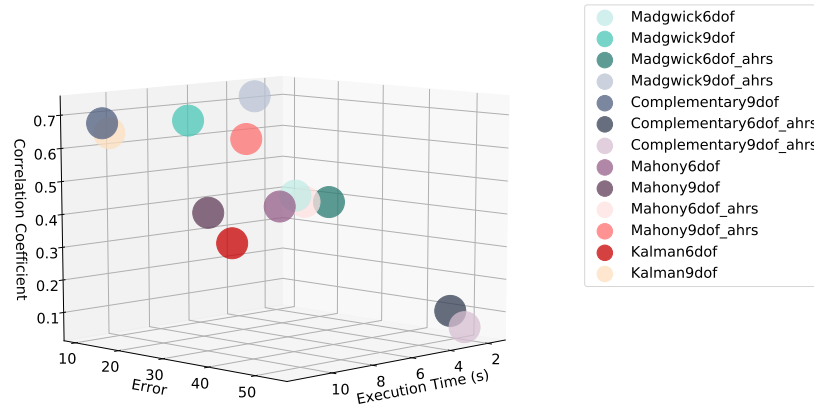


Figure 4.6: Sensor fusion algorithms execution times, angular RMSE and R^2 . SFAs tested were Complementary, Madgwick and Mahony filters by Fraunhofer, and Kalman, Complementary, Madgwick and Mahony filters from AHRS.

4.4.2 Angular Extraction

In respect to the angular extraction, OpenSim software Python’s Application Programming Interface (API) was used to perform IK and in order to estimate angular data from orientation data (i.e. quaternions).

Particularly, the OpenSim API pipeline for IK, regarding IHMT, is named of OpenSense (OpenSense, 2021) and it consists of three main steps, depicted in the next sections.

Before going through OpenSense steps, the OpenSim (kinematic) model utilised to describe the upper body motion is briefly depicted.

Highly complex biomechanical models are being deployed to estimate the upper body motion (3.1.4.3). However, a simpler model was selected for this dissertation’s project, the Rajagopal model. It was developed by the authors of Rajagopal et al., 2016, and it was chosen because the final application did not require very accurate estimates, such as in rehabilitation and sports performance. In addition, more complex models present higher computational complexity, and their joints’ motion description and interpretation may not be trivial.

Concerning the Rajagopal model, in Figure 4.7, it is a full-body model mainly used in gait analysis. Nevertheless, it also provides a neat description of the joints from the human upper body, which is enough for this project.

The tracked DoFs were the lumbar flexion/extension, lateral bending and rotation; the upper arm extension/flexion, abduction/adduction and rotation; the elbow extension/flexion and the forearm supination/pronation; and the wrist extension/flexion and deviation. In Table 4.3, the Rajagopal model DoFs tracked and their respective RoMs are pointed out.

4. MATERIALS AND METHODS

Table 4.3: Upper body joints' DoFs and their respective RoMs. Note that forearm supination/pronation RoM is from 0° - 180° , which is equivalent to -60° - 90° .

DoF	RoM
Lumbar flexion/extension	-90° - 90°
Lumbar lateral bending to left/right	-90° - 90°
Lumbar rotation to right/left	-90° - 90°
Upper arm extension/flexion	-90° - 180°
Upper arm abduction/adduction	-180° - 90°
Upper arm outward/inward rotation	-90° - 90°
Elbow extension/flexion	0° - 160°
Forearm supination/pronation	0° - 180°
Wrist extension/flexion	-90° - 90°
Wrist radial/ulnar deviation	-30° - 40°

The three steps to the angular extraction using OpenSense are detailed next.

4.4.2.1 Convert the Orientation Data File in Storage Format

This step converts orientation files to OpenSim file format (i.e. *sto.*) and associates them with the OpenSim model.

Firstly, the orientation files were converted to APDM wearable sensors (Technologies, n.a) data format to be compatible with OpenSense. Usually, APDM exports an acquisition as a *.h5* file and as a *.csv* ASCII text file, i.e. comma-delimited. The OpenSense APDM Reader can only read the *.csv* file type, which was the type of the file generated. In the *.csv* file data columns labels are associated with OpenSim model segments.

A settings/XML file was constructed, in which each *< experimental sensor >* (i.e. a string identifying the columns in the *.csv* file that correspond to data from the sensor *experimental sensor*) and *< segment in model_imu >* (i.e. a string defining the name of the segment in the OpenSim Model *segment in model*) were specified for each pair of sensor-segment.

Secondly, using the OpenSense APDM Reader and STO File Adapter Quaternion, APDM files were converted to *sto.* files.

Figures C.6, C.7 and C.8 show examples of APDM *.csv* format, settings/XML and the resulting *sto.* files, respectively, about data collected in laboratory during a dynamic trial.

4.4.2.2 Calibrate the Model

The calibration step takes the OpenSim model and the IMU calibration data (i.e. first time point in the orientation data) and finds the initial orientation of the IMU frames on the OpenSim model segments. Note that OpenSense calibration assumes that the pose of the subject in the calibration data matches the default pose of the model, which can be defined beforehand on the OpenSim Graphical User Interface (GUI). In this project, the calibration pose chosen was the N-Pose.

Toward calibration, the OpenSense IMU Placer was implemented in order to add each IMU frame to the respective OpenSim model segment. The input parameters of IMU Placer are:

- OpenSim model filename (*.osim* file, i.e. OpenSim models are described in *.osim* file format);
- Orientation data filename (*.csv* file);

- Sensor to opensim rotations, which is a vector that provides the rotation needed to convert the IMU Earth frame to the OpenSim Earth frame (Y up, Z to the right);
- Base IMU (optional), the label of the IMU frame that represents the segment from which other segments move as a kinematic chain (concept described in section 3.1.4.3);
- Base heading axis (optional), which is the direction (i.e. axis) the base IMU is facing in the initial (calibration) pose. The axis can be 'x', '-x', 'y', '-y', 'z' or '-z';
- Output model filename (.osim file). The output is the calibrated OpenSim model, where each IMU is registered to an OpenSim model segment.

Initial pose in the orientation data, sensor to opensim rotations, base IMU and base heading axis inputs enable to compute the angular offset between the two poses (i.e. initial calibration pose in orientation data and default pose of the model). Then, sensor to opensim rotations input is used to rotate the orientation data, so that the heading of the base IMU is redirected along the x -axis of the OpenSim model Earth frame. If neither base IMU nor base heading axis are provided, then no heading correction is performed.

Figure 4.7 shows an example of the input parameters selection to the initial angular offset calculation and the sensor frames orientation on the OpenSim model segments.

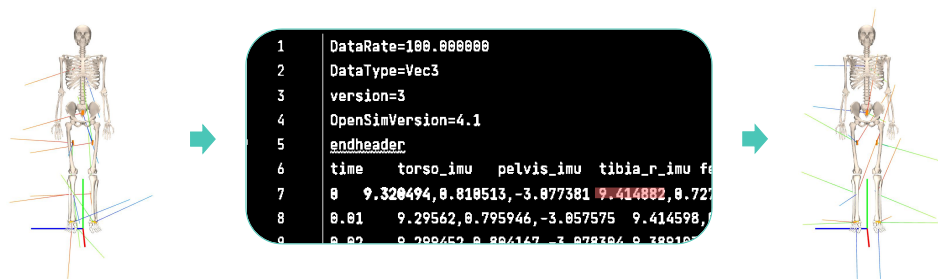


Figure 4.7: An example of the OpenSense input parameters selection. Before (left) and after (right) sensor frames calibration. The selected input parameters to the initial angular offset calculation were: *pelvis* as base IMU with the heading axis z , and sensor to opensim rotations equal to $-\frac{\pi}{2}$ around the OpenSim x -axis, and 0 around the y - and the z -axis. The sensor to opensim rotations were selected by observing sensor orientation data, in which *pelvis* x -axis acceleration is identical to the gravitational acceleration in the initial calibration pose, so the sensors' x -axis should be pointing in the UP direction of the sensors' Earth frame, i.e. the direction of the gravitational force application. As follows, the sensors' frames were rotated by $-\frac{\pi}{2}$ around the OpenSim x -axis, and 0 around the y - and the z -axis, in order to achieve it. The pelvis acceleration x -axis component in the initial calibration pose is highlighted in the sensor orientation data *sto*. file (middle) - in coral color.

The base IMU and its heading axis were differently chosen for the laboratory and the field data, being *pelvis* and $-z$, and *torso* and z , respectively. For both settings, sensor to opensim rotations was $-\frac{\pi}{2}$, π and 0, around the x -, y - and z -axis of the OpenSim Earth frame, respectively.

4.4.2.3 Inverse Kinematics

The IK step finds the pose of the model at each timestamp that minimises, in the least-squares sense, the difference between the orientation data from the IMU sensors and the IMU frames on the calibrated model. The computed kinematics results depended on both calibrated model and sensors' orientation data.

With regard to IK, the OpenSense IMU Inverse Kinematics Tool was deployed, whose input parameters are:

4. MATERIALS AND METHODS

- Orientation data filename;
- OpenSim calibrated model filename, the name/path to the calibrated model file to be used in tracking;
- Sensor to opensim rotations;
- Time range, from t_{start} to t_{end} , to perform the IK tracking (in seconds);
- Results directory, that is the directory wherein the results were printed to files.

For each acquisition, the inverse kinematics results were: the orientation error, as a *.sto* file, and the angular orientation data, as a *.mot* file (i.e. OpenSim motion file format that can be loaded in the OpenSim GUI for visual inspection of the estimated motion).

Note that an orientation error is the orientation difference between the experimental IMU and the corresponding IMU frame in the model, quantified by an angle when representing the orientation difference as rotation about a single axis (i.e. a coordinate rotation).

4.5 Systems Comparison

The angular data obtained through the methods formerly described was compared with the angular data provided by the ground truth system, i.e. the MVN Awinda system plus the MVN Analyze software. The results from this comparison are the validation scenario outputs.

Firstly, the angular data provided by the XSens' system had to be reprocessed and its joints' angular estimates adjusted to the Rajagopal model joints' RoMs. Reprocessing was necessary to obtain estimates with higher quality, but it was a time-consuming task, especially for field data long-term acquisitions. Furthermore, XSens joints' angular estimates adjustments were not trivial, as there is no detailed description of the kinematic model used by XSens. However, it was noted that a few joints presented RoMs opposite to the OpenSim model, being adjusted. In addition, RoMs of the OpenSim model DoFs were also "extended" to match with the XSens DoFs RoMs. The extended ranges are those presented in Table 4.3.

Secondly, systems data synchronisation is required to compare the angular data provided by the systems. It was observed that the resulting angular data streams were morphologically alike, such as the example in Figure 4.8.

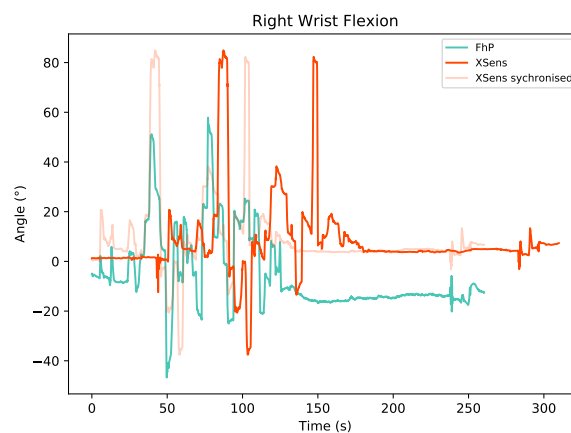


Figure 4.8: An example of the wrist flexion DoF angular data from Fraunhofer's - in turquoise color - and from XSens' - in orange-red color - systems.

Therefore, the maximum values of the straight and the reverse cross-correlation between the data streams from different systems were computed to calculate the lag between the systems data streams. Notice that, for that purpose, only systems angular data streams of a selected DoF (i.e. the reference DoF) were used in the calculation. The reference DoF used in laboratory and field acquisitions was the arm flexion.

The lag of the XSens system data stream with respect to the Fraunhofer's system data stream (i.e. FhP subscribed) was calculated by the following expression:

$$L = \max(|l_{x_{FhP}} - i_{max}|, |l_{x_{FhP}} - i_{max_r}|) \quad (4.1)$$

Where i_{max} and i_{max_r} are the indexes of the straight and reverse cross-correlation function maximum values, respectively, and $l_{x_{FhP}}$ equals to Fraunhofer's system data stream length.

In Figure 4.9 the lag expression terms are clarified with an example.

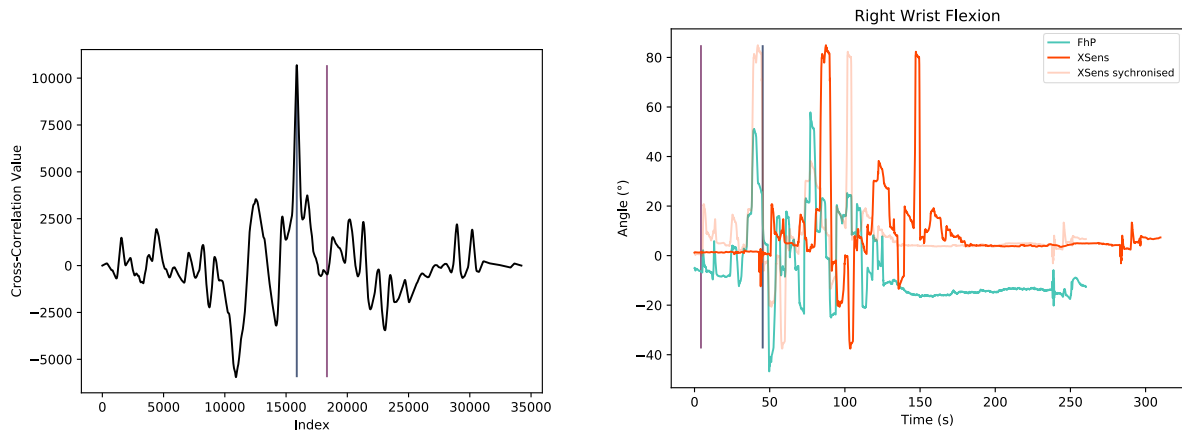


Figure 4.9: An example of the lag expression terms with respect to angular data in Figure 4.8. Cross-correlation values (left) and angular data streams from Fraunhofer's - in turquoise color - and from XSens' - in orange-red color - systems (right). In the cross-correlation plot, i_{max} and i_{max_r} are represented by the vertical lines in blue color and purple color, respectively. In the angular data plot, the points in the time-axis with the indexes of $|l_{x_{FhP}} - i_{max}|$ and $|l_{x_{FhP}} - i_{max_r}|$ are displayed by the vertical lines in blue color and purple color, respectively. Note that the maximum cross-correlation value was observed for i_{max} , so the index corresponding to the lag was $|l_{x_{FhP}} - i_{max}|$.

4.5.1 Performance Metrics

Toward joints' angular estimates comparison, Root Mean Squared Error (RMSE), Determination Coefficient (R^2) and Cumulative Distribution Function (CDF) were computed. These performance metrics have been used to validate alternative inertial motion capture systems, comparing them with a ground truth system (Pedro et al., 2021, Weygers et al., 2020, Santos et al., 2020, Bouvier et al., 2015). A few of these authors calculated Coefficient of Multiple Correlation (CMC), which equals the square root of R^2 .

4.5.1.1 Mean Squared Error and Root Mean Squared Error

The Mean Squared Error (MSE) measures the average of the squares of the errors, and its estimation over n samples is defined as:

$$\text{MSE}(y, \hat{y}) = \frac{1}{n} \sum_{i=0}^{n-1} (y_i - \hat{y}_i)^2 \quad (4.2)$$

4. MATERIALS AND METHODS

Where \hat{y}_i is the predicted value of the i -th sample (i.e. the Fraunhofer's system data stream i -th value), and y_i is the corresponding true value (i.e. the ground truth system's data stream i -th value).

The square root of the MSE is the RMSE, and, while MSE corresponds to the residuals' variance, the RMSE corresponds to the residuals' standard deviation. Greater values of MSE and RMSE suggest worse Fraunhofer's system predictions.

4.5.1.2 Determination Coefficient

The R^2 is a statistical measure that represents the goodness of fit of a regression model. R^2 mathematical expression is:

$$R^2 = 1 - \frac{SS_{res}}{SS_{tot}} \quad (4.3)$$

Where SS_{res} is the residual sum of squares, the summation of squares of perpendicular distance between data points (i.e. Fraunhofer's system data points) and the best-fitted line to the data (i.e. the ground truth system's data); and SS_{tot} is the total sum of squares, the summation of squares of perpendicular distance between the Fraunhofer's system data points and the ground truth system's data average line.

The ideal value for R^2 is 1. The closer the value of R^2 is to 1, the better is the model fitted. Note that the R^2 value can also be negative when the distance to the best-fitted model is greater than the distance to the average fitted model (i.e. $SS_{res} > SS_{tot}$).

4.5.1.3 Cumulative Distribution Function

The CDF, $F_X(x)$, is the probability that X will take a value less than or equal to x , and it can be described as:

$$F_X(x) = P(X \leq x) \quad (4.4)$$

CDF captures the probability distribution of the variable X , e.g. Fraunhofer's system error (i.e. the difference (element-wise) between the angular data calculated using the developed framework and the angular data provided by the ground truth system).

4.6 Ergonomic Assessment

In the present section, ergonomic assessment steps are pointed out and pictured in Figure 4.10. These were adopted taking into account the *case study* of automotive assembly lines, i.e. are based on the protocols used by ergonomists at the time of the study. The computational implementations to ergonomic risk assessment, described within the current section, were ones of the main contributions of the dissertation to the OPERATOR.

4.6.1 Work-Cycle Annotation

Firstly, notice that the work-cycle concept was introduced in section 4.1.3. Work-cycles in each acquisition data were annotated because there was a need to perform the ergonomic assessment, i.e. extraction of the metrics to the ergonomic risk evaluation for each work-cycle in data.

The annotations were performed in the NOVA software version 1.0.7.1 (Baur et al., 2021), and the video recordings were used to annotate the data itself, previously synchronised with the respective video. NOVA's annotation outputs are:

1. An *.annotation* file, which characterises every label assigned to data, such as “<item name=“*label name*” id=“*label id*” color=“*label color*” / >”;
2. A *.txt* file, that shows a list of “*start time; end time; label id; label assignment confidence*” to each label assignment in data.

Note that each work-cycle data comprised angular data, i.e. time series, of every DoF for each segment tracked: lumbar flexion/extension, lateral bending and rotation; upper arm extension/flexion, abduction/adduction and rotation; elbow extension/flexion and forearm supination/pronation; and wrist extension/flexion and deviation. As of right and left upper limbs were tracked, work-cycle data comprehended seventeen time series.

4.6.2 Angular Ranges Quantisation

The angular ranges quantisation consisted of downsampling the angular data, using linear interpolation, from 100Hz to 1Hz and, posteriorly, assigning each data point (i.e. angular value) to an angular range. The data downsampling was conducted as an angular value per second gives us enough detail for the further ergonomic analysis, reducing the computational complexity.

Angular ranges of interest were selected to each DoF based on International Organisation for Standardisation (ISO) guidelines (i.e. ISO norm 11226) and the proforma sheet European Assembly Worksheet (EAWS).

4.6.3 Ergonomic Assessment Implementations

From angular ranged data, implementations of the ISO norm 11226 and proforma sheet EAWS were made in order to assess the biomechanical exposure to risk factors related work and to determine the consequent ergonomic risk, respectively.

Note that if a segment is within an angular range about one of its DoFs, it can be said that it is in the posture defined by that angular range relative to that DoF. A segment's or the body's condition consists of a segment's or the combination of segments' postures, respectively.

The ISO norm 11226 characterises working static postures, in terms of segments' conditions, as “Acceptable” or “Not recommended”. Notice that being “Acceptable” or “Not recommended” can depend on the holding time in the static posture, i.e. the duration that it is maintained. The ISO norm's criteria implementation is outlined in the risk assessment guidelines sheet, in Appendix C.11, for the trunk, upper arm, forearm and hand segments. The output from ISO implementation is the percentage of values in a “Not Recommended” posture/condition for each DoF and work-cycle in data. This percentage reports the biomechanical exposure to risk factors related to work about the posture being assessed. Note that, for extreme postures, the criteria selected was the one described in EAWS, instead of the criteria depicted in the ISO norm 11226. The EAWS considers a wider range of values as extreme postures, increasing the biomechanical exposure to risk factors when compared to ISO norm criteria.

The ergonomic risk score can be computed according to the rating scale proposed in the proforma sheet EAWS (Appendix C.10). In this dissertation, an “adapted” EAWS concerning its table “Basic Positions / Postures and movements of trunk and arms (per shift)” was implemented. In particular, the

4. MATERIALS AND METHODS

implementation focused on the table's section "Standing (and Walking)", which evaluates the percentage of cycle time in which the worker is at specific postural conditions. The implementation is an "adaptation" of the EAWS because there are variables assessed in its sections that cannot be quantified using the setup (section 4.2.2). This implementation is also detailed in the risk assessment guidelines sheet in Appendix C.11. The outputs from EAWS implementation are the percentage of cycle time in each specific condition, depicted in the EAWS' section, and the respective risk score value. Plus, the total risk score was calculated as the sum of the conditions risk score values. Note that, for the conditions of the upper limbs, only the highest sum value, assigned to the right or left limb, was considered in the final total risk score sum.

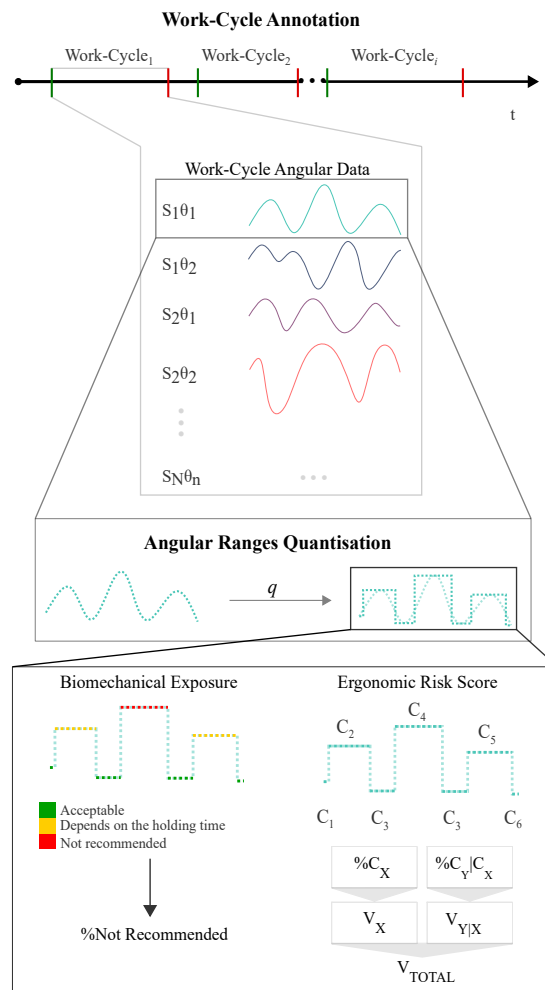


Figure 4.10: **Ergonomic Assessment Steps.** Work-cycles annotations were performed from the 1st to the i^{th} cycle in data from an acquisition. Work-cycle angular data is a set of angular time series, one for each segment's S_N DoF θ_n , where N varies from 1-7 and n from 1-3. Angular ranges quantisation: a function q was implemented for each DoF. The angular ranges were taken as input to the ergonomic assessment. Biomechanical exposure assessment (ISO norm): each segment's condition was characterised over cycle time, as "Acceptable" or "Not Recommended"; Ergonomic risk determination (EAWS): each percentage of cycle time in an EAWS condition, and the respective risk score were computed. C_X or $C_Y|C_X$ and V_X or $V_{Y|X}$, denotes a single or a combined condition percentages and single or a combined risk score values, respectively. Single and combined condition concepts are explained in the risk assessment guidelines sheet in Appendix C.11.

The biomechanical exposure and consequent ergonomic risk score assessment outputs were used to construct an individual ergonomic report, i.e. a report for each worker and fitting process he performed, and compare the work-method of different workers for the same fitting process. These are the evaluation scenario outputs.

An example of an individual ergonomic report is laid out in Appendix C.12. For each report, an appendix was also generated. It displays the percentages of cycles times in each EAWS' condition in order to clarify the risk score values computed. Plus, the risk assessment guidelines sheet, which can be consulted in Appendix C.11, was designed to support the individual ergonomic report analysis.

4.7 Chapter Conclusions

In Figure 4.11, it is shown the relationship of methods and their respective outputs. Accordingly, the modelling framework results are the DoFs' angular data, from Fraunhofer's system data, and IK errors, which enable the assessment of the impact of IK on the angular data estimation. The comparison results are the outputs of the validation scenario and are used to evaluate the trueness and precision of Fraunhofer's DoFs' angular data estimates. The biomechanical exposure and consequent ergonomic risk measurements were used for the evaluation scenario outputs: the individual ergonomic report and group-level analysis.

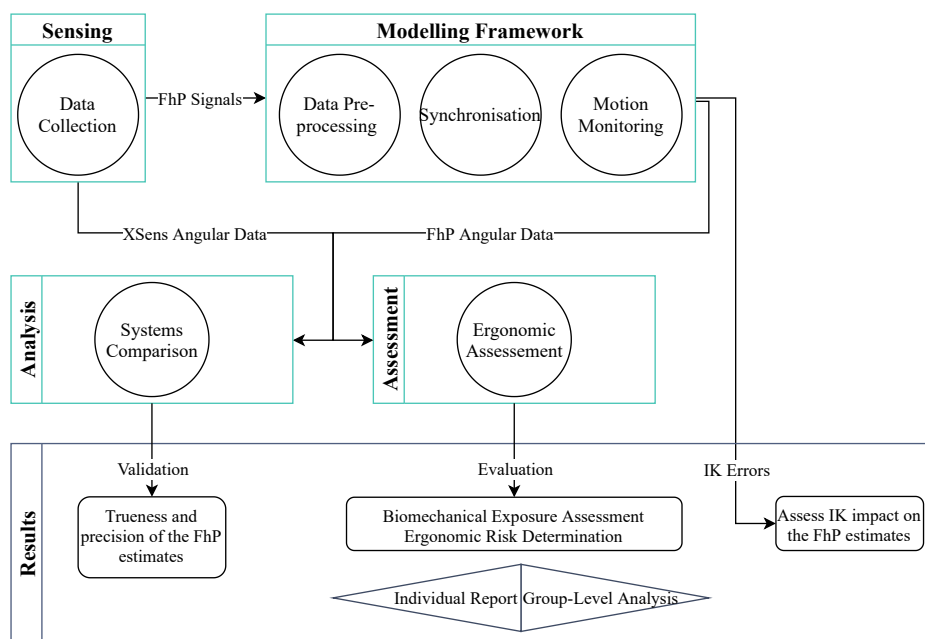


Figure 4.11: Block diagram of the dissertation methods and their respective outputs.

5. Results and Discussion

This section presents the dissertation's results and raises matters of discussion. It starts with system design recommendations (5.1), followed by the characterisation of the study population (5.2). Then, it depicts the results related to motion tracking, the estimation's orientation errors (5.3), i.e. differences between the estimates with and without IK; and the system's validation outputs (5.4), i.e. performance metrics values associated to the angular data estimated using the developed framework when compared to the angular data provided by the ground truth system. After that, the evaluation scenario outputs are presented (5.5).

5.1 Design Recommendations

This section summarises recommendations considered to be crucial to the development of the design, which is being idealised by OPERATOR's team designers, that aim to create with a feasible, reliable and secure solution to the IMU sensors' placement and attachment.

Firstly, it must be remembered that IMU-based joint angles estimation is dependent on the IMU sensors placement and attachment to segments. At the time of this project, the IMUs' placement and attachment were performed by the research team. However, in the future, it should be done by the ergonomist or the operator his/herself. For this reason, the final solution should be a *plug and wear* sensing wearable.

Regarding field acquisitions, motion estimates were affected by sensor falls and increased STAs effects. The more rigidly attached an IMU is to the segment, the more rigorous and less sensitive to STAs are its motion estimates. In order to avoid STAs, the placement on the upper arm segment is considered the hardest. According to Zabat et al., 2019 and Alderman et al., 2018, and based on preliminary tests conducted in the laboratory, the following placement of each IMU to the respective segment was selected:

- Torso IMU: on the flat portion of the sternum;
- Upper Arm IMU: on the central third of the upper arm, laterally (or slightly posterior if judged useful to reduce the occurrence of STA);
- Forearm IMU: dorso-distally on the forearm;
- Hand IMU: dorsally on the hand;
- Pelvis IMU: centrally on the back and at the lumbar region.

The IMUs' placement was reported to the designers that are presently constructing the attaching system.

5. RESULTS AND DISCUSSION

5.2 Population Characterisation

Dataset characteristic values can be consulted in Appendix D.2. Table D.2 displays the summary statistics for each characteristic concerning the laboratory and field populations. The boxplots in Figure 5.1 enable to visualise the body measurements distributions in consideration of both settings and allow to compare them.

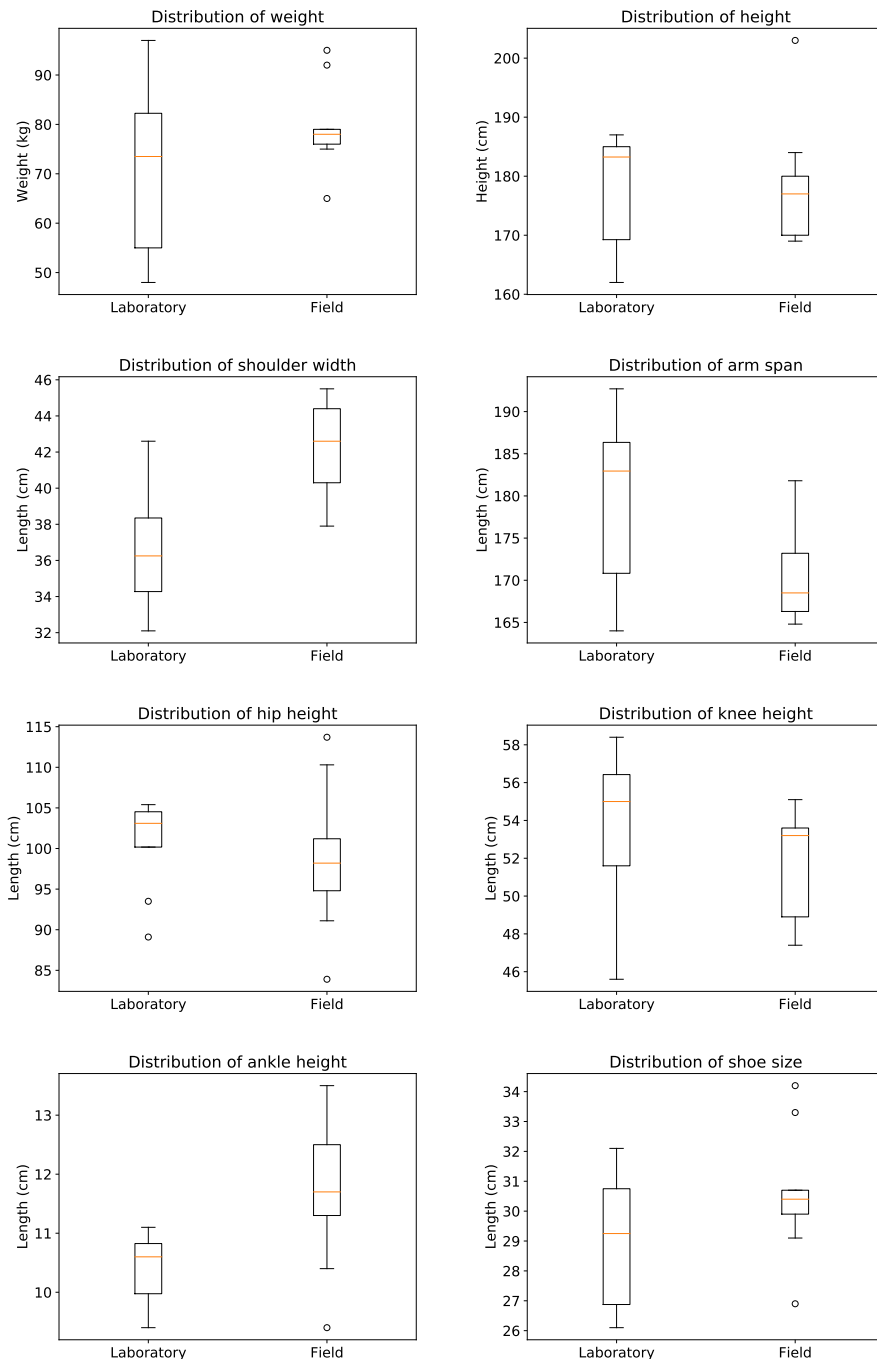


Figure 5.1: Body measurements values distributions, concerning laboratory and field settings. Weight, height, shoulder width, arm span, hip height, knee height, ankle height and shoe size body measurements.

As expected, as participants were not the same in both settings' acquisitions, each body measurement

distribution is different between laboratory and field data. Moreover, the laboratory acquisitions were only performed to validate the motion estimation; thus, people of both genders participated in those acquisitions.

As it can be observed in Figure 5.1, for height, shoulder width, hip height, ankle height and shoe size, the subjects in the laboratory setting has narrower distributions of values than subjects in the field setting. The reason is that subjects in the field setting present greater values for these body measurements than the subjects in the laboratory setting, mainly due to field population outliers. Nonetheless, field data were also considered in orientation errors and validation results. Hence, the body measurements differences observed between settings do not nullify the validation scenario conclusions and, subsequently, the feasibility of the angular estimates to the subsequent ergonomic risk assessment.

Table D.1 presents the values of the body measurements for each operator that conducted one or more fitting processes. For group A, worker 9 is larger than other operators, namely workers 5 and 6. Regarding group B, worker 5 has smaller measures than other operators, workers 4 and 8. Concerning group C, it is clear that worker 1 is taller than the others, workers 2 and 3 have similar body profiles, and worker 7 is the smallest.

5.3 Orientation Errors

In this section the orientation errors results are shown, i.e. the differences between the orientation with and without IK, in terms of coordinate rotations. These results are pictured in Figures 5.2 and 5.3. About Figures inspection, note that: x -axis' limits differs from laboratory (Figure 5.2) to field (Figure 5.3) results visualisations; and each figure's diagonal shows the CDFs with regard to orientation errors for each segment in the figure's horizontal x -axis.

In terms of magnitude, static trials show minimal errors in both settings compared to dynamic trials, but existing, which can be related to an initial misalignment between the calibration pose and the model's default pose.

Remember that, during functional trials acquisitions, a set of movements about joints' DoFs mobilisation were performed, respecting the arms (i.e. shoulders, elbows and wrists joints) - part 1 - and trunk (i.e. spine) - part 2. In Figure 5.2, it can be noticed that the least dynamic trial (i.e. functional part 2) shows lower values of orientation errors than other dynamic trials, i.e. functional part 1 and simulation.

Functional part 1 compromised the mobilisation of the upper limbs' joints, showing higher errors than functional part 2 for trunk and, notably, for upper limbs segments over the acquisitions times, as it can be observed in the CDFs in Figure 5.2. A reason for this can be that, in segments' motion description through a kinematic chain, there can be an "error propagation" from a moving segment to its adjacent segments. In addition, it can be noticed that the kinematic chain's terminal segments (i.e. hands) show the highest errors, which, again, suggest an "error propagation" to subsequent segments in the chain.

Additionally, the results show that the effect on the estimation performed by IK about functional part 1 and simulation trials data was significant. Recall that simulation trials movements were less controlled than functionals, as they were designed based on processes conducted by operators in the automotive assembly lines. Thus, the results encourage the implementation of IK in order to track human motion about industrial processes.

Moreover, the effect of IK in the angular estimates was higher, in terms of magnitude, for field motion tracking than for laboratory. This can be related to data collection problems, e.g. sensor falls and STAs, and orientation estimation issues (described in section 3.3.6). As it can be observed in Figure 5.3 CDFs, the orientation errors over the acquisitions times vary very much among segments, but upper

5. RESULTS AND DISCUSSION

limbs show higher errors than trunk; in general, group B's acquisitions show lower orientation errors than groups A's and C's; and the errors related to the left upper limb's segments were higher than right's. No explanations were found for these observations.

In terms of correlations among IMUs' orientation errors, successive segments (e.g. forearm and hand of the same limb) in the model show a "positive" correlation for the effect of the IK in the segments angular estimates. As expected, these results report that the model describes the upper body segments movements like a kinematic chain.

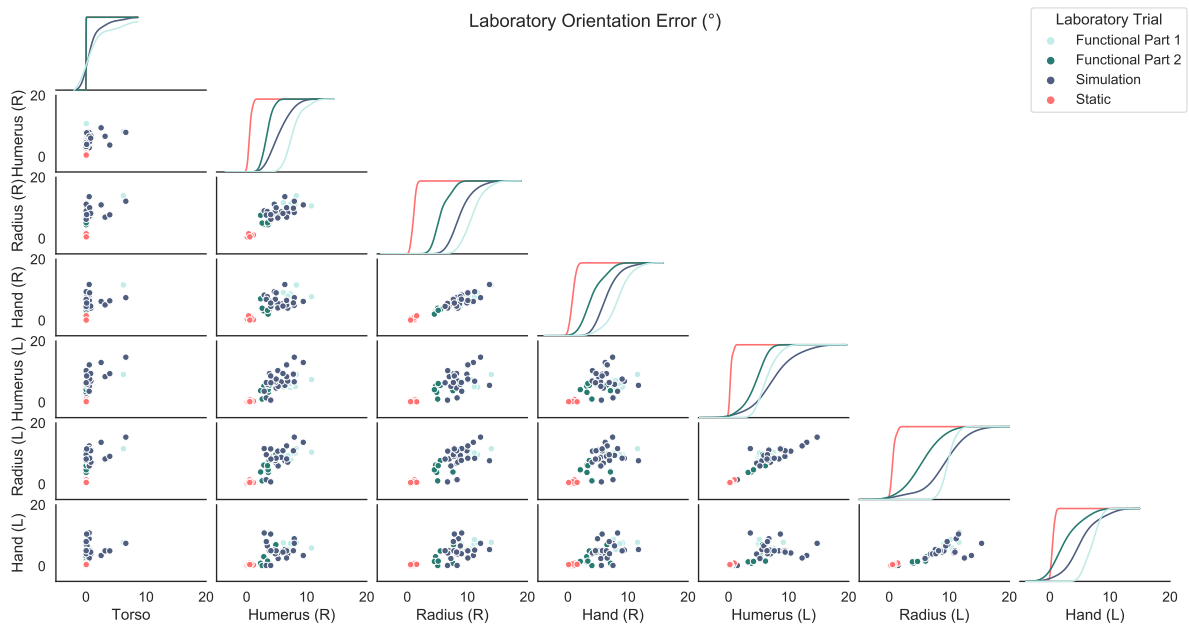


Figure 5.2: Orientation error data from laboratory data collection.

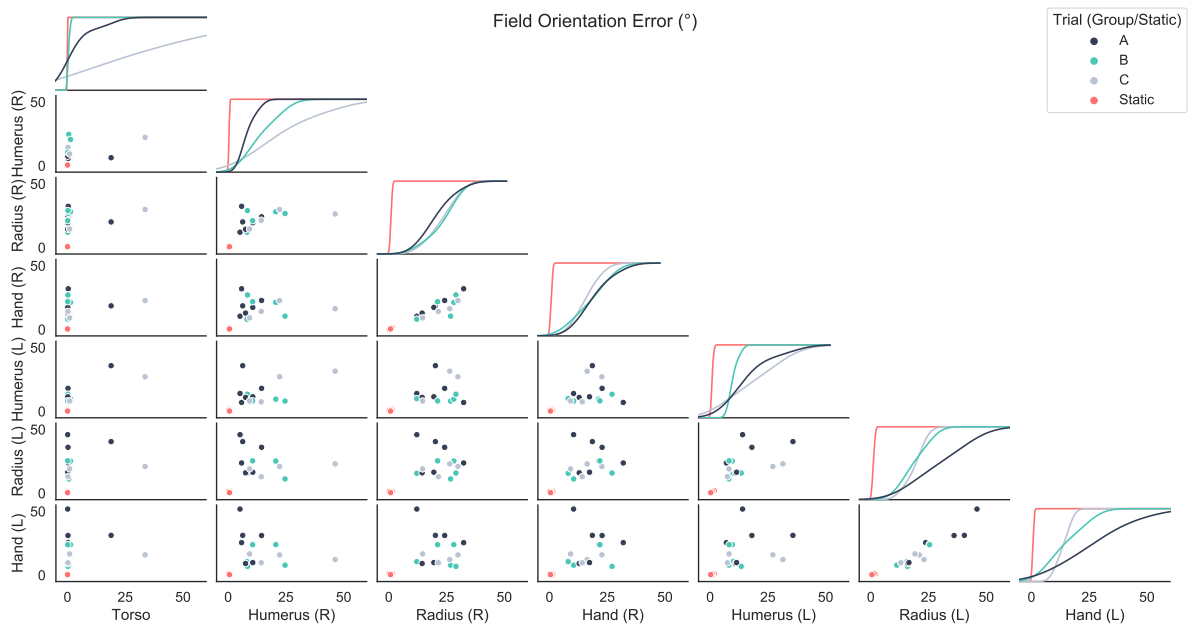


Figure 5.3: Orientation error data from field data collection.

5.4 Validation

Next, performance metrics values for laboratory and field settings acquisitions are presented.

5.4.1 Root Mean Squared Error and Determination Coefficient

In Figures 5.4 and 5.5 are represented the RMSE and R^2 mean values for each DoF tracked, and the respective standard deviations, for laboratory and field acquisitions, respectively. In Figure 5.6, the relationship between RMSE and R^2 values with regard to laboratory and field acquisitions can be noticed and for each participant.

In general, observing mean R^2 values, these fluctuate very much, as well as their standard deviation, especially for field results. No trend was found for these measurements.

Regarding laboratory results, in Figures 5.4 and 5.6, it can be noticed that the RMSE values were mainly located between 0° and 30° . It was also noted that RMSE values for the right forearm supination/pronation DoF were consistently the highest. No explanation was found for the specificity of the right forearm supination/pronation. However, note that forearms supination/pronation monitoring is highly dependent on the sensors' attachment to the forearms in order to avoid STAs.

Functional part 1 data shows higher values of RMSE than other laboratory acquisitions, particularly for both arms extension/flexion, rotation and forearms supination/pronation. This was already expected because, within the functional part 1 trial, the participants performed a highly complex and extreme series of upper limbs postures. With regard to the remaining DoFs, it was observed that RMSE and R^2 values were relatively low and high, respectively.

Functional part 2 data displays the lowest values of RMSE, which could be associated with less dynamic motion tracking, as those trials only compromised the spine's DoFs mobilisation. It was noticed that R^2 values were not very high for most of the DoFs tracked, excluding right arm extension/flexion; no explanation for this fact was found. Notice that lumbar's movements have RMSE values of $\approx 10^\circ$ to 20° , and R^2 values from ≈ 0.5 to 0.75 . As the functional part 2 trial was intended to validate lumbar's movements, which describe spine's DoFs, then it can be considered that those were fairly tracked (i.e. RMSE values of $\approx 10^\circ$ and R^2 values from ≈ 0.5 for lumbar's movements).

Simulation trials display RMSE values mostly below 20° and have a eleven DoFs' R^2 mean values above 0.5. These results are satisfactory, as simulation trials replicated processes carried out in automotive assembly lines, supporting the validation of Fraunhofer's motion tracking system to the *case study* of automotive assembly lines.

Analysing the field results, in Figures 5.5 and 5.6, it can be observed that the RMSE values were mostly located between 20° and 60° and the R^2 values strongly decreased from group C to group A and then group B.

The group B results were the worst, notably concerning R^2 values. The reason can be that the group B's workstations are in different locations of the shop floor, one of them being located in an elevated platform, which can degrade the estimates as no multi-scenario tracking was pursued. Multi-scenario tracking considers each segment position, assuming that the user can be walking on terrain or varying

5. RESULTS AND DISCUSSION

height, e.g. climbing stairs. In this dissertation, segments positions were not computed; instead, the dissertation focused only on segments orientations.

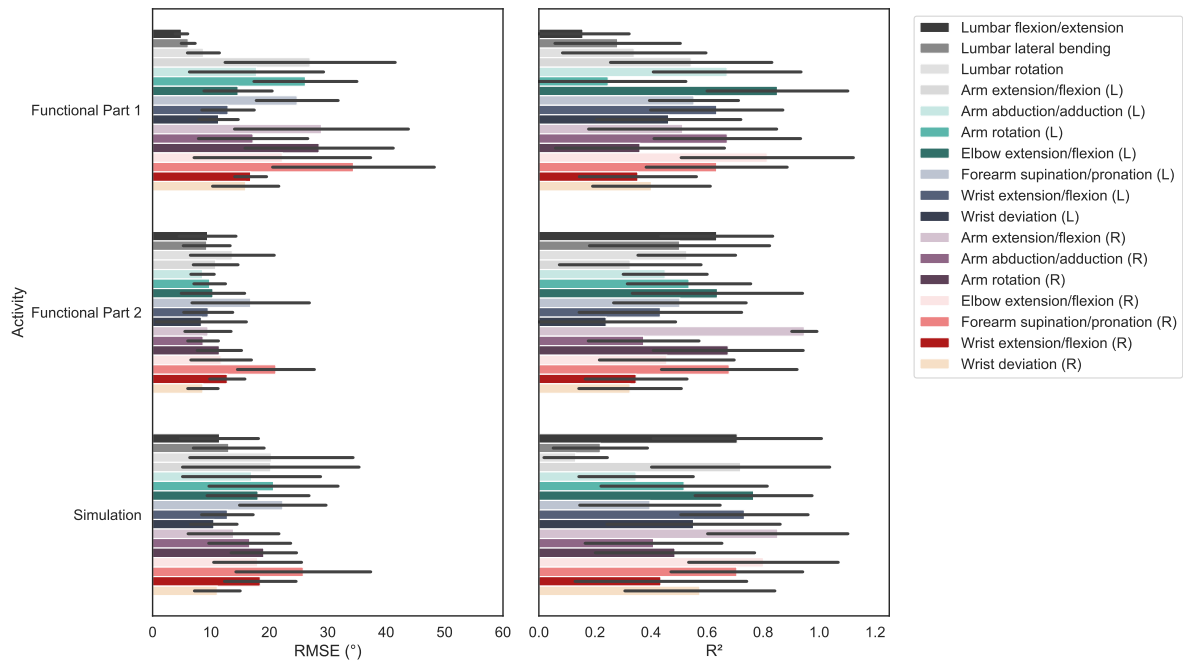


Figure 5.4: RMSE (left) and R^2 (right) mean values and the respective standard deviation, depicted in the horizontal error bar, for each DoF and acquisition trial conducted in laboratory setting.

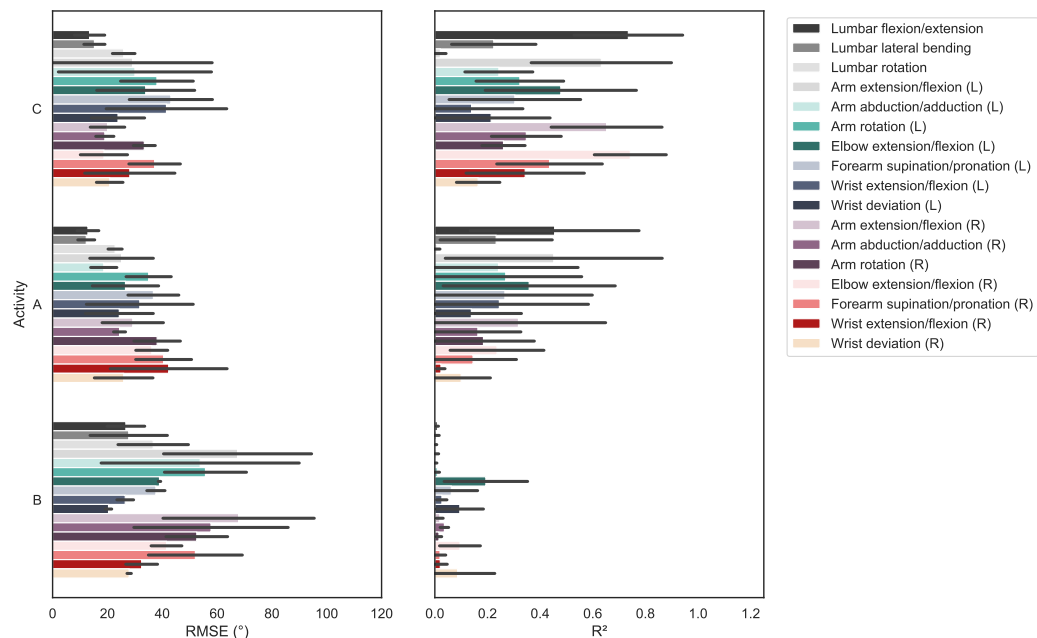


Figure 5.5: RMSE (left) and R^2 (right) mean values and the respective standard deviation, depicted in the horizontal error bar, for each DoF and acquisition set conducted in field setting.

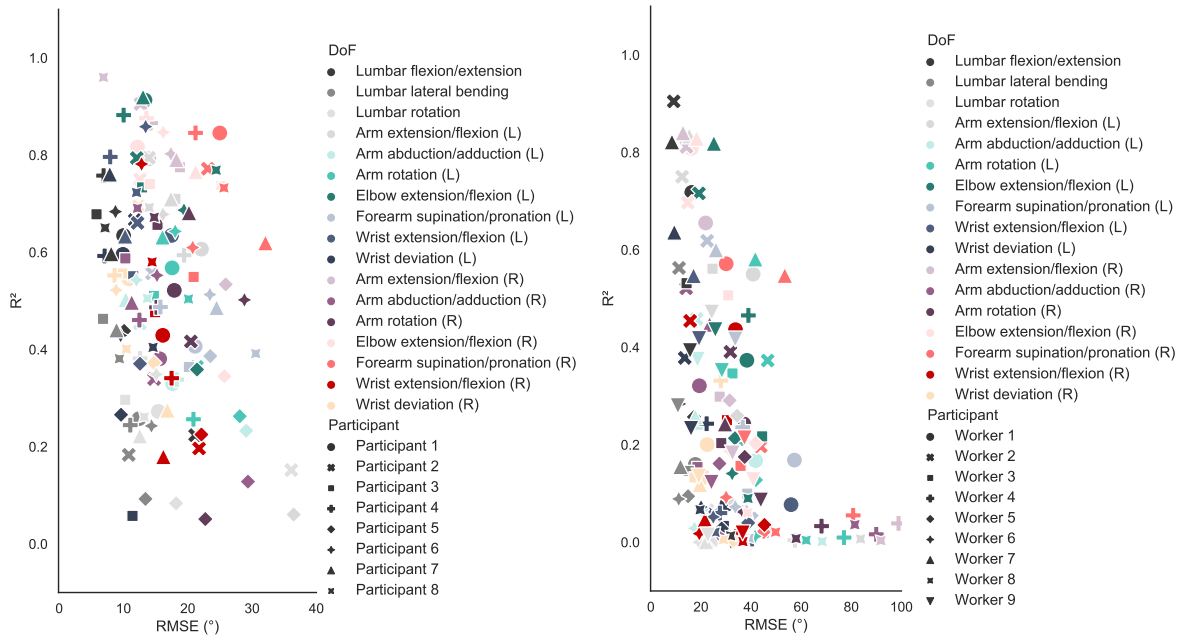


Figure 5.6: Relation plot of RMSE and R^2 values for each DoF and acquisition trial conducted in laboratory (left) and field (right) settings.

In contemplation of participants' results (Figure 5.6), the R^2 values are disperse in magnitude between participants/workers, while the RMSE values are slightly different in magnitude but also vary much among the DoFs tracked. Dissimilarities in results from different participants can be due to differences in their body measurements and, afterwards, the lack of the kinematic model's adjustment to each participant; and marginal differences in IMU sensors' placement on each participant's body segments.

For both settings, the reasons for higher RMSE and lower R^2 values can be: the occurrence of STAs during the acquisition; the model minimal DoFs description; and an existing offset between the real initial participant's pose and the model's default pose. Particularly to field settings, additional reasons are sensors falls and sampling frequency instabilities; and orientation estimation issues (described in section 3.3.6). On the whole, concerning laboratory's and field's RMSE and R^2 values and standard deviations, these were worst to field due to disturbing variables that arise in uncontrolled settings.

5.4.2 Cumulative Distribution Function

Figure 5.7 shows the mean CDFs for each segment's DoFs and set of acquisitions, i.e. in laboratory and field.

Concerning CDFs shape, it can be observed that: for functional trials, CDFs shapes vary significantly from segment to segment, which can be explained by the fact that each functional trial consisted of a set of controlled movements of selected segments; about simulation trials, a more dynamic motion was tracked and the CDFs present identical shapes among segments; respecting field results, each segment's CDF was different for each group.

The differences among field's acquisitions CDFs results verify that the error depends on the fitting process being performed. CDF can be affected by the sequence of movements that completes the tasks conducted within each fitting process. For example, in order to estimate an extreme posture performed

5. RESULTS AND DISCUSSION

during an acquisition, if there is a slight difference between the user's initial pose and the model's default pose, IK can lead to an estimate of the segment orientation that deviates in a greater extent from its actual orientation. The model's segment can reach its extreme posture before it is performed by the user, further compensating on the estimates from other segments.

Regarding CDFs' values, during 80% of the mean between total acquisitions' times, it can be observed that:

- For functional part 1, the error associated with: lumbar is lower than 10° , shoulders and left elbow is lower than $\approx 25^\circ$, right elbow is lower than 40° , left wrist is lower than $\approx 15^\circ$, and right wrist is lower than 20° ;
- For functional part 2, the error is lower than 20° respecting almost every segment, excluding right elbow for which it is slightly higher than 20° ;
- For simulation, the error is lower than $\approx 40^\circ$ concerning every segment, excluding left wrist for that it is lower than $\approx 20^\circ$;
- For group A, the error is lower than $\approx 50^\circ$ to every segment, excluding lumbar for which it is lower than 20° ;
- For group B, the error associated with: lumbar is lower than $\approx 70^\circ$, shoulders are lower than $\approx 120^\circ$, left elbow is lower than $\approx 50^\circ$, as well as right wrist, right elbow is lower than 80° , and left wrist is lower than $\approx 30^\circ$;
- For group C, the error associated with: lumbar is lower than 20° , left shoulder and elbow are lower than 40° , right elbow is lower than $\approx 50^\circ$, wrists are lower than $\approx 30^\circ$, as well as for right shoulder.

Since field acquisitions were much longer than laboratory acquisitions and were conducted within highly magnetic surroundings, it was already expected that the error values over time were higher for acquisitions performed in field settings due to orientation estimation issues.

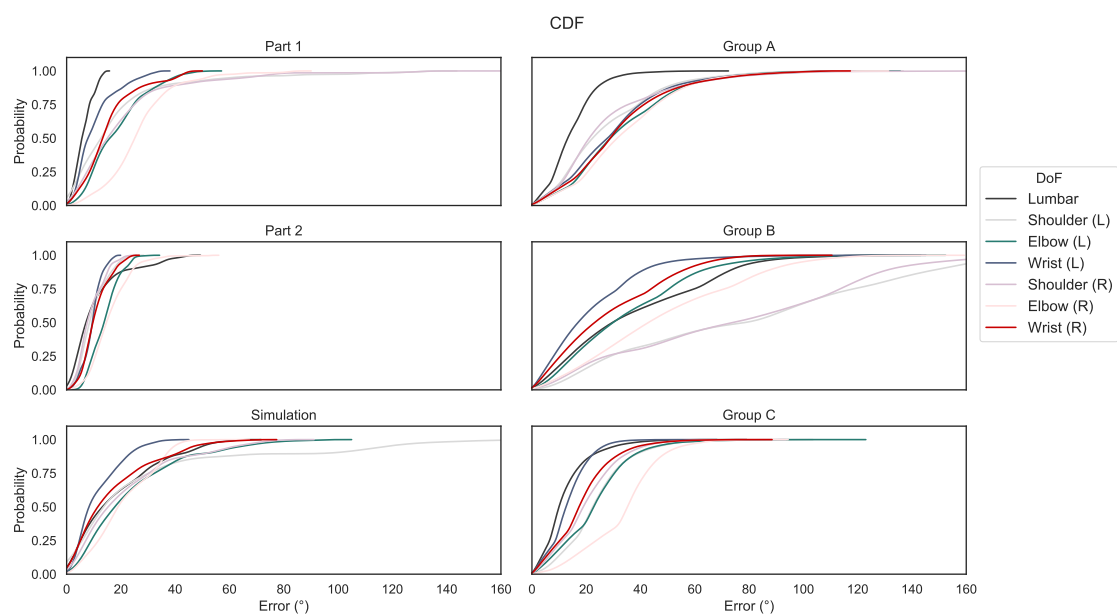


Figure 5.7: Mean error CDFs with respect to laboratory (left) and field acquisitions (right) results for each segment.

5.5 Evaluation

This section provides an ergonomic risk assessment with regard to the *case study* of automotive assembly lines (described in section 4.1). Figure 5.8 shows a diagram of the analysis carried out and the respective research questions this dissertation aimed to answer about ergonomic risk assessment. Note that only Fraunhofer's angular data was used to generate the results presented in this section.

Moreover, the analysis provided is divided into two components:

- **Workstation-Level:** comparison of the ergonomic assessment results between different fitting processes;
- **Operator-Level:** comparison of the ergonomic assessment results between operators who executed the same fitting process for each fitting process.

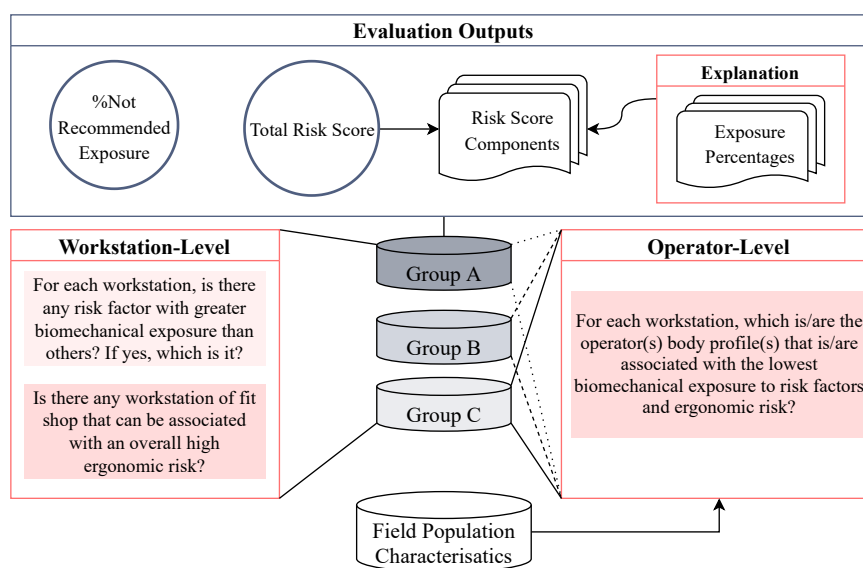


Figure 5.8: Block diagram about the risk assessment results analysis and the respective research questions.

Figure 5.9 presents the total risk score associated with each workstation and operator. The total risk scores were calculated through the implementation of the EAWS rating scale. Observe that group B's workstations present higher total risk scores than groups A's and C's, worker 4 bearing the maximum values.

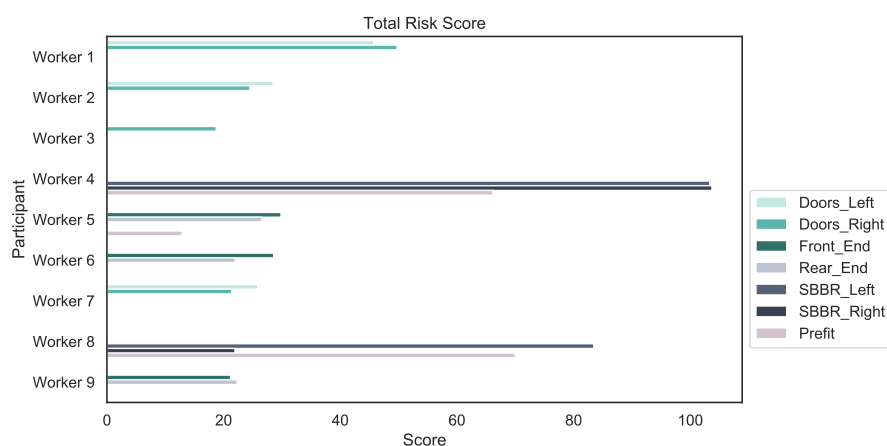


Figure 5.9: Total risk score values for each workstation and operator.

5. RESULTS AND DISCUSSION

Note that the sections 5.5.1 and 5.5.2 use a list of abbreviations depicted in the risk assessment guidelines sheet in Appendix C.11, which describes the considerations taken into account to evaluate the operators' postures/conditions.

5.5.1 Workstation-Level

Firstly, the mean and standard deviation measurements of the ergonomic assessment metrics were computed for each fitting process tracked and posture/condition assessed in the ergonomic implementations performed.

Appendix D.1 shows a summary of the results from a self-reported ergonomic assessment conducted by the Volkswagen Autoeuropa team to characterise the physical effort felt by the fit shop's operators for each body region concerning each fitting process.

Table 5.1 indicates low to high criteria for mean values classification (i.e. low to high biomechanical exposure/ergonomic risk).

Table 5.1: Ergonomic outputs mean values classification criteria. The biomechanical exposure refers to the percentage of the work-cycle time in a not recommended posture and the ergonomic risk is about the score units depicted in the EAWS.

Criteria	Biomechanical Exposure	Ergonomic Risk
Low	≤20%	≤5
Medium	20%-50%	5-10
High	≥50%	≥10

Table 5.2 summarises the mean and the standard deviation of the percentages of mean work-cycle times in not recommended ranges for postures evaluated in the ISO norm 11226, divided by workstation. According to the ISO norm, note that for trunk flexion and upper arms elevation postures, the holding time is accounted to classify if the posture is not recommended or acceptable.

Table 5.2: Mean and standard deviation of the percentages of work-cycle times in not recommended conditions with regard to postures described in the ISO norm 11226 for each workstation. Values in bold present high biomechanical exposure. The list of abbreviations used is in the risk assessment guidelines sheet in Appendix C.11.

Fitting process Condition	Doors Left	Doors Right	Front End	Prefit	Rear End	SBBR Left	SBBR Right
TSymRot	28 ± 8	30 ± 12	21 ± 7	46 ± 10	29 ± 15	82 ± 13	59 ± 48
TSymBend	8 ± 5	9 ± 7	7 ± 6	28 ± 24	3 ± 3	78 ± 29	51 ± 69
TFlex	14 ± 4	29 ± 14	12 ± 9	24 ± 3	21 ± 4	30 ± 10	21 ± 19
left AwkUA	23 ± 11	41 ± 22	22 ± 5	49 ± 19	32 ± 10	91 ± 13	62 ± 54
right AwkUA	31 ± 21	33 ± 11	58 ± 11	55 ± 7	43 ± 16	60 ± 57	77 ± 32
left UAElev	20 ± 3	25 ± 21	20 ± 10	34 ± 30	21 ± 9	85 ± 17	57 ± 59
right UAElev	23 ± 5	20 ± 7	18 ± 3	46 ± 25	17 ± 5	43 ± 61	5 ± 7
left ExtElbFE	23 ± 17	44 ± 15	23 ± 3	33 ± 18	38 ± 16	40 ± 37	16 ± 11
right ExtElbFE	35 ± 5	36 ± 12	29 ± 18	46 ± 27	40 ± 18	19 ± 22	14 ± 15
left ExtElbPS	18 ± 19	17 ± 15	15 ± 2	16 ± 11	13 ± 7	15 ± 3	8 ± 1
right ExtElbPS	26 ± 24	19 ± 13	24 ± 9	29 ± 14	26 ± 30	39 ± 14	33 ± 17
left ExtWr	58 ± 22	65 ± 25	75 ± 12	66 ± 4	63 ± 19	77 ± 2	56 ± 13
right ExtWr	74 ± 13	79 ± 15	66 ± 16	72 ± 11	70 ± 25	61 ± 12	54 ± 3

5.5 Evaluation

Table 5.3 shows the mean and standard deviation of the ergonomic risk score values related to each condition evaluated in the EAWS section "Standing (and Walking)" (i.e. the components of the total risk scores displayed in Figure 5.9), and for each workstation. Note that the ergonomic risk score values were assigned according to the percentage of mean work-cycle times spent in the condition. The ergonomic risk score value depended on the condition's number of occurrences and intensity for some conditions.

Table 5.3: Mean and the standard deviation of the score for the mean work-cycle with regard to conditions described in the EAWS section "Standing (and Walking)" for each workstation. Values in bold present high ergonomic risk. Note that conditions showing null values among workstations were excluded. The list of abbreviations used is in the risk assessment guidelines sheet in Appendix C.11.

Fitting process Condition	Doors Left	Doors Right	Front End	Prefit	Rear End	SBBR Left	SBBR Right
U	1 ± 0	1 ± 0	1 ± 0	1 ± 0	2 ± 2	-	1 ± 0
BF	13 ± 4	11 ± 3	9 ± 2	13 ± 7	3 ± 2	20 ± 9	12 ± 2
BS	3 ± 4	1 ± 1	0 ± 1	5 ± 5	-	5 ± 4	0 ± 1
left AbduOS	-	3 ± 6	-	2 ± 4	-	13 ± 17	16 ± 22
left FlexOS	1 ± 1	4 ± 6	6 ± 3	4 ± 4	9 ± 4	3 ± 4	1 ± 1
right AbduOS	-	-	-	2 ± 3	-	3 ± 4	-
right FlexOS	4 ± 4	2 ± 2	4 ± 2	4 ± 3	3 ± 3	3 ± 5	-
right OH	-	-	1 ± 1	-	-	-	-
TR x U	1 ± 2	-	1 ± 1	2 ± 1	2 ± 1	9 ± 8	7 ± 9
TR x BF	-	1 ± 1	-	2 ± 3	-	9 ± 1	5 ± 6
TR x BS	-	-	-	3 ± 2	-	2 ± 3	-
TR x left FlexOS	-	-	-	-	1 ± 1	0 ± 1	-
TR x right AbduOS	-	-	-	-	-	0 ± 1	-
TR x right FlexOS	-	-	-	-	-	1 ± 1	-
TB x U	-	-	1 ± 1	4 ± 2	-	9 ± 8	7 ± 10
TB x BF	-	0 ± 1	-	3 ± 3	-	9 ± 8	7 ± 10
TB x BS	-	-	-	1 ± 1	-	2 ± 0	0 ± 1
TB x right AbduOS	-	0 ± 1	-	-	-	-	-
left FR x U	1 ± 1	1 ± 0	2 ± 1	2 ± 1	1 ± 1	1 ± 1	1 ± 1
left FR x BF	1 ± 2	-	-	1 ± 1	-	1 ± 0	2 ± 2
left FR x BS	1 ± 2	-	-	2 ± 3	-	2 ± 2	-
right FR x U	2 ± 1	1 ± 1	1 ± 1	2 ± 1	1 ± 1	6 ± 7	3 ± 3
right FR x BF	-	-	3 ± 4	1 ± 1	0 ± 1	4 ± 4	5 ± 7
right FR x BS	-	-	-	1 ± 1	-	1 ± 0	-
right FR x right FlexOS	2 ± 1	1 ± 1	-	-	-	-	-

Respecting group A fitting processes (i.e. front and rear end), it was observed that:

- Front end accommodates high biomechanical exposure to risk factors of right upper arm awkward posture and wrists' extreme postures. It also compromises low valued ergonomic risk score for work over the shoulder with respect to right upper arm flexion and medium valued ergonomic risk score for bent forward and left upper arm flexion over the shoulder.
- Rear end carries high biomechanical exposure to risk factors of wrists extreme postures. It shows an ergonomic risk score higher than for the front end fitting process to left upper arm flexion over

5. RESULTS AND DISCUSSION

the shoulder.

These workstations are associated with an overall medium biomechanical exposure to risk factors related to work. However, the degree of the exposure must be evaluated individually, mainly concerning the rear end fitting process, as standard deviation values are greater for it, supporting the presence of more significant differences among operators. According to Appendix D.1, it was expected that the front end had consistently higher ergonomic risk score values than the rear end, but it not always happened, i.e. it depended on each operator's work-method. Generally, the risk score associated with these workstations is medium/low.

About group B fitting processes (i.e. prefit and SBBR, right and left), it can be noticed that:

- Prefit shows a medium to high biomechanical exposure to risk factors of almost all the conditions assessed by the ISO norm, and the highest values are observed about right upper arm awkward posture and wrists extreme postures. It displays positive risk score values for most of the conditions described in the EAWS section, which makes it a high-risk workstation. The condition with the highest risk score value is bent forward, followed by strongly bent forward.
- SBBR fitting process biomechanical exposure to risk factors highly depends on the SBBR's side, the left side presenting a higher exposure than the right side, especially to the trunk and most of the upper arms conditions. However, SBBR right biomechanical exposure to risk factors is significantly higher than other fitting processes, excluding SBBR left, mainly for trunk symmetries and upper arms awkward postures. As prefit, SBBRs are also high-risk workstations, with SBBR left as the fit shop's riskiest workstation for almost all risk score values. However, SBBR right fitting process is riskier than the left concerning left upper arm abduction over the shoulder.

These workstations are associated with the highest biomechanical exposure and risk score values. As it was expected, i.e. from results in Appendix D.1, prefit is a high-risk workstation, as well as SBBR's, left and right. Nonetheless, it was expected that prefit was the riskiest instead of SBBR left. Nevertheless, the ergonomic assessment results show to be very much dependent on the operator who performed the fitting processes, as standard deviation values are very high among group B's workstations.

Regarding group C fitting processes (i.e. doors, left and right), it can be noted that:

- Doors fitting processes are identical but flipped; thus and so, as expected, these display similar ergonomic assessment results. Regarding biomechanical exposure to risk factors related to work, it is high for both wrists' postures regarding both doors sides. Concerning ergonomic risk score results, the doors left fitting process shows a higher risk score value for bent forward than the doors right fitting process. Plus, while the doors left fitting process shows a higher risk score value for the right arm's flexion over the shoulder than doors right's, the doors right fitting process shows a higher risk score value for the left arm's flexion over the shoulder. This difference was expected, as operators frequently used the arm opposite (to the doors side) to support their body within their work-method.

These workstations are associated with medium biomechanical exposure to risk factors related to work. The similarity between the processes can be the reason for their similar results among conditions. Besides, there are also differences between operators' work-methods to account. Also, these are

associated with medium/low values of ergonomic risk score.

Notice that, for front end and prefit fitting processes, which consisted of bilateral tasks, the biomechanical exposure and consequent ergonomic risk mean values for both body's segments sides are similar. Additionally, at the time of the field's acquisitions, the rear end and SBBRs fitting processes were carried out by two operators in a kind of collaborative work, each having tasks on the right and left side. No distinction between rear end left and right side tasks were made because those were not easily distinguishable.

5.5.2 Operator-Level

Regarding operator-level analysis, heatmaps were constructed in order to inspect the ergonomic assessment results with respect to each operator tracked. Heatmaps are displayed in Figures 5.10 and, 5.11 and 5.12, about ISO and, EAWS implementations' results, respectively.

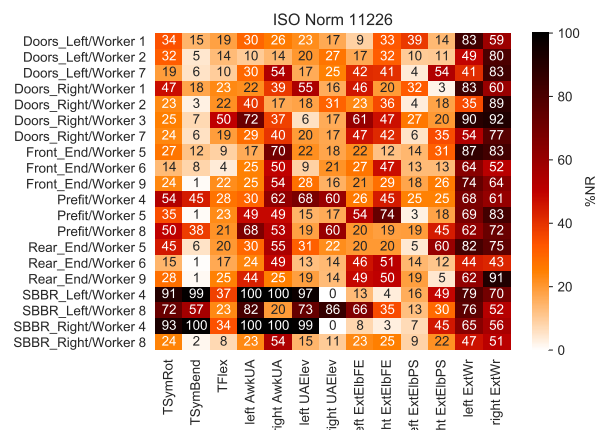


Figure 5.10: Biomechanical exposure outputs with regard to postures described in the ISO norm 11226 for each workstation and operator. Percentage of the mean work-cycle time in a not recommended condition.

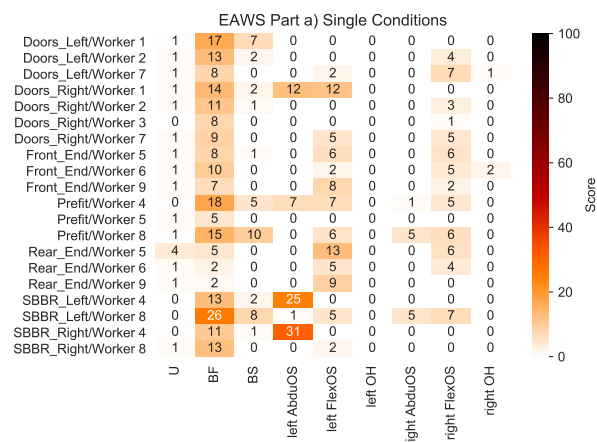


Figure 5.11: Ergonomic risk score outputs with regard to conditions described in the EAWS section "Standing (and Walking)" - Part a (corresponding to single conditions) - for each workstation and operator. Score with respect to each condition.

5. RESULTS AND DISCUSSION

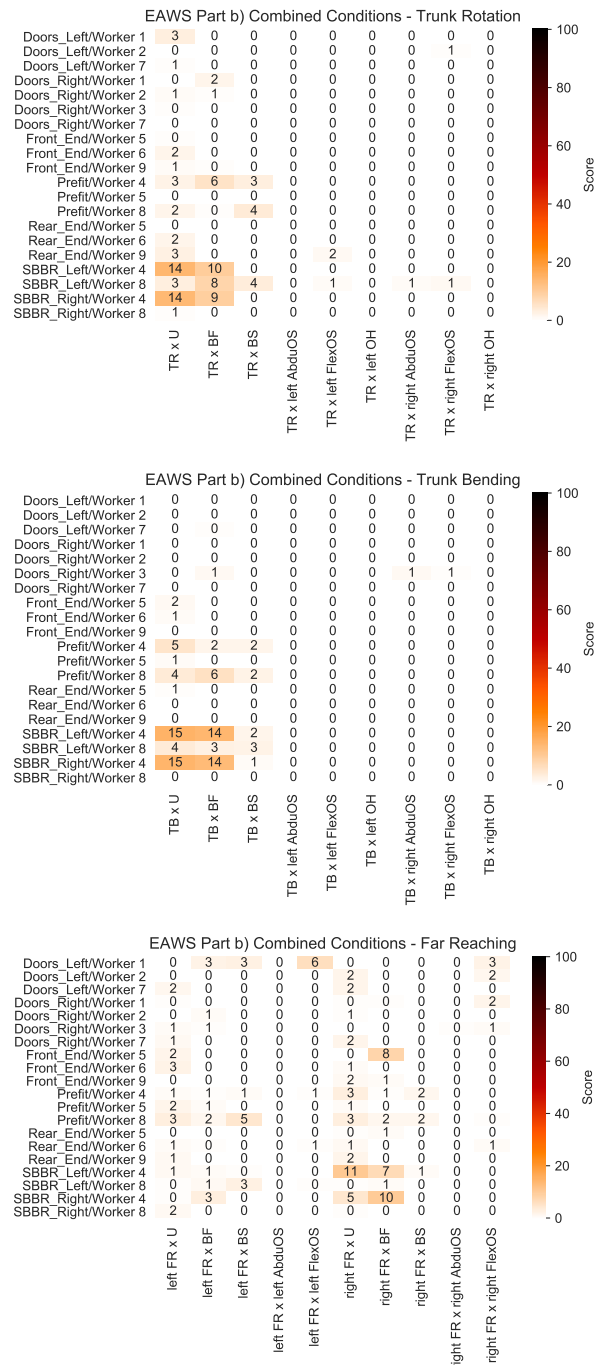


Figure 5.12: Ergonomic risk score outputs with regard to conditions described in the EAWs section "Standing (and Walking)" - Part b (corresponding to combined conditions) - for each workstation and operator. Score with respect to each condition.

Next, a comparison among operators was undertaken for conditions that satisfied the minimum standard deviation threshold of $\geq 20\%$ for biomechanical exposure assessment and ≥ 5 for ergonomic risk determination. Also, consider the distributions from operators' body measurements, in Figure 5.1, and the total risk score values, in Figure 5.9.

Respecting group A fitting processes, note that results do not significantly vary among workers, i.e. standard deviations of percentages $\leq 20\%$ and scores ≤ 5 .

For the front end, about biomechanical exposure to risk factors related to work, right extreme el-

bow flexion/extension and right extreme wrist posture percentages vary to a greater extent than others' postures, workers 6 and 5 bearing the highest values, respectively. About ergonomic risk score results, workers 5 and 6 present higher total risk scores than worker 9. Worker 9 is the highest and has the greatest arm span, followed by worker 6 and worker 5; but note that workers 5 and 6 have similar body profiles and total risk score values (i.e. higher than worker 9's total risk score value). Also, notice that worker 9 is an experienced operator in group A's fitting processes.

For the rear end, about biomechanical exposure to risk factors, right elbow extreme pronation/supination and right wrist extreme posture vary substantially between workers, being the greatest for workers 5 and 9, respectively. These results were not expected as worker 6, the less proficient, showed lower biomechanical exposure to risk factors than others. A reason for this can be that, as the rear end is conducted in collaborative work and worker 6 was learning how to perform the workstation, he did not perform a few tasks, because he was learning how to perform them from his buddy. Worker 5 shows the greatest overall ergonomic risk score value concerning ergonomic risk score results, but these do not vary much among workers.

For prefit, about the biomechanical exposure to risk factors, it can be seen that values considerably vary for: trunk bending symmetry and upper arms elevation postures, which are the highest for worker 4; and right elbow extreme flexion/extension that is the highest for worker 5. Regarding ergonomic risk score results, worker 5 presents a total risk score value smaller than others, which can be due to the worker's expertise in group B's fitting processes. Worker 4 displays the highest risk score for bent forward, while worker 8 displays the greatest risk score value for strongly bent forward. Nonetheless, considering both trunk and arm's conditions, worker 4 work-method reports the highest total risk score among the operators.

SBBR left and right workstation results exhibit more significant differences between workers than other workstations'. Worker 4 supports the highest values of biomechanical exposure to risk factors respecting trunk, awkward upper arms' postures and left upper arm elevation. Notice that worker 4's height and arm span is greater than worker 8. Concerning ergonomic risk score results, these highly depend on the condition analysed. SBBR left shows a larger degree of positive risk score values for worker 8 among conditions when compared to worker 4's. However, both workers present a high total risk score associated with the SBBR left fitting process. Otherwise, worker 4 distinctly shows the highest total risk score related to SBBR right fitting process, mainly due to the high risk score values about the single condition of left arm abduction over the shoulder and the combined conditions of trunk rotation and bending asymmetries.

As it was noted before, fitting processes of left and right doors are identical. Furthermore, regarding biomechanical exposure to risk factors, the most significant gaps between operators are:

For doors left, with regard to right upper arm awkward posture, right extreme elbow pronation/supination and left wrist extreme posture, having the highest percentage in a not recommended postures for workers 7, 7 and 1, respectively;

For doors right, about left upper arm awkward posture and elevation, and left wrist extreme posture, bearing the highest percentage in a not recommended postures for workers 3 and 1, and 3, respectively.

Concerning ergonomic risk score results, worker 1 presents the highest values for doors fitting processes. Nevertheless, worker 2 displays high risk scores for bent forward, and worker 7 shows medium risk scores for upper arms flexion over the shoulder.

5. RESULTS AND DISCUSSION

According to the criteria presented in Table 5.1, Figure 5.13 shows a summary of the operator-level results. In Figure 5.13, note that: regarding biomechanical exposure, the mean between the percentages in not recommended conditions was calculated for each segment's postures; concerning ergonomic risk, for trunk and full arms, right and left, the sum of risk score values was calculated.

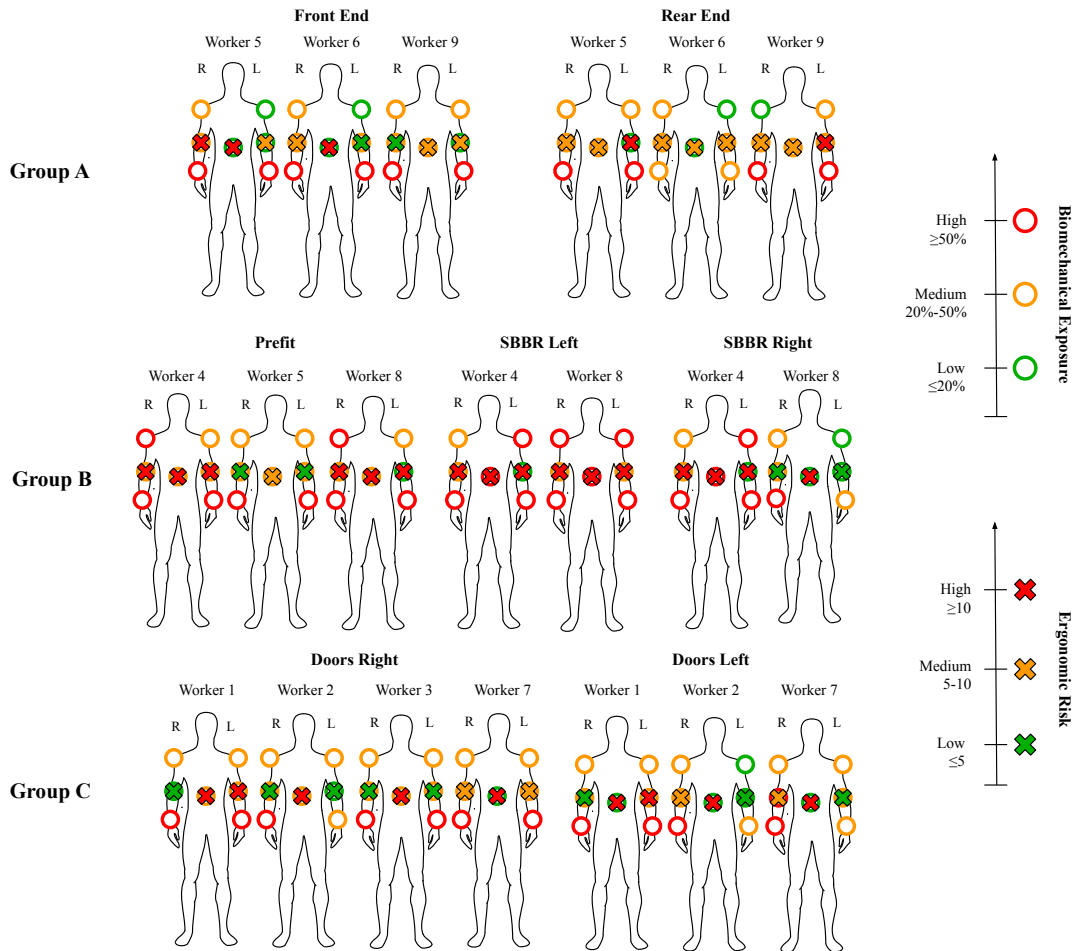


Figure 5.13: Operator-level biomechanical exposure and ergonomic risk results.

Note that, when observing Figure 5.13, there is not always a linear and positive relationship between the biomechanical exposure and the ergonomic risk results. Nevertheless, possibly the criteria used to judge the ergonomic risk value was too harsh. Another reason for the mismatch can be that: biomechanical exposure assessment results presented take into account the holding time in the assessed posture, while the ergonomic risk score calculation only considers the number of times the operator reaches the condition; in other words, the first assess the duration in the posture, while the latter evaluates the condition's number of occurrences. In addition, according to the ISO norm 11226, the percentage of values in a not recommended condition of trunk flexion considers trunk flexion below 0° (i.e. trunk extension), while EAWS does not consider it.

5.6 Study Limitations

Several study limitations should be considered, as it follows:

- **Hardware and design issues:** both Fraunhofer's hardware and case design are *in development*. Thus, there were some technical issues, reported in sections C.1 and 5.1, that affected the accuracy of the methods developed during this dissertation, as the results highly depend on the integrity of the collected data.
- **Low complexity kinematic model:** as a low complexity kinematic model was deployed, it may have failed on upper body segments' motion estimation, particularly concerning extreme segments' postures. In the future, the usage of a more complex upper body model that uses ISB standards to describe the upper body's joints' motion can be a valuable approach to obtain better motion estimates, whose accuracy is captured through validation.
- **Small sample size in the field setting:** sample size is too small to generalise the results to the fit shop's population. Remark that only two to four operators with different body profiles were tracked by workstation, while the real population size is ≈ 100 workers. Plus, a sample size closer to the population's would enable a significant statistical analyses about variables correlation and/or cause-effect.
- **Reduced and naive body measures collection:** the upper body motion was tracked; thus, the collection of more measures of the upper body segments is relevant to the definition of the most suitable body profile for each process, specifically, the collection of the trunk and upper limbs anthropometric measurements.

5. RESULTS AND DISCUSSION

5.7 Chapter Conclusions

In the course of this dissertation, design recommendations were provided to the designers' team for the IMU sensors placement/attachment.

With respect to population characterisation, it was noted that participants from laboratory data collection present narrower distributions of body measurements than participants from field data collection, mainly due to disruptive body profiles. Moreover, it was observed that, for each workstation, there are not more than two operators with distinct body profiles, which limited the ergonomic assessment operator-level analysis.

Concerning orientation errors results, for every IMU, static trials compromise lower errors values than dynamic trials; the highest errors values were observed to upper limbs DoFs; field's data errors were higher than laboratory's. Additionally, the kinematic model, used to the IK is describing joints' movements as a kinematic chain since relations between segments errors were exposed.

Toward validation outputs analysis, and inspired by the authors of Bouvier et al., 2015, the concepts of trueness - "close to a reference system", i.e. RMSE and R^2 values closeness to 0° and 1, respectively - and precision - i.e. similarities of RMSE and R^2 values among different participants' acquisitions - can be used. RMSE and R^2 values show that, generally, RMSE and R^2 values trueness and precision are fair for laboratory's results, while field's show lower trueness and precision. As expected, over the acquisitions times, the errors also increased in a greater extent for field than for laboratory results.

Regarding evaluation results and group-level analysis, the biomechanical exposure to risk factors related to work of extreme wrists' postures is the highest; prefit and SBBR left workstations present a higher overall ergonomic risk than other workstations. Regarding operator-level analysis, as the sample size is too small to generalisations, it can be only pointed out the worker with presenting the work-method, at the time of the acquisition, that represents the lowest biomechanical exposure to risk factors and consequent ergonomic risk for each workstation: for front end, worker 5/6; for the rear end, worker 6; for prefit, worker 5; for SBBR, left and right, worker 8; for doors right, worker 3; and for doors left, worker 2. Plus, please note that an example of an individual ergonomic report is provided in Appendix C.12.

6. Conclusions and Future Work

This chapter summarises the developed work and the obtained results throughout this dissertation. Guidelines for future research are also proposed.

6.1 Conclusions

Nowadays, in industrial contexts, ergonomic risk assessment is conducted using self-reported or observational methods. Notwithstanding, there has been an exponential growth of wearable technologies used to directly measure the biomechanical exposure to risk factors and the related ergonomic risk; currently available solutions have several weaknesses, as those do not offer a good trade-off between system's explainability, scalability and invasiveness. Often, whereas a system requires many elements, its explainability is fair, though its scalability and invasiveness are not.

Therefore, to provide a preferable solution, under the sphere of the ongoing R&D project, entitled OPERATOR, this dissertation answer the research question of “how to quantify the ergonomic risk and biomechanical exposure in automotive assembly lines?” throughout the application and development of computational tools *in tandem with* inertial MoCap technology.

Firstly, as the study focused on upper body motion tracking, the sensors should be rigidly attached to the user's upper body segments to prevent them from falling. IMUs best placement location is usually the flattest and most regular segment's surface portion, minimising the STAs.

Secondly, the data-driven synchronisation technique designed cannot be extended to data already collected because it demands the execution of a pre-defined synchronisation sequence, which should be “equally” identified in data streams from different sensors. However, using common patterns/events displayed in data streams coming out of different sensors can be the answer to a post-hoc and data-driven synchronisation solution. Regarding the data collected, the synchronisation sequences were remarkably detected and used to synchronise sensors' data streams with respect to short- and long-term acquisitions. Depending on the acquisition duration, the synchronisation sequence should be performed at least one to three times.

Thirdly, the usage of a biomechanical model, in order to apply real motion constraints to the orientation data, calculated from IMUs signals, corrects orientation errors through IK; it enables monitoring the user's upper body segments motion as a chain, connecting adjacent segments' motion and computing their relative movements with respect to each other. These relative movements are translated into angular data of DoFs from the upper body segments' joints. In fact, IK affected the orientation estimates and, mainly, about the field's data collection, whose orientation errors were greater

6. CONCLUSIONS AND FUTURE WORK

than laboratory's. Additionally, Fraunhofer's system validation results show that it fairly tracked its user's upper body segments' motion, especially in controlled settings.

The following topics are related to the *case study* of automotive assembly lines about fit shop's workstations ergonomic analysis and assessment.

Fourthly, implementations of the ISO norm 11226 and the EAWS proforma sheet were done, in order to provide biomechanical exposure and consequent ergonomic risk assessment by workstation and operator, in terms of the percentages of work-cycle time spent in a not recommended posture for each upper body segment, defined in the ISO norm; and the ergonomic risk scores, associated with each condition evaluated in the EAWS. Biomechanical exposure and consequent ergonomic risk assessments' results were computed for each work-cycle in data. Also, mean and standard deviation values were calculated among operators' acquisitions for each fitting process.

Fifthly, evaluation results were exploited in a group-level analysis, divided into workstation-level and operator-level, and it was found out that: generally, among workstations and operators, the biomechanical exposure to risk factors related to work of extreme wrists postures was the highest; the workstations associated with greater biomechanical exposure and ergonomic risk are from group B, particularly, prefit and SBBR left; and, for each workstation, different operators (i.e. with different body profiles) are associated with different ergonomic assessment outputs; thus and so, at the time of the acquisitions, specific work-methods lead to lower biomechanical exposure and consequent ergonomic risk than others, but no further generalisations can be made.

Lastly, for each workstation and operator, an individual ergonomic report was automatically generated, wherein biomechanical exposure and consequent ergonomic risk assessment results are provided for each work-cycle. It enables ergonomists to focus their analysis on each operator work-method and assess its variability over the monitored work-cycles.

6.2 Future Work

This dissertation leaves some unsolved problems and opens new research questions to which it will be devoting additional research effort in the future. Topics to explore are pointed out in Figure 6.1, and their descriptions are detailed next.

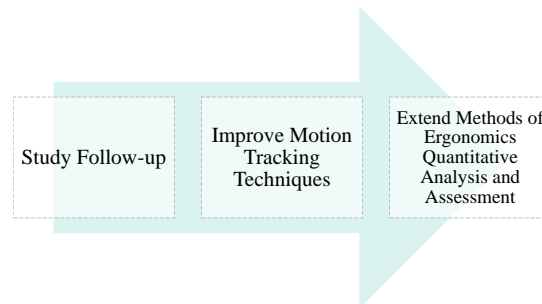


Figure 6.1: The main research topics for future work.

Improvements in motion tracking techniques Throughout the (1) comparison of the angular estimates using the simplest and a complex biomechanical model to describe joints' motion, the (2) comparison of angular estimates using a reduced number of inertial sensors, the (3) tracking of position, and the (4) usage of a visual MoCap to provide an extra validation of the angular estimates.

Extension of the ergonomic quantitative analysis and assessment The analysis can consist of (1) characterising the ergonomic risk as a multi-dimensional approach, through the design of concrete measures to assess duration, repetition and intensity, using multi-time series data (acceleration, angular velocity, magnetic field, orientation), (2) coming up with an elegant solution to visualise the ergonomic risk assessment outputs over a work-cycle to target the periods that contribute the most to high ergonomic risk values, (3) conducting machine learning techniques to multiclass classification task of simplest movements (e.g. picking, placing) performed in industrial contexts which increased occurrences can be related to a greater ergonomic risk value. Additionally, other mining time series tasks can be carried out, namely: event detection and pattern recognition, which can hold advanced synchronisation techniques to detect synchronisation opportunities; methods to characterise industrial movements that can be related to greater ergonomic risk, such as *hard fits* (i.e. tasks carried out in fitting processes which experts classify as the most harmful).

Study follow-up Compromise the (1) data collection for a larger sample size in order to provide representative relationships among body measures, other variables and the ergonomic risk assessment outputs, and the (2) crossing of quantitative and qualitative data collected within a longitudinal study, and medical department's back data.

Bibliography

- ABfal, Johannes et al. (2009). “Probabilistic similarity search for uncertain time series”. In: *Lect. Notes Comput. Sci. (including Subser. Lect. Notes Artif. Intell. Lect. Notes Bioinformatics)* 5566 LNCS, pp. 435–443. ISSN: 03029743. DOI: 10.1007/978-3-642-02279-1_31.
- Acuna, Miguel and Andrew R. Karduna (2012). “Wrist activity monitor counts are correlated with dynamic but not static assessments of arm elevation exposure made with a triaxial accelerometer”. In: *Ergonomics* 55.8, pp. 963–970. ISSN: 00140139. DOI: 10.1080/00140139.2012.676672.
- Alaee, Sara, Kaveh Kamgar, and Eamonn Keogh (2020). “Matrix Profile XXII: Exact Discovery of Time Series Motifs under DTW”. In: arXiv: 2009.07907.
- Alderman, Elizabeth, Kevin Brenner, and Caitlin Hogan (2018). *Development of Upper-Extremity IMU to OpenSim Data Conversion Method - OpenSim Documentation - Global Site*. URL: <https://simtk-confluence.stanford.edu/display/OpenSim/Development+of+Upper-Extremity+IMU+to+OpenSim+Data+Conversion+Method> (visited on 09/14/2021).
- Álvarez, Diego et al. (2016). “Upper limb joint angle measurement in occupational health”. In: *Comput. Methods Biomech. Biomed. Engin.* 19.2, pp. 159–170. ISSN: 14768259. DOI: 10.1080/10255842.2014.997718.
- Anderson, Jennifer et al. (2019). “Exploring occupational standing activities using accelerometer-based activity monitoring”. In: *Ergonomics* 62.8, pp. 1055–1065. ISSN: 13665847. DOI: 10.1080/00140139.2019.1615640.
- Arus, Emeric (2018). *The Fundamentals of Biomechanics*, pp. 109–177. ISBN: 9780387493114. DOI: 10.1201/b22446-8.
- AXS (n.a). *AXS - Home*. DOI: <https://axsco.com/>. URL: <https://axsco.com/> (visited on 01/04/2021).
- Badihi, Behnam (2020). “Overview of Time Synchronization for IoT Deployments : Clock Discipline Algorithms”. In: DOI: 10.3390/s20205928.
- Baur, Tobias et al. (2021). *NOVA Documentation*. URL: <https://rawgit.com/hcmlab/nova/master/docs/index.html> (visited on 09/04/2021).
- Bell, Peter (2021). *scipy/_savitzky_golay.py at v1.7.1 · scipy/scipy*. URL: https://docs.scipy.org/doc/scipy/reference/generated/scipy.signal.savgol{_}filter.html (visited on 08/30/2021).
- Bennett, Terrell R (2017). “Data-Driven Synchronization for Internet-of-Things Systems”. In: December 2019. DOI: 10.1145/2983627.
- Berlin, Cecilia and Caroline Adams (2017). *Production Ergonomics: Designing Work Systems to Support Optimal Human Performance*. ISBN: 9781911529125. DOI: 10.5334/bbe.
- Bleser, Gabriele, Gustaf Hendeby, and Markus Miezal (2011). “Using egocentric vision to achieve robust inertial body tracking under magnetic disturbances”. In: *2011 10th IEEE Int. Symp. Mix. Augment. Reality, ISMAR 2011* November 2014, pp. 103–109. DOI: 10.1109/ISMAR.2011.6092528.

BIBLIOGRAPHY

- Bouvier, Brice et al. (2015). “Upper limb kinematics using inertial and magnetic sensors: Comparison of sensor-to-segment calibrations”. In: *Sensors (Switzerland)* 15.8. ISSN: 14248220. DOI: 10.3390/s150818813.
- Brandt, Mikkel et al. (2015). “Participatory intervention with objectively measured physical risk factors for musculoskeletal disorders in the construction industry: Study protocol for a cluster randomized controlled trial Epidemiology of musculoskeletal disorders”. In: *BMC Musculoskelet. Disord.* 16.1. ISSN: 14712474. DOI: 10.1186/s12891-015-0758-0.
- Brandt, Mikkel et al. (2018). “Accuracy of identification of low or high risk lifting during standardised lifting situations”. In: *Ergonomics* 61.5, pp. 710–719. ISSN: 0014-0139. DOI: 10.1080/00140139.2017.1408857.
- Brankovic, Milutin et al. (2020). *(k, l)-Medians Clustering of Trajectories Using Continuous Dynamic Time Warping*. Vol. 1. 1. Association for Computing Machinery, pp. 99–110. ISBN: 9781450380195. DOI: 10.1145/3397536.3422245. arXiv: arXiv:2012.00464v1.
- Butterworth Filter - an overview — ScienceDirect Topics* (n.a). URL: <https://www.sciencedirect.com/topics/computer-science/butterworth-filter> (visited on 05/14/2021).
- Cao, Zhe et al. (2021). “OpenPose: Realtime Multi-Person 2D Pose Estimation Using Part Affinity Fields”. In: *IEEE Trans. Pattern Anal. Mach. Intell.* 43.1, pp. 172–186. ISSN: 1939-3539. DOI: 10.1109/TPAMI.2019.2929257.
- Carmichael, Presenter., Ong Moderator, and Jen Hicks (n.a). *OpenSim Webinar Which Simulation Pipeline Should I Use? An Overview of Common Workflows [Accessed: 15- Nov- 2020]*. Tech. rep. URL: <http://opensim.stanford.edu/downloads/>.
- Cdn.bitrix24.ru* (2021). URL: https://cdn.bitrix24.ru/b7382791/landing/7c5/7c5c0c57872267e15ad42690082766bb/Awind2a{_}1x.jpg (visited on 08/26/2021).
- Chen, Yanping et al. (2013). “DTW-D: Time series semi-supervised learning from a single example”. In: *Proc. ACM SIGKDD Int. Conf. Knowl. Discov. Data Min.* Part F1288, pp. 383–391. DOI: 10.1145/2487575.2487633.
- De Nul, Lars, Maija Breque, and Athanasios Petridis (2021). *Industry 5.0 : towards a sustainable, human-centric and resilient European industry*. URL: <https://op.europa.eu/en/publication-detail/-/publication/468a892a-5097-11eb-b59f-01aa75ed71a1/> (visited on 01/11/2021).
- Diebel, James (2006). “Representing attitude: Euler angles, unit quaternions, and rotation vectors”. In: *Matrix* 58, pp. 1–35. ISSN: 14602431.
- Direção-Geral da Saúde (2008). “Lesões Musculoesqueléticas Relacionadas com o Trabalho: Guia de Orientação para a Prevenção”. In: *Programa Nac. Contra as Doenças Reumáticas*, p. 28. URL: <https://www.dgs.pt/documentos-e-publicacoes/lesoes-musculoesqueleticas-relacionadas-com-o-trabalho-pdf.aspx>.
- Douphrate, David I. et al. (2012). “Full shift arm inclinometry among dairy parlor workers: A feasibility study in a challenging work environment”. In: *Appl. Ergon.* 43.3, pp. 604–613. ISSN: 18729126. DOI: 10.1016/j.apergo.2011.09.007.
- Eleksen (n.a). *WEARABLE TECHNOLOGIES — Improving Workforce Safety*. URL: <https://eleksen.com/> (visited on 01/04/2021).
- Equivital (n.a). *When human data matters most - Equivital*. URL: <https://www.equivital.com/> (visited on 01/04/2021).
- Executive, Health and Safety (2016). “Health and Safety Executive Risk assessment of pushing and pulling (RAPP) tool Risk assessment of pushing and pulling (RAPP) tool”. In.

- Fan, Thomas J. (2021). *scikit-learn/_base.py at 844b4be24d20fc42cc13b957374c718956a0db39 · scikit-learn/scikit-learn*. URL: https://scikit-learn.org/stable/modules/generated/sklearn.linear_model.LinearRegression.html (visited on 08/30/2021).
- Ferreira, J. et al. (2009). “Development of an assessment tool for repetitive tasks of the upper limbs (ART).” In: *undefined*.
- Filippeschi, Alessandro et al. (2017). “Survey of motion tracking methods based on inertial sensors: A focus on upper limb human motion”. In: *Sensors (Switzerland)* 17.6, pp. 1–40. ISSN: 14248220. DOI: 10.3390/s17061257.
- Folgado, Duarte et al. (2018). “Time Alignment Measurement for Time Series”. In: *Pattern Recognit.* 81, pp. 268–279. ISSN: 00313203. DOI: 10.1016/j.patcog.2018.04.003.
- Foxlin, Eric (2002). “Motion tracking requirements and technologies”. In: *Handb. virtual Environ. Technol.*, pp. 163–210.
- Fraunhofer Portugal, Center for Assistive Information and Communication Solutions – AICOS (2020). *OPERATOR*. DOI: https://www.aicos.fraunhofer.pt/en/our_work/projects/operator.html. URL: https://www.aicos.fraunhofer.pt/en/our_work/projects/operator.html (visited on 01/11/2021).
- Gamboa, Hugo (n.a). *GitHub*. 2021. *novainstrumentation/filter.py at master · hgamba/novainstrumentation*. URL: <https://github.com/hgamboa/novainstrumentation/blob/master/novainstrumentation/filter.py> (visited on 08/30/2021).
- Gamboa, Hugo Filipe Silveira (2013). “Time Series Clustering Algorithm for Two-Modes Cyclic Biosignals”. In: *Biomed. Eng. Syst. Technol.* Ed. by Ana Fred Gamboa, Joaquim Filipe, and Hugo. Springer Berlin Heidelberg, pp. 233–245. ISBN: 978-3-642-29751-9 / 978-3-642-29752-6.
- Garcia, Mario (n.d.). *Ahrs.readthedocs.io*. 2021. *Complementary Filter — AHRS 0.3.0-rc1 documentation*. [online] Available at: <https://ahrs.readthedocs.io/en/latest/filters/complementary.html> [Accessed 26 August 2021]. URL: <https://ahrs.readthedocs.io/en/latest/filters/complementary.html> (visited on 08/13/2021).
- (n.a[a]). *Ahrs.readthedocs.io*. 2021. *AHRS: Attitude and Heading Reference Systems — AHRS 0.3.0-rc1 documentation*. URL: <https://ahrs.readthedocs.io/en/latest/> (visited on 08/30/2021).
- (n.a[b]). *Ahrs.readthedocs.io*. 2021. *Extended Kalman Filter — AHRS 0.3.0-rc1 documentation*. URL: <https://ahrs.readthedocs.io/en/latest/filters/ekf.html> (visited on 08/14/2021).
- (n.a[c]). *Ahrs.readthedocs.io*. 2021. *Madgwick Orientation Filter — AHRS 0.3.0-rc1 documentation*. URL: <https://ahrs.readthedocs.io/en/latest/filters/madgwick.html> (visited on 08/14/2021).
- Hansson, Gert Åke et al. (2010). “Physical workload in various types of work: Part II. Neck, shoulder and upper arm”. In: *Int. J. Ind. Ergon.* 40.3, pp. 267–281. ISSN: 01698141. DOI: 10.1016/j.ergon.2009.11.002.
- Haslwanter, Thomas (2018). *Thomas Haslwanter 3D Kinematics*. Springer Nature Switzerland AG. ISBN: 9783319752761.
- Hassan, Mohammed Mehedi et al. (2018). “A robust human activity recognition system using smartphone sensors and deep learning”. In: *Futur. Gener. Comput. Syst.* 81, pp. 307–313. ISSN: 0167739X. DOI: 10.1016/j.future.2017.11.029.
- He, Jingjing, Changku Sun, and Peng Wang (2019). “Noise reduction for MEMS gyroscope signal: A novel method combining ACMP with adaptive multiscale SG filter based on AMA”. In: *Sensors (Switzerland)* 19.20. ISSN: 14248220. DOI: 10.3390/s19204382.

BIBLIOGRAPHY

- Hodder, Joanne N., Michael W.R. Holmes, and Peter J. Keir (2010). “Continuous assessment of work activities and posture in long-term care nurses”. In: *Ergonomics* 53.9, pp. 1097–1107. ISSN: 00140139. DOI: 10.1080/00140139.2010.502252.
- Holzbaur, Katherine R.S., Wendy M. Murray, and Scott L. Delp (2005). “A model of the upper extremity for simulating musculoskeletal surgery and analyzing neuromuscular control”. In: *Ann. Biomed. Eng.* 33.6, pp. 829–840. ISSN: 00906964. DOI: 10.1007/s10439-005-3320-7.
- Hosseinian, Seyed Mohammadreza et al. (2019). “Static and Dynamic Work Activity Classification from a Single Accelerometer: Implications for Ergonomic Assessment of Manual Handling Tasks”. In: *IISE Trans. Occup. Ergon. Hum. Factors* 7.1, pp. 59–68. ISSN: 2472-5838. DOI: 10.1080/24725838.2019.1608873.
- JM, Kapellusch et al. (2017). “Risk assessments using the Strain Index and the TLV for HAL, Part I: Task and multi-task job exposure classifications”. In: *J. Occup. Environ. Hyg.* 14.12, pp. 1011–1019. ISSN: 1545-9632. DOI: 10.1080/15459624.2017.1366037.
- JM, Kapellusch et al. (2018). “Risk assessments using the Strain Index and the TLV for HAL, Part II: Multi-task jobs and prevalence of CTS”. In: *J. Occup. Environ. Hyg.* 15.2, pp. 157–166. ISSN: 1545-9632. DOI: 10.1080/15459624.2017.1401709.
- Kalman, R. E. (1960). “A new approach to linear filtering and prediction problems”. In: *J. Fluids Eng. Trans. ASME* 82.1, pp. 35–45. ISSN: 1528901X. DOI: 10.1115/1.3662552.
- Keir, Peter J. et al. (2021). “Relationships and Mechanisms Between Occupational Risk Factors and Distal Upper Extremity Disorders”. In: *Hum. Factors* 63.1, pp. 5–31. ISSN: 15478181. DOI: 10.1177/0018720819860683.
- Keogh, Eamonn (2006). *Introduction to Time Series Mining Slides from Keogh Eamonn’s tutorial*. Tech. rep. URL: http://didawiki.cli.di.unipi.it/lib/exe/fetch.php/dm/time_series_from_keogh_tutorial.pdf.
- (n.a). *Eamonn Keogh*, [Cs.ucr.edu]. URL: <https://www.cs.ucr.edu/~eamonn/> (visited on 01/09/2021).
- Kim, Sunwook and Maury A. Nussbaum (2014). “An evaluation of classification algorithms for manual material handling tasks based on data obtained using wearable technologies”. In: *Ergonomics* 57.7, pp. 1040–1051. ISSN: 13665847. DOI: 10.1080/00140139.2014.907450.
- Klussmann, André et al. (2010). “The Key Indicator Method for Manual Handling Operations (KIM-MHO) - evaluation of a new method for the assessment of working conditions within a cross-sectional study”. In: *BMC Musculoskelet. Disord.* 2010 111 11.1, pp. 1–8. ISSN: 1471-2474. DOI: 10.1186/1471-2474-11-272.
- Kok, Jan De et al. (2019). “Work-related MSDs: prevalence, costs and demographics in the EU (European Risk Observatory Executive summary)”. In: *Publ. Off. Eur. Union*, pp. 1–18.
- KUIPERS, JACK B. (2020). “Quaternion Algebra”. In: *Quaternions Rotat. Seq.*, pp. 103–140. DOI: 10.2307/j.ctvx5wc3k.10.
- L, McAtamney and Nigel Corlett E (1993). “RULA: a survey method for the investigation of work-related upper limb disorders”. In: *Appl. Ergon.* 24.2, pp. 91–99. ISSN: 0003-6870. DOI: 10.1016/0003-6870(93)90080-S.
- Lim, Sol and Clive D’Souza (2020). *A narrative review on contemporary and emerging uses of inertial sensing in occupational ergonomics*. DOI: 10.1016/j.ergon.2020.102937.
- Lipton, Howard L. and Brian P. Schlitt (2002). “ISB recommendation on definitions of joint coordinate system of various joints for the reporting of human joint motion—part I: ankle, hip, and spine”. In: *J. Neuroimmunol.* 126.1-2, pp. 1–2. ISSN: 01655728. DOI: 10.1016/S0165-5728(02)00065-6.

- Madgwick, Sebastian O H (2010). “An efficient orientation filter for inertial and inertial/magnetic sensor arrays”. In.
- Mahony, Robert et al. (2008). “Nonlinear complementary filters on the special orthogonal group”. In: *IEEE Trans. Automat. Contr.* 53.5, pp. 1203–1218. ISSN: 00189286. DOI: 10.1109/TAC.2008.923738.
- Malaise, Adrien et al. (2019). “Activity Recognition for Ergonomics Assessment of Industrial Tasks with Automatic Feature Selection”. In: *IEEE Robot. Autom. Lett.* 4.2, pp. 1132–1139. ISSN: 23773766. DOI: 10.1109/LRA.2019.2894389.
- Marteau, Pierre François (2009). “Time warp edit distance with stiffness adjustment for time series matching”. In: *IEEE Trans. Pattern Anal. Mach. Intell.* 31.2, pp. 306–318. ISSN: 01628828. DOI: 10.1109/TPAMI.2008.76.
- Maurer-Grubinger, Christian et al. (2021). “Combining ergonomic risk assessment (Rula) with inertial motion capture technology in dentistry—using the benefits from two worlds”. In: *Sensors* 21.12, pp. 1–17. ISSN: 14248220. DOI: 10.3390/s21124077.
- Maurice, Pauline et al. (2019). “Human Movement and Ergonomics: an Industry-Oriented Dataset for Collaborative Robotics Human Movement and Ergonomics: an Industry-Oriented Dataset for Collaborative Robotics Journal Title XX(X):1-8”. In: DOI: 10.1177/0278364919882089.
- McGee, P. (2019). *Germany invests to prolong employees’ working lives*. URL: <https://www.ft.com/content/f1b294b8-9cbe-11e8-88de-49c908b1f264> (visited on 01/11/2021).
- Menolotto, Matteo et al. (2020). “Motion Capture Technology in Industrial Applications: A Systematic Review”. In: *Sensors* 20.19, p. 5687. ISSN: 1424-8220. DOI: 10.3390/s20195687.
- Modjoul (n.a). *Modjoul Home Page*. URL: <https://www.modjoul.com/> (visited on 01/04/2021).
- Möller, Thérèse et al. (2004). “Job enlargement and mechanical exposure variability in cyclic assembly work”. In: *Ergonomics* 47.1, pp. 19–40. ISSN: 00140139. DOI: 10.1080/0014013032000121651.
- Monnington S.C. et al. (2003). *Development of Manual Handling Assessment Charts (MAC) for Health and Safety Inspectors. — Request PDF*. URL: https://www.researchgate.net/publication/331374663/Development_of_Manual_Handling_Assessment_Charts_MAC_for_Health_and_Safety_Inspectors (visited on 08/20/2021).
- Nazarahari, Milad and Hossein Rouhani (2021). “40 years of sensor fusion for orientation tracking via magnetic and inertial measurement units: Methods, lessons learned, and future challenges”. In: *Inf. Fusion* 68, pp. 67–84. ISSN: 15662535. DOI: 10.1016/j.inffus.2020.10.018.
- Nedoma, Jiri et al. (2011). *MATHEMATICAL AND COMPUTATIONAL METHODS IN BIOMECHANICS OF HUMAN SKELETAL SYSTEMS*. Ed. by Wiley Series, Yi Pan, and Albert Y. Zomaya, pp. 9–30. ISBN: 9780470408247.
- O, Karhu, Kansu P, and Kuorinka I (1977). “Correcting working postures in industry: A practical method for analysis”. In: *Appl. Ergon.* 8.4, pp. 199–201. ISSN: 0003-6870. DOI: 10.1016/0003-6870(77)90164-8.
- OCCHIPINTI, E. (2010). “OCRA: a concise index for the assessment of exposure to repetitive movements of the upper limbs”. In: <http://dx.doi.org/10.1080/001401398186315> 41.9, pp. 1290–1311. DOI: 10.1080/001401398186315.
- OpenSense (2021). *OpenSense - Kinematics with IMU Data - OpenSim Documentation - Global Site*. URL: <https://simtk-confluence.stanford.edu/display/OpenSim/OpenSense+-Kinematics+with+IMU+Data> (visited on 01/09/2021).

BIBLIOGRAPHY

- OSHWiki (2020). “Assessment of physical workloads to prevent work-related MSDs - OSHWiki”. In: pp. 1–10. DOI: https://oshwiki.eu/wiki/Assessment_of_physical_workloads_to_prevent_work-related_MSDs.
- Pedro, Bruno, Sílvia Cabral, and António Prieto Veloso (2021). “Concurrent validity of an inertial measurement system in tennis forehand drive”. In: *J. Biomech.* 121. ISSN: 00219290. DOI: 10.1016/j.jbiomech.2021.110410.
- Peppoloni, L et al. (2016). “International Journal of Industrial Ergonomics (WMSDs issue) A novel wearable system for the online assessment of risk for biomechanical load in repetitive efforts *”. In: *Int. J. Ind. Ergon.* 52, pp. 1–11. ISSN: 0169-8141. DOI: 10.1016/j.ergon.2015.07.002.
- Rajagopal, Apoorva et al. (2016). “Full-Body Musculoskeletal Model for Muscle-Driven Simulation of Human Gait”. In: *IEEE Trans. Biomed. Eng.* 63.10, pp. 2068–2079. ISSN: 15582531. DOI: 10.1109/TBME.2016.2586891.
- Rakthanmanon, Thanawin et al. (2012). “Searching and Mining Trillions of Time Series Subsequences under Dynamic Time Warping”. In: pp. 262–270. DOI: 10.1145/2339530.2339576.
- Reatec (n.a). *HAVS Hand Arm Vibration & Workplace Social Distancing - Reactec*. URL: <https://www.reactec.com/> (visited on 01/04/2021).
- Reporting, WakeCap Real-Time Site and Analytics (n.a). *WakeCap - Real-Time Site Reporting and Analytics*. URL: <https://www.wakecap.com/> (visited on 01/04/2021).
- Ribeiro, Pedro Manuel Santos et al. (2020). “Machine learning improvements to human motion tracking with imus”. In: *Sensors (Switzerland)* 20.21, pp. 1–21. ISSN: 14248220. DOI: 10.3390/s20216383.
- Roetenberg, Daniel, Henk Luinge, and Per Slycke (2009). “Xsens MVN: full 6DOF human motion tracking using miniature inertial sensors”. In: *Xsens Motion Technol. BV, ...* February, pp. 1–7.
- Rombit (n.a). *Rombit Worker Safety solutions*. URL: <https://rombit.com/worker-safety-solutions/> (visited on 01/04/2021).
- Romero, David et al. (Oct. 2016). “Towards an Operator 4.0 Typology: A Human-Centric Perspective on the Fourth Industrial Revolution Technologies”. In.
- Roy, Pamphile (2021). *scipy/_peak_finding.py at v1.7.1 · scipy/scipy*. URL: https://docs.scipy.org/doc/scipy/reference/generated/scipy.signal.find_peaks.html (visited on 08/30/2021).
- Sabatini, Angelo Maria (2011). “Estimating three-dimensional orientation of human body parts by inertial/magnetic sensing”. In: *Sensors* 11.2, pp. 1489–1525. ISSN: 14248220. DOI: 10.3390/s110201489.
- Santos, Sara et al. (2020). “Explaining the ergonomic assessment of human movement in industrial contexts”. In: *BIOSIGNALS 2020 - 13th Int. Conf. Bio-Inspired Syst. Signal Process. Proceedings; Part 13th Int. Jt. Conf. Biomed. Eng. Syst. Technol. BIOSTEC 2020* March, pp. 79–88. DOI: 10.5220/0008953800790088.
- Scalefit (n.a). *Home - scalefit english*. URL: <https://www.scalefit.de/home.html{\#}top> (visited on 08/01/2021).
- Schafer, Ronald W. (2011). “What is a savitzky-golay filter?” In: *IEEE Signal Process. Mag.* 28.4, pp. 111–117. ISSN: 10535888. DOI: 10.1109/MSP.2011.941097.
- Schaub, K. et al. (2013). “The European Assembly Worksheet”. In: *Theor. Issues Ergon. Sci.* 14.6, pp. 616–639. ISSN: 1464536X. DOI: 10.1080/1463922X.2012.678283.
- Schaub, Karlheinz G. (2004). “Das Automotive Assembly Worksheet (AAWS)”. In: *undefined*.

- Scheurer, Sebastian et al. (2020). “Using domain knowledge for interpretable and competitive multi-class human activity recognition”. In: *Sensors (Switzerland)* 20.4. ISSN: 14248220. DOI: 10.3390/s20041208.
- Seidel, David H. et al. (2019). “Quantitative measures of physical risk factors associated with work-related musculoskeletal disorders of the elbow: A systematic review”. In: *Int. J. Environ. Res. Public Health* 16.1, pp. 1–23. ISSN: 16604601. DOI: 10.3390/ijerph16010130.
- Sensry (n.a[a]). “IoT Sensor Solution Kit”. In: pp. 1–3. URL: <https://sensry.net/>.
- (n.a[b]). *Kallisto Toolbox*. URL: https://play.google.com/store/apps/details?id=de.sensry.kallistotoolbox&hl=en_US&gl=US (visited on 08/26/2021).
- Seth, Ajay et al. (2016). “A biomechanical model of the scapulothoracic joint to accurately capture scapular kinematics during shoulder movements”. In: *PLoS One* 11.1. ISSN: 19326203. DOI: 10.1371/journal.pone.0141028.
- Shaabana, A L A and Rong Zheng (2019). “CRONOS : A Post-hoc Data Driven Multi-Sensor”. In: 15.3. SoterAnalytics (n.a). *Soter Analytics - Ergonomic Injury Prevention in the Workplace*. URL: <https://soteranalytics.com/> (visited on 01/04/2021).
- Sybele, Williams, Ralf Schmidt, and Catherine Disselhorst-klug (2006). “An upper body model for the kinematical analysis of the joint chain of the human arm”. In: 39, pp. 2419–2429. DOI: 10.1016/j.jbiomech.2005.07.023.
- Technologies, APDM Wearable (n.a). *Wearable Sensors - APDM Wearable Technologies*. URL: <https://apdm.com/wearable-sensors/> (visited on 08/30/2021).
- Teslabs (n.a). *Teslabs Engineering - A way to calibrate a magnetometer*. URL: <https://teslabs.com/articles/magnetometer-calibration/> (visited on 08/16/2021).
- The International Ergonomics Association (2000). *Human Factors/Ergonomics (HF/E) — The International Ergonomics Association is a global federation of human factors/ergonomics societies, registered as a nonprofit organization in Geneva, Switzerland*. URL: <https://iea.cc/what-is-ergonomics/> (visited on 12/27/2020).
- Varandas, Rui, Duarte Folgado, and Hugo Gamboa (2019). “Evaluation of spatial-temporal anomalies in the analysis of human movement”. In: *BIOSIGNALS 2019 - 12th Int. Conf. Bio-Inspired Syst. Signal Process. Proceedings; Part 12th Int. Jt. Conf. Biomed. Eng. Syst. Technol. BIOSTEC 2019* Biostec, pp. 163–170. DOI: 10.5220/0007386701630170.
- Vicon Motion Systems (n.a). *Site Home - Vicon Documentation*. URL: <https://docs.vicon.com/dashboard.action> (visited on 01/04/2021).
- Vignais, Nicolas et al. (2013). “Innovative system for real-time ergonomic feedback in industrial manufacturing”. In: *Appl. Ergon.* 44.4, pp. 566–574. ISSN: 18729126. DOI: 10.1016/j.apergo.2012.11.008.
- VIT (n.a). *Vigilant Technologies (VIT) - Reduce workplace injuries*. URL: <https://www.vitinitiative.com/> (visited on 01/04/2021).
- ViveLab (n.a). *ViveLab Ergo — 3D Virtual Ergonomic Verification*. URL: <https://www.vivelab.cloud/> (visited on 01/04/2021).
- W3 (2017). *Motion Sensors Explainer*. URL: <https://www.w3.org/TR/motion-sensors/> (visited on 11/30/2020).
- Wang, Shuliang and Wenzhong Shi (2012). *Data mining and knowledge discovery*, pp. 123–142. ISBN: 9783540726807. DOI: 10.1007/978-3-540-72680-7_5.
- WearHealth (n.a). *AI insights for a safer, healthier and productive workforce — WearHealth*. URL: <https://www.wearhealth.com/> (visited on 01/04/2021).

BIBLIOGRAPHY

- WearKinetic (n.a). *Injury Reduction — Safe Distancing — Contact Tracing*. URL: <https://www.wearkinetic.com/> (visited on 01/04/2021).
- Weygers, Ive et al. (2020). “Drift-Free Inertial Sensor-Based Joint Kinematics for Long-Term Arbitrary Movements”. In: *IEEE Sens. J.* 20.14, pp. 7969–7979. ISSN: 15581748. DOI: 10.1109/JSEN.2020.2982459.
- Wikipedia (n.a). *Conversion between quaternions and Euler angles*. URL: https://en.wikipedia.org/wiki/Conversion_between_quaternions_and_Euler_angles (visited on 01/14/2021).
- Wu, Ge et al. (2005). “ISB recommendation on definitions of joint coordinate systems of various joints for the reporting of human joint motion - Part II: Shoulder, elbow, wrist and hand”. In: *J. Biomech.* 38.5, pp. 981–992. ISSN: 00219290. DOI: 10.1016/j.jbiomech.2004.05.042.
- Xsens (2015). “MVN User Manual”. In: *Mv0319P* March, p. 162. URL: <https://www.cleancss.com/user-manuals/QIL/MTW2-3A7G6>.
- XSens (2021). *Xsens Knowledge Base*. URL: https://base.xsens.com/knowledgebase/s/article/Sensor-Placement-in-Xsens-Awinda-System-1605791447430?language=en_US (visited on 08/26/2021).
- Xsens (n.a). *Home - Xsens 3D motion tracking*. URL: <https://www.xsens.com/> (visited on 01/05/2021).
- XSens (n.a). *Validation Research*. URL: <https://www.xsens.com/validation-research-list> (visited on 08/26/2021).
- Yahya, Muhammad et al. (2019). “Motion capture sensing techniques used in human upper limb motion: a review”. In: *Sens. Rev.* 39.4, pp. 504–511. ISSN: 02602288. DOI: 10.1108/SR-10-2018-0270.
- Yoshimura, Genta (2019). “Enumerating Hub Motifs in Time Series Based on the Matrix Profile”. In.
- Zabat, Mahdi et al. (2019). “IMU-based sensor-to-segment multiple calibration for upper limb joint angle measurement—a proof of concept”. In: *Med. Biol. Eng. Comput.* 57.11, pp. 2449–2460. ISSN: 17410444. DOI: 10.1007/s11517-019-02033-7.
- Zhou, Huiyu and Huosheng Hu (2007). “Inertial sensors for motion detection of human upper limbs”. In: *Sens. Rev.* 27.2, pp. 151–158. ISSN: 02602288. DOI: 10.1108/02602280710731713.

Appendices

A. State of the Art

Table A.1: Proforma sheets used whilst observational ergonomic risk assessment (based on OSHwiki, 2020).

Method	Description
Ovako Working posture Assessment System (OWAS) (O et al., 1977)	<ul style="list-style-type: none"> • Developed and introduced in Finland in a steel production company (Ovako) in the 1970s; • Aspects to be observed include the weight of the load and postures of the back, arms, and lower extremities.
Key Indicator Methods (KIM) (Klussmann et al., 2010)	<ul style="list-style-type: none"> • Developed in Germany by the Federal Institute for occupational safety and health; • The screening methods cover six types of workload: lifting, holding and carrying; pushing and pulling; manual handling operations; whole body forces; awkward postures and body movements.
Manual handling Assessment Chart (MAC) (Monnington S.C. et al., 2003)	<ul style="list-style-type: none"> • Developed in United Kingdom (UK) by the Health and Safety Executive (HSE); • Addresses lifting and carrying, and manual handling operations; • Based on a checklist, sets out 11 items of manual handling to be evaluated.
Assessment of Repetitive Tasks (ART) (Ferreira et al., 2009)	<ul style="list-style-type: none"> • Developed in UK by the HSE; • Assesses repetitive tasks associated with upper limb disorders; • Uses a numerical score to indicate the level of risk for twelve factors grouped into four categories (frequency/repetition of movements, force, postures and additional factors, such as duration).
Risk Assessment of Pushing and Pulling (RAPP) (Executive et al., 2016)	<ul style="list-style-type: none"> • Developed in UK by the HSE; • Assesses pushing and pulling operations; • Makes a distinction between pushing and pulling associated with moving loads on wheeled equipment and moving loads without wheels.
Rapid Upper Limb Assessment (RULA) (L et al., 1993)	<ul style="list-style-type: none"> • Based on the observation of the postures of individual body segments; • Consists in giving a numerical value about how far the body segments deviate from their neutral pose; • Additional weights are given to the postures according to forces/loads handled and the occurrence of static/repetitive muscular activity.
Occupational Repetitive Action (OCRA) (OCCHIPINTI, 2010)	<ul style="list-style-type: none"> • Based on the observation of actions and, then, the attribution of weights for six risk factors (movements, posture, external force, vibration, contact forces and others).
Hand Activity Level (HAL) (JM et al., 2017, JM et al., 2018)	<ul style="list-style-type: none"> • Developed by the American Conference of Governmental Industrial Hygienists; • Evaluates job risk factors associated with MSDs of the hand and wrist; • Based on an assessment of hand activity and the level of effort for a typical posture while performing a short cycle task.
Exertion Atlas	<ul style="list-style-type: none"> • Developed under the supervision of the Institute of Ergonomics of Darmstadt Technical University (IAD); • Involves physical exertion and/or exposure to force.
Automotive Assembly Worksheet (AAWS) (Schaub, 2004) and European Assembly Worksheet (EAWS) (Schaub et al., 2013)	<ul style="list-style-type: none"> • Both developed by the IAD; • Assess different types of workload and particularly for cyclic activities in the automotive and supply industry; • EAWS resulted from a revision of AAWS, performed to increase the field of application of the later.

A. STATE OF THE ART

Table A.3: Examples of countries/entities codes, standards and guidelines primarily aimed to prevent WRMSDs. Table from Berlin et al., 2017 p. 152-153.

Country / Entity	Document
Australia	<ul style="list-style-type: none"> • National Code of Practice for Manual Handling [NOHCs: 2005(1990)]; • National Code of Practice for the Prevention of Occupational Overuse Syndrome [NOHCs: 2013 (1994)]; • Manual Tasks Advisory Standard 2000 – Queensland; • Code of Practice for Manual Handling 2000 – Victoria.
China	<ul style="list-style-type: none"> • Law on Prevention and Control of Occupational Diseases (Article 13 of Chapter II Preliminary Prevention). 2002; • Occupational exposure limits for hand-transmitted vibration in the workplace (GBZ 2.2-2007), Measurement methods (GBZ/T 189.9), and Diagnostic criteria of occupational hand-arm vibration disease (GBZ 7); • Hygienic Standards for the Design of Industrial Enterprises (GBZ1) on workplace lighting and illumination; • Guidelines for occupational hazards prevention and control (GBZ/T 211-2008).
European Community	<ul style="list-style-type: none"> • Directive 89/391 Introduction of measures to encourage improvements in the safety and health of workers at work; • Directive 90/269/EEC Minimum health and safety requirements for the manual handling of loads where there is a risk, particularly of back injuries to workers; • Directive 2002/44/EC Minimum health and safety requirements regarding the exposure of workers to the risks arising from physical agents (vibration).
ISO	<ul style="list-style-type: none"> • ISO 11228-1 Ergonomics – Manual Handling – Part 1: Lifting and Carrying; • ISO 11226 Ergonomics – Evaluation of static working postures; • ISO/FDIS 6385:2003 Ergonomic Principles in the Design of Work Systems.
Japan	<ul style="list-style-type: none"> • Guidelines on the prevention of lumbago in the workplace (1994).
Netherlands	<ul style="list-style-type: none"> • Working Conditions Act 1998.
New Zealand	<ul style="list-style-type: none"> • Code of Practice for Manual Handling; • Approved Code of Practice for the Use of Visual Display Units in the Place of Work; • Occupational Overuse Syndrome (OOS) – Guidelines for prevention and management (1991) and Occupational Overuse Syndrome. Checklists for the evaluation of work (1991).
Norway	<ul style="list-style-type: none"> • Act Relating to Worker Protection and Working Environment (2003).
South Africa	<ul style="list-style-type: none"> • Occupational Health and Safety Act 1993.
Spain	<ul style="list-style-type: none"> • Royal Decree 487/1997 Minimum health and safety provision relating to manual load handling involving risks for workers, particularly to the dorsolumbar region and the associated technical guide for the evaluation and prevention of risks associated with manual load handling; • Royal decree 488/1997 Minimum health and safety dispositions relating to work with equipment fitted with visual display units and the associated technical guide for evaluating and preventing risks associated with the use of equipment with visual display units.
Sweden	<ul style="list-style-type: none"> • AFS 2001:1 – Provisions of the Swedish Work Environment Authority on Systematic Work Environment Management, together with General Recommendations on the Implementation of the Provisions; • AFS 1998:1 – Provisions of the Swedish National Board of Occupational Safety and Health on Ergonomics for the Prevention of Musculoskeletal Disorders, together with the Board’s General Recommendations on the Implementation of the Provisions.
UK	<ul style="list-style-type: none"> • The Manual Handling Operations Regulations 1992; • The Health and Safety (Display Screen Equipment) Regulations 1992; • Upper limb disorders in the workplace. HSE, 2002; • Aching arms (or RSI) in small businesses, HSE, 2003; • Manual Handling Assessment Charts. HSE, 2003.

- OSHA, 2003: Ergonomics for the Prevention of Musculoskeletal Disorders. Guidelines for Poultry Processing;
- NIOSH: Simple Solutions: Ergonomics For Farm Workers, 2001;
- California Dept of Industrial Relations, 1999: Easy Ergonomics. A Practical Approach for Improving the Workplace;
- California Dept of Industrial Relations, 2000: Fitting the Task to the Person: Ergonomics for Very Small Businesses;
- State of Washington, Dept of Labor: WAC 296-62-051. Ergonomics;
- State of Washington, Dept of Labor: Fitting the Job to the Worker: An Ergonomics Program Guideline,

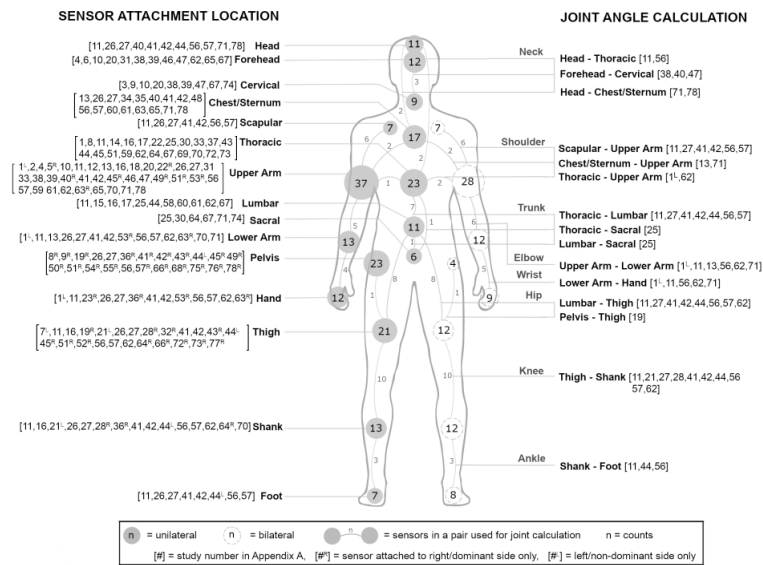


Figure A.1: Inertial Systems *Setups* used in Occupational Ergonomics (Lim et al., 2020).

B. Theoretical Background

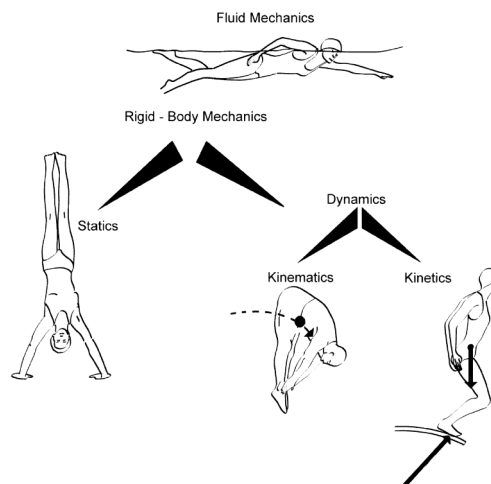


Figure B.1: The major branches of mechanics used in most biomechanical studies (Arus, 2018).

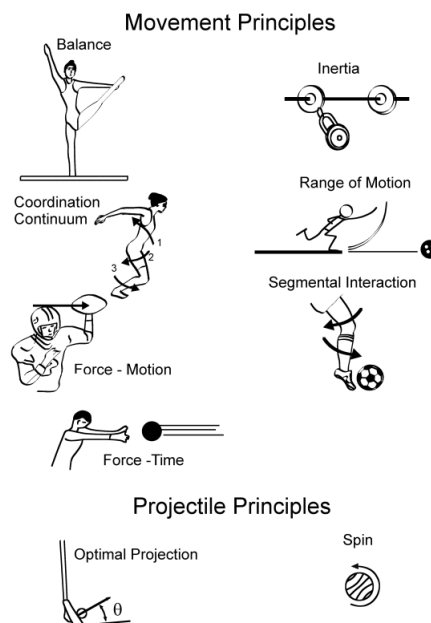


Figure B.2: The nine principles of biomechanics (Arus, 2018).

C. Materials and Methods

C.1 Motion Capture Systems

The MVN Awinda system (Figure C.1), developed by XSens, includes 17 (plus 1 prop) Wireless Motion Trackers (MTw) with battery inside, an Awinda Station (1 per person tracked), a full body strap set (3 T-shirts + straps), charging stations for Awinda sensors, a BNC connector to synchronisation and a sturdy backpack. Its main characteristics are an update rate (in its software) of 60Hz, a wireless range (i.e. wireless coverage) up to $\sim 50\text{m}$, battery life of 6h, wireless communication using a radio protocol (Awinda protocol), a system latency, i.e. the amount of time the audio signal takes to travel from the sensor (the source) to the computer, of 30ms, and an on-body buffering, i.e. the amount of time it takes for the computer to process any incoming audio signal, of 30 s (XSens, 2015).

The MVN Analyze software non-paid version only allows the usage of very basic features. As follows, for this work, the paid version, provided by Volkswagen Autoeuropa, as a 1-year license, was used. It was used the MVN Analyze Pro software 2020.2.0 version.



Figure C.1: MVN Awinda XSens system setup (source: *Cdn.bitrix24.ru* 2021).

The Fraunhofer's system compromised the set up of 8 to 9 wireless and *low-cost* IMU kallisto sensors, formerly developed by Fraunhofer and currently sold by Sensry (Sensry, n.a[a]), using the attaching system *in development*.

C. MATERIALS AND METHODS

Notice that the communication protocol between the sensors and one or more the servers, the hardware for data storage and update, and the software features are also *in development*. The servers update rate was changeful, as it depended on the distance of the sensors to the smartphones, and if the distance to the smartphone was higher than $\sim 10\text{m}$, they disconnected. At the time, Wi-Fi connection and local storage were being considered to solve these problems.

A Kallisto has its battery inside and is charged through induction. Meanwhile, tests are being held to evaluate sensor battery life accurately, but it is certainly longer than a MTw.

C.2 Laboratory Protocol

PROTOCOLO DE RECOLHA

Validação – Laboratório

OBJETIVOS

- ✓ Avaliação da integridade dos sinais recolhidos com sistema de sensorização inercial desenvolvido pela Fraunhofer;
- ✓ Validação da montagem dos sensores e do algoritmo na reconstrução de movimentos funcionais, conjuntos de movimentos de mobilização articular;
- ✓ Validação da montagem dos sensores e do algoritmo na reconstrução de movimentos mais dinâmicos, simulando processos levados a cabo em linha de montagem da Volkswagen Autoeuropa pelos seus operadores. Os *trials* realizados nesta fase serão orientados por objetivos que os participantes deverão completar ao longo do *trial*.

LOCAL DA RECOLHA: [Fraunhofer AICOS, Lisboa](#)

MATERIAL

- Sistema inercial de captura de movimento XSens - MVN Awinda:
 - 17(+1) *Wireless Motion Trackers* (MTw) e respectivo material de colocação;
 - 1 Estação Awinda;
 - 2 Estações de Carregamento Awinda;
 - 1 Segmómetro.
- PC com o software MVN Analyze instalado;
- Sistema inercial de captura de movimento desenvolvido pela Fraunhofer:
 - 8 Kallistos (sensores inerciais, *wireless*) e respectivo material de colocação;
 - 2 smartphones com as Apps Recorder (App interna da Fraunhofer) e a Kallisto ToolBox (disponível na App Store) instaladas.
- Câmara;
- Ferramentas que integram os *trials* relativos à Simulação:
 - Chave de roquete;
 - Carrinho de ferramentas/mesa com rodas;

PROCEDIMENTO

Preparação

1. Verificação da concordância do participante com o consentimento informado;
2. Registo dos dados pessoais do participante;
3. Recolha e registo das medidas corporais do participante, usando o segmómetro;
4. Explicação dos próximos passos ao participante;

Montagem

5. Montagem do sistema XSens;
6. Montagem do sistema desenvolvido pela Fraunhofer;
7. Captura fotográfica da montagem inicial dos sistemas;

Emparelhamento

8. Registo do participante e da aquisição na App Recorder;
9. Começo de uma nova sessão no *software* MVN Analyze, preenchendo o campos afetos às medidas corporais obrigatórias;

C. MATERIALS AND METHODS

Calibração

10. Explicação dos procedimentos de calibração;
11. Calibração do sistema XSens, seguida da calibração estática do sistema desenvolvido pela Fraunhofer;

Ensaio

12. Explicação do procedimento de sincronização sistemas-vídeo e entre sistemas, e dos movimentos a realizar em contexto:
 - a. Postura anatómica ou *N-pose* (10 s);
 - b. Salto vertical;
 - c. Postura anatómica ou *N-pose* (5 s);
 - d. Flexão do braço direito a 90° (5 s);
 - e. Postura anatómica ou *N-pose* (10 s).

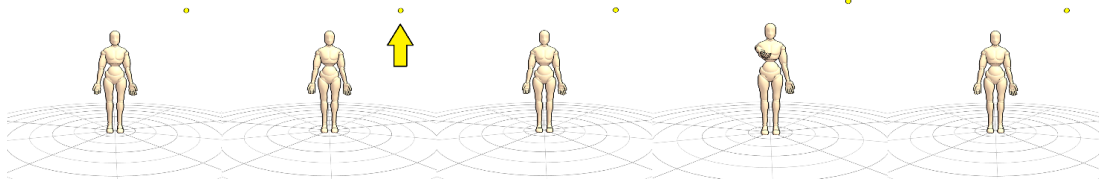


Figure 1: Ilustração dos movimentos integrantes do procedimento de sincronização.

13. Posicionamento da câmara de registo de vídeos;
14. Explicação dos conjuntos de movimentos a realizar a cada *trial*;
15. Realização de um treino dos movimentos explicados - movimentos realizados “em espelho” com o conductor(a) da recolha;

AQUISIÇÃO

16. Inicialização da gravação vídeo;
17. Inicialização da gravação com o sistema XSens;
18. Inicialização da gravação com o sistema desenvolvido pela Fraunhofer;
19. Realização os movimentos de sincronização, descritos na secção Ensaio;
20. Realização dos movimentos descritos no *trial* em questão;
21. Realização os movimentos de sincronização, descritos na secção Ensaio;
22. Paragem da gravação com o sistema desenvolvido pela Fraunhofer;
23. Paragem da gravação com o sistema XSens;
24. Paragem da gravação vídeo;

TRIALS

Funcional – Parte 1 – Membro Superior

Começar com o membro superior direito e permanecer 2 segundos em cada posição:

1. *N-pose*;
2. Abdução do ombro a 90°;
3. Abdução do ombro a 180°;
4. Adução do ombro a 90°;
5. Flexão do cotovelo a 90°;
6. Flexão do pulso a 70°;
7. Rotação do ombro no sentido horário cerca de 90°;
8. Pulso em postura neutra;

9. Pronação do antebraço cerca de 90°;
10. Rotação do ombro no sentido anti-horário cerca de 90°;
11. Extensão do pulso a 70°;
12. Pulso em postura neutra;
13. Supinação do antebraço cerca de 90°;
14. Adução do ombro a 0°;
15. Supinação do antebraço cerca de 90°;
16. Rotação do ombro no sentido anti-horário cerca de 90°;
17. Pronação do antebraço cerca de 90°;
18. Rotação do ombro no sentido horário cerca de 90°;
19. Desvio radial do pulso a 25°;
20. Pulso em posição neutral;
21. Desvio ulnar do pulso a 35°;
22. Pulso em posição neutra;
23. Flexão do ombro a 90°;
24. Flexão do pulso a 70°;
25. Pulso em posição neutral;
26. Supinação do antebraço cerca de 90°;
27. Rotação do ombro no sentido anti-horário a 90°;
28. Extensão do cotovelo a 0°;
29. Flexão do ombro a 180°;
30. Extensão do ombro a 90°;
31. *N-pose*;
32. **Repetir os pontos 2-30 com o membro superior esquerdo.**

C. MATERIALS AND METHODS

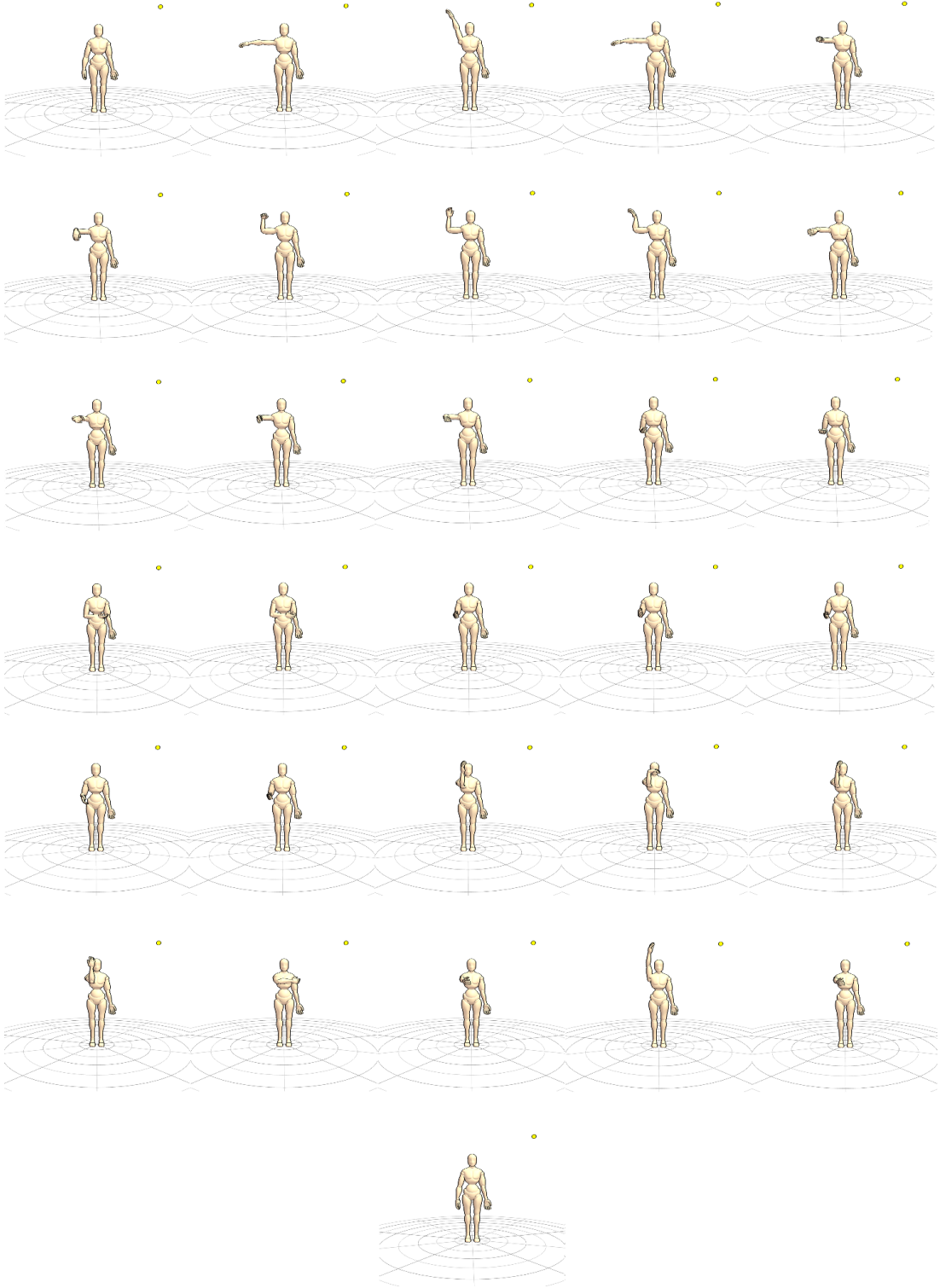


Figure 2: Ilustração do *trial* funcional - mobilização articular do membro superior.

Funcional – Parte 2 – Tronco

Permanecer 5 segundos em cada posição:

1. Postura anatômica ou *N-pose*;
2. Flexão do tronco a 45°;
3. Postura anatômica ou *N-pose*;
4. Extensão do tronco 15°;
5. Postura anatômica ou *N-pose*;
6. Curvar o tronco lateralmente para o lado direito a 20°;
7. Postura anatômica ou *N-pose*;
8. Curvar o tronco lateralmente para o lado esquerdo a 20°;
9. Postura anatômica ou *N-pose*;
10. Rotação do tronco no sentido horário (direita) a 35°;
11. Postura anatômica ou *N-pose*;
12. Rotação do tronco no sentido anti-horário (esquerda) a 35°;
13. Postura anatômica ou *N-pose*.

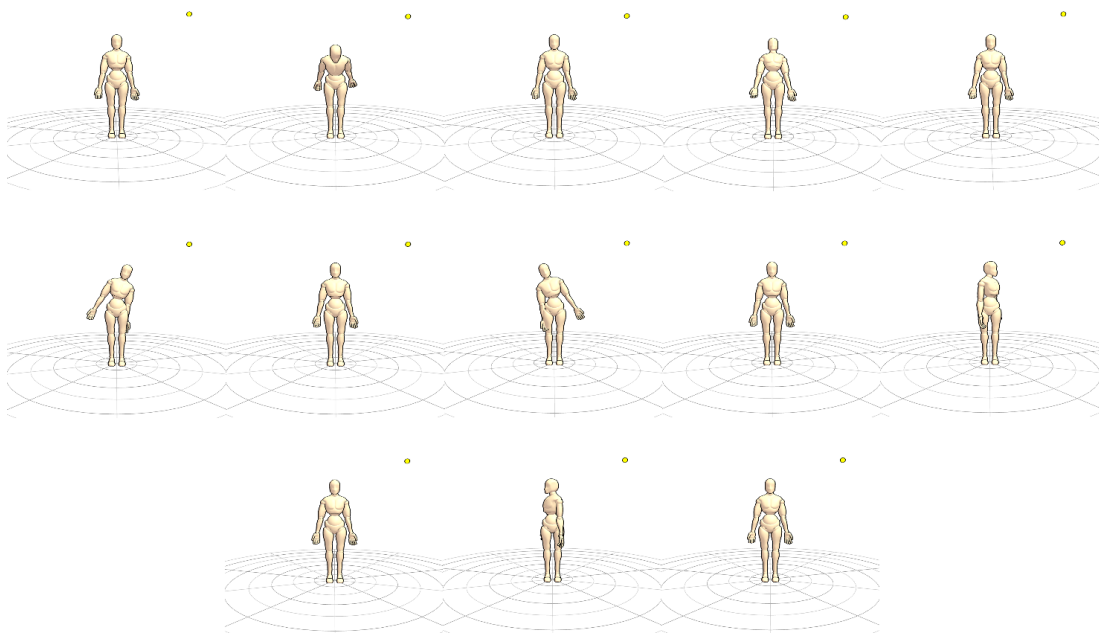


Figure 3: Ilustração do *trial* funcional - mobilização articular do tronco ("em espelho").

Simulação - Sequência 1

1. Empurrar o carrinho de ferramentas para perto do armário;
2. Escolher uma chave de roquete;
3. Simular a ação de desaparafusar numa prateleira acima do nível da cabeça (3x);
4. Pousar a chave de roquete;
5. Inspeccionar o armário;
6. Escolher uma chave de roquete;

C. MATERIALS AND METHODS

7. Simular a ação de desaparafusar numa prateleira ao nível do diafragma (3x);
8. Pousar a chave de roquete;
9. Inspeccionar o armário;
10. Escolher uma chave de roquete;
11. Simular a ação de desaparafusar numa prateleira abaixo do nível da cintura (3x), realizando a flexão do tronco;
12. Pousar a chave de roquete;
13. Inspeccionar o armário.

Simulação - Sequência 2

1. Empurrar o carrinho de ferramentas para perto do armário;
2. Segurar extremidades do armário com as mãos acima do nível da cabeça e realizar um movimento de torção (1x);
3. Inspeccionar o armário;
4. Segurar extremidades do armário com as mãos ao nível do diafragma e realizar um movimento de torção (1x).

Simulação - Sequência 3

1. Empurrar o carrinho de ferramentas para perto da mesa;
2. Aplicar pressão sobre o tampo com ambas as mãos (1x, 5 s);
3. Inspeccionar a mesa;
4. Aplicar pressão sobre o tampo com a mão direita (1x, 5 s);
5. Inspeccionar a mesa;
6. Aplicar pressão sobre o tampo com a mão esquerda (1x, 5 s);
7. Inspeccionar a mesa.

C.3 Laboratory Informed Consent

CONSENTIMENTO PARA PARTICIPAÇÃO EM INVESTIGAÇÃO PROJECTO OPERATOR – FASE 1

O projeto “Operator - Transformação Digital na Indústria com foco no Operador 4.0” pretende realizar um estudo de investigação para o desenvolvimento de tecnologia que seja capaz de promover o bem-estar físico e mental dos trabalhadores sem comprometer a produtividade.

Neste estudo participam as seguintes entidades: Zenithwings (empresa privada), Associação Fraunhofer Portugal Research (Fraunhofer), Faculdade de Psicologia e de Ciências da Educação da Universidade do Porto (FPCEUP), Faculdade de Ciências e Tecnologia da Universidade Nova de Lisboa (NOVA), Volkswagen Autoeuropa, NST Apparel (Europe) Lda., ControlConsul (empresa privada), Universidade do Minho e MIT – Institute for Medical Engineering and Science.

No âmbito deste estudo, pretendemos colocar sensores sobre os membros superiores para recolha de dados de movimento.

Objetivos da atividade

Com a colocação de sensores sobre os membros superiores procuraremos medir movimentos durante a execução das tarefas. O objetivo principal visa a comparação da estimativa de movimento obtida através de ferramentas computacionais desenvolvidas ao longo do projeto, com dados de movimento fornecidos por um sistema de referência.

Materiais usados

Nesta atividade iremos proceder à recolha de dados sociodemográficos, medidas corporais e dados de sensores inerciais, que serão utilizados durante o período de recolha de dados. Serão, adicionalmente, gravados vídeo, som e imagem, com vista à construção de um registo que ajudará o trabalho de processamento dos dados resultantes da aquisição. A análise dos dados recolhidos será realizada pela Fraunhofer (Portugal).

Procedimentos

Iremos equipar os seus braços e tronco com um conjunto de sensores de movimento, o que pode tardar 30 a 40 minutos. Em seguida, iremos pedir-lhe que execute conjuntos de movimentos, desenhados pelos investigadores da Fraunhofer, durante cerca de 30 a 40 minutos. Os sensores estarão a medir os seus movimentos.

Os seus dados pessoais serão analisados pelos investigadores da Fraunhofer. Os dados recolhidos são confidenciais. As entidades envolvidas no estudo tomarão todas as medidas necessárias à salvaguarda e proteção dos dados recolhidos, evitando que venham a ser acedidos por terceiros não autorizados.

Gostaríamos de contar com a sua participação. A participação não envolve qualquer prejuízo ou dano material, nem qualquer benefício. Todo o material necessário para este estudo será fornecido. A sua participação não envolve qualquer tipo de pagamento, não terá consequências no seu trabalho ou avaliação, nem terá custos para si ou para a empresa para quem trabalha.

A sua participação é voluntária, podendo em qualquer altura cessá-la sem qualquer tipo de consequência. Também poderá pedir a retificação ou destruição da informação recolhida a qualquer momento. Para isso, basta que nos contacte através do e-mail fornecido abaixo.

Agradecemos muito o seu contributo, fundamental para a nossa investigação.

C. MATERIALS AND METHODS

CONSENTIMENTO PARA PARTICIPAÇÃO EM INVESTIGAÇÃO PROJECTO OPERATOR – FASE 1

O/A participante:

*Declaro ter lido e compreendido este documento, bem como as informações verbais fornecidas e aceito participar nesta investigação. Permito a utilização dos dados que forneço de forma voluntária, confiando que apenas serão utilizados para investigação e com as garantias de confidencialidade e anonimato que me são dadas pelas investigadoras. Autorizo a comunicação de dados de forma **anónima** a outras entidades parceiras do estudo para fins académicos e de investigação científica.*

Nome da/o participante: _____

Assinatura: _____ Data ___ / ___ / _____

Investigador responsável:

Nome: Maria Lua Nunes

Assinatura: _____

Telefone: 220 430 345

E-mail: maria.nunes@fraunhofer.pt

C.4 Signals Example

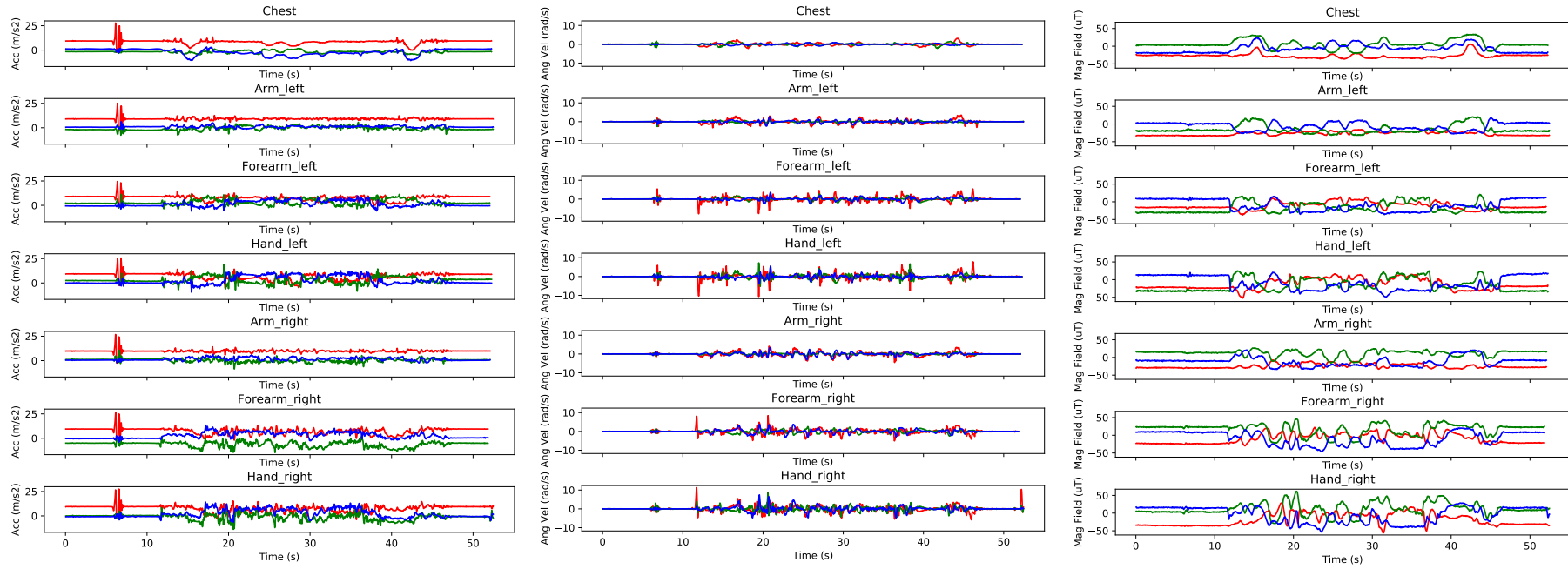


Figure C.2: An example of Fraunhofer's sensors signals' components - acceleration (upper right), angular velocity (upper left) and magnetic field (bottom) - for each IMU attached to a body segment.

C. MATERIALS AND METHODS

C.5 Computational Tools

This section provides a widely description of the computational tools used. The tasks described in sections 4.3 to 4.6 were mainly carried out in Python 3.7, using PyCharm 2020.2.3 (Community Edition) as the Integrated Development Environment (IDE), with the Anaconda 3.0 distribution.

C.5.1 Python Packages

Next, are listed the Python packages basis requirements to the framework developed during the dissertation project.

Data Structure

```
numpy==1.17.5  
pandas==1.0.5
```

Signal/Data Processing/Analysis

```
biosignalsnotebooks==0.6.3  
novainstrumentation==0.4  
scipy==1.6.1  
statsmodels==0.10.0
```

Sensor Fusion

```
AHRS==0.3.0  
pyquaternion==0.9.9
```

Inverse Kinematics

```
opensim===4.2-2021-01-13-642235a
```

Reporting

```
html5lib==1.0.1  
htmlmin==0.1.12  
Jinja2==2.11.2  
Markdown==3.3.3
```

Visualisation

```
matplotlib==3.1.3  
seaborn==0.11.1  
streamlit==0.80.0  
xhtml2pdf==0.2.5
```

C.6 Filtering Example

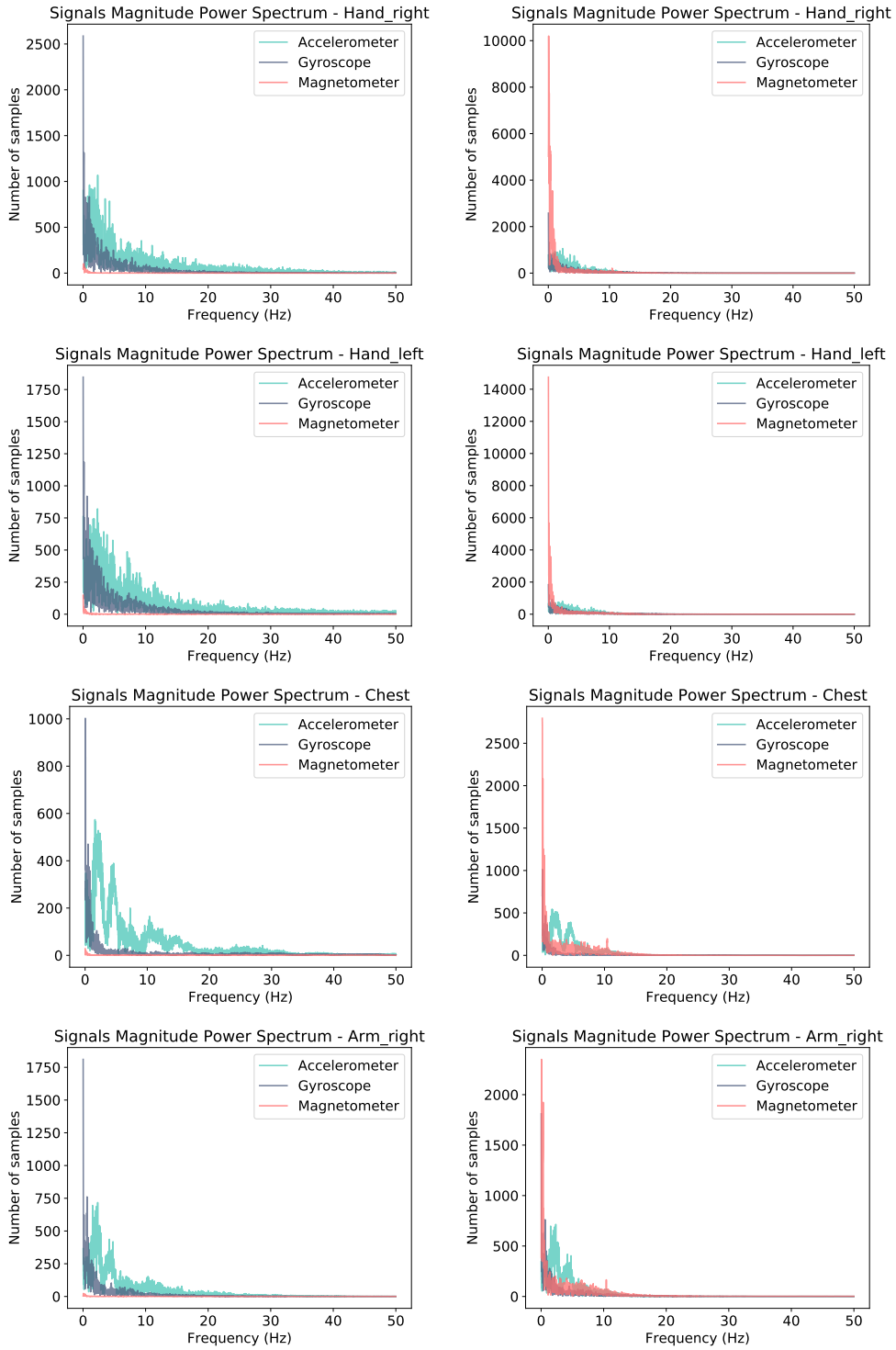


Figure C.3: An example of IMU sensors signals magnitude power spectrum for each body segment tracked before (left) and after (right) filtering. Hand, right and left, chest and arm right body segments.

C. MATERIALS AND METHODS

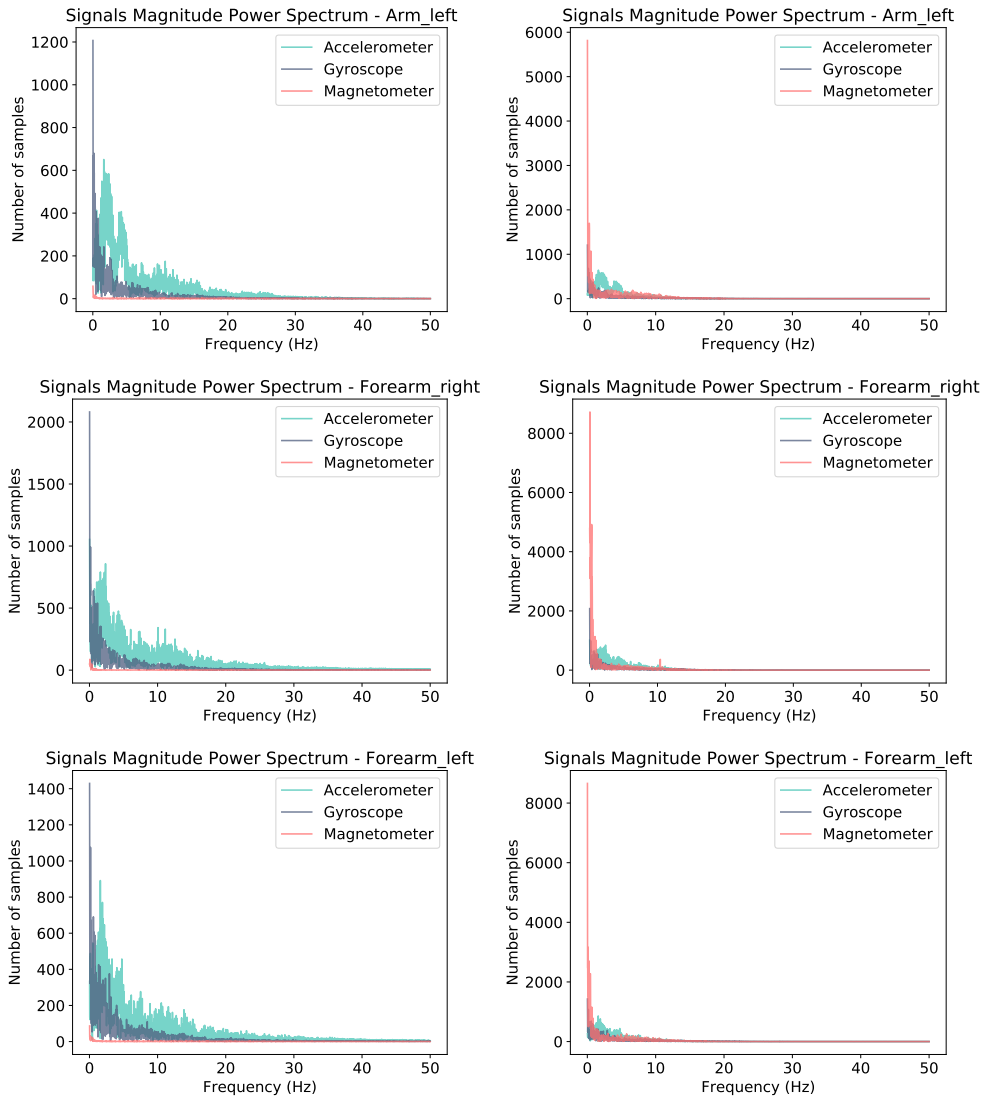


Figure C.4: An example of IMU sensors signals magnitude power spectrum for each body segment tracked before (left) and after (right) filtering. Arm right and forearm, right and left, body segments.

C.7 Synchronisation Method Algorithm

Table C.1: Synchronisation Method Algorithm.

Input parameters: Master signal, M_s , and axis, M_{ax} ; Peaks height, h ; Reference segment, S_r ; Interval maximal threshold, t_A ; Sampling frequency, f_s .

1. Identify the synchronisation opportunities \mathbf{O} s in the M_s and M_{ax} for each segment. It uses Scipy signal function find peaks (Roy, 2021) to detect the peaks with a height equal or higher to h (i.e. \mathbf{O} s).
2. Alignment of segments' time series by their initial \mathbf{O} . It consists in cutting off the samples with an index anterior to the first \mathbf{O} 's index for each signal of each segment data.
3. Match the \mathbf{O} s in the time series from the reference segment with the \mathbf{O} s in time series from another segments, and drop \mathbf{O} s without matching. Matching \mathbf{O} s consists in pointing out \mathbf{O} s in the M_s and M_{ax} from a segment S time series (to be synchronised) that correspond to the \mathbf{O} s in the M_s and M_{ax} from the S_r time series, using the t_A as the maximal threshold for the time interval between an \mathbf{O} in S and an \mathbf{O} in S_r . Matched \mathbf{O} s are named as alignment points, \mathbf{A} s.
4. Compute the correction times between a S time series and the S_r time series. The result is an array \mathbf{c} of the differences in time between each \mathbf{A} in S and the corresponding \mathbf{A} in S_r . The array describes S 's sensor drift over time.
5. Determine the linear regression that translates each S 's sensor drift over time \mathbf{L} , using scikit learn linear model Linear Regression class (Fan, 2021).
6. Remove the linear regression \mathbf{L} element-wise to each S sensor time axis t_S .
7. Interpolate correction of each segment data (S_r data included). It searches in time-axes from all the segments data which one ends up earlier in time, and uses its last point in time, t_f , to arrange a vector T starting at 0 and finishing in t_f , from $1/f_s$ to $1/f_s$. T is the selected time-axis for all the segments data and it is used to interpolate sensors signals data.

C. MATERIALS AND METHODS

C.8 Synchronisation Example

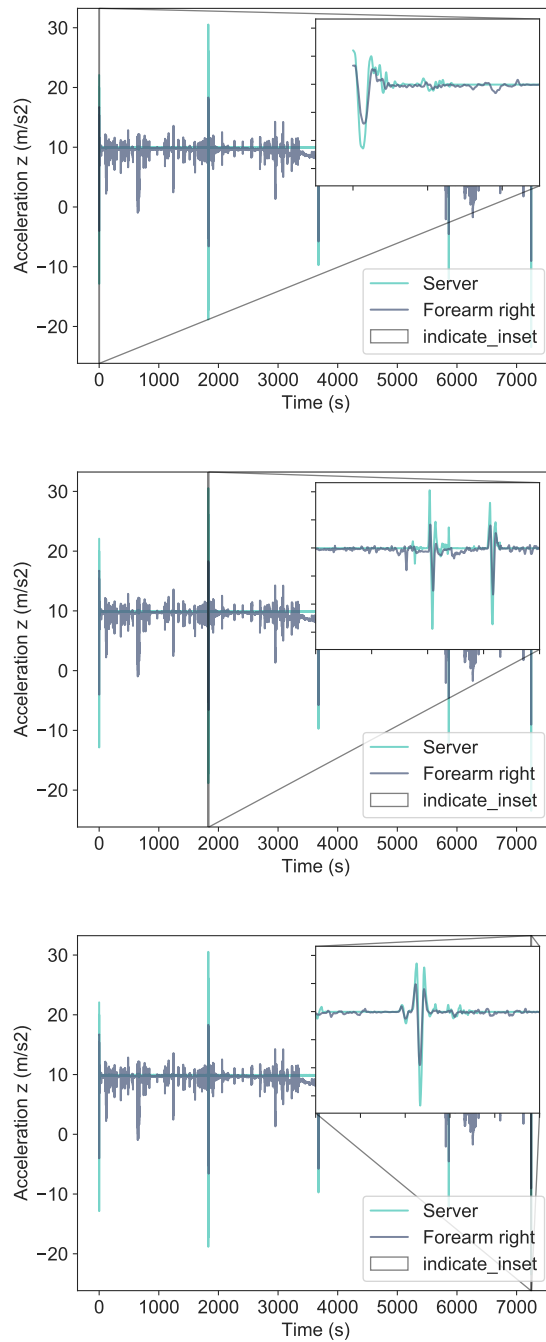


Figure C.5: An example of usage of the synchronisation method for a long-term acquisition (of 2h). The input parameters chosen were: Accelerometer as M_s and z as M_{ax} , h of 16, "Server" as r , t_A of 0.2s and f_s of 100Hz. Zoom in into the first (top), a middle and the last (bottom) As in Accelerometer z data, from Server - in turquoise color - and Forearm right - in purple color.

C. MATERIALS AND METHODS

```
1 DataRate=100.000000
2 DataType=Quaternion
3 version=3
4 OpensimVersion=4.2-2021-01-13-642235a
5 endheader
6 time torso_lmu humerus_r_lmu radius_r_lmu hand_r_lmu humerus_l_lmu radius_l_lmu hand_l_lmu
7 0 0.5745670475992742, 0.3747948540751853, -0.5157171440173082, 0.5132614855397248 0.7223506101110406, 0.1199431682984516, -0.6767429514479714, 0.07643435167662101 0.6619023793194083,
8 0.01 0.5747052086816635, 0.3746838654387471, -0.5155252587724525, 0.5133805914345034 0.7225389707425981, 0.1196910606529262, -0.6765920601001396, 0.07638501140573133 0.66220396942811
9 0.02 0.574822069483224, 0.3745862494255424, -0.515325241348656, 0.5135218643184087 0.722670831716804, 0.1196241219429366, -0.67645006939391817, 0.07649994863684795 0.66258240011557
10 0.03 0.57495702530566, 0.374475736282654, -0.5150802369243631, 0.5136970805246324 0.72281637571393929, 0.119727776352264, -0.6762946798784574, 0.07671642561564051 0.6630398901785969,
11 0.04 0.575088990626966, 0.374357828334418, -0.5148405665173741, 0.513875490252272 0.7228784415384094, 0.1201299230721468, -0.676065370775339, 0.07714385769511393 0.6635608249916809,
12 0.05 0.5752486966767467, 0.3742042832321722, -0.5146060968731591, 0.514043138983222 0.7230026806695314, 0.1212966007582299, -0.6752961105411709, 0.07807387420908932 0.66411385606901
13 0.06 0.5754026348467467, 0.3740120208534293, -0.5144512922817354, 0.5141660081512325 0.7230026806695314, 0.1212966007582299, -0.6752961105411709, 0.07807387420908932 0.66411385606901
14 0.07000000000000001 0.5755356376484809, 0.3737787051539363, -0.5143908083126967, 0.5142473195782475 0.723123852679449, 0.1220127017875614, -0.67478483509431, 0.0785076080930045 0.664670409550
15 0.08 0.575664636056764, 0.373498505270325, -0.5143811177813663, 0.5143162052905381 0.7233634025104009, 0.1227798528215108, -0.6742257523303346, 0.0788779196474254 0.6656820040710226,
16 0.09 0.5757798498385708, 0.373199369862121, -0.5144032091211623, 0.5143823906531453 0.72430310319278, 0.123584046825037, -0.6736498210036023, 0.07917388196204712 0.666105575458899, -0.311
17 0.09999999999999999 0.57586764500207, 0.372914848015322, -0.5144417308755828, 0.5144518219456647 0.7246849414406658, 0.1244013747152327, -0.673092584289153, 0.07938769799565112 0.666441
18 0.11 0.575921935734587, 0.3726747240023452, -0.5144765126439957, 0.5145302633993367 0.7250097988865616, 0.1251829652742268, -0.672850461778798, 0.0794948019528584 0.66670206199595
19 0.12 0.5759281020288961, 0.372497774115121, -0.5145106396855506, 0.5146173638549599 0.7253014239933843, 0.1258583389719589, -0.672148727735822, 0.0794562361300087 0.66687840997161
20 0.13 0.5759818470950283, 0.3723277314040369, -0.5145485904328729, 0.5147104792402396 0.725511541360217, 0.1263486102560381, -0.6717911810856764, 0.07924101203039607 0.66700960880597
21 0.14 0.5758302056852076, 0.3722170552040481, -0.5145836521629281, 0.514817925677829 0.7258264775796092, 0.126605032592697, -0.6715150497944399, 0.07883291232822831 0.6671303666081
22 0.15 0.5757971014975367, 0.3721490814969793, -0.5145776325239865, 0.5149491422895439 0.7262051707923506, 0.1266405483119393, -0.6713239999286058, 0.0782773012040892 0.66726279550661
23 0.16 0.5757560714433205, 0.3720219439748602, -0.5146058103353103, 0.5150587144845319 0.7262585492874206, 0.1265208462803647, -0.6712014967228114, 0.07765015029276798 0.6674099661938
24 0.17 0.5756982321965238, 0.3718916709642109, -0.514696112736179, 0.515127095778973 0.7264165186065974, 0.126355970682098, -0.671131792177416, 0.07704172846626089 0.6675561835658583,
25 0.18 0.575638541055649, 0.371752245775263, -0.514826192698081, 0.5151645505154614 0.726532733748243, 0.1262487417953798, -0.671097657366863, 0.076494599759855 0.6676842104454402,
26 0.19 0.575557980699247, 0.371626815679992, -0.51498783613834, 0.5151835103627878 0.7265963931143838, 0.1262601198570915, -0.6710712439843587, 0.07602268835108372 0.6677902305251725,
27 0.2 0.575453637656291, 0.371526437090299, -0.5151568953213592, 0.5152035284773102 0.7266431541886568, 0.1263875285521069, -0.6710471487757512, 0.075575414105285 0.6678735116389429, -0.31637
28 0.21 0.5753338185275871, 0.3714483707900684, -0.515309166261142, 0.5152412718941642 0.7266749218060813, 0.1265781292121523, -0.6710307463200144, 0.07509509116102106 0.6679217103430729,
29 0.22000000000000001 0.5751880451288569, 0.3713948509052076, -0.515454043606885, 0.5152976871588445 0.7267112291593756, 0.126744881247233, -0.6710247707369104, 0.0745136330808236 0.66794
30 0.23000000000000001 0.575018096053553, 0.3713549323125607, -0.515597954262317, 0.5153733080891041 0.7267836280603857, 0.1268106138718918, -0.6710132835373401, 0.07379564395522303 0.66794
31 0.24000000000000001 0.5748416767152591, 0.3713086296126754, -0.515733578955771, 0.5154666078251425 0.726916374617889, 0.1267379157893555, -0.6709765040568706, 0.0729425258754257 0.66794
32 0.25000000000000001 0.574671314247105, 0.3712412547344258, -0.515862945801962, 0.5155756321949994 0.7271013460845207, 0.1265375567938041, -0.6709172865546154, 0.0719825351997332 0.66780
33 0.26000000000000001 0.5745286559401266, 0.3711390935113901, -0.5159659487190191, 0.5157050867828027 0.7273097712878599, 0.126258766186483, -0.6708505397072623, 0.07098432168262819 0.66780
34 0.27000000000000001 0.5744266094339928, 0.3709966197450132, -0.516022849623881, 0.5158648853475072 0.7274992297289101, 0.1259685155333944, -0.670800804026776, 0.070028930506074 0.66780
35 0.28000000000000001 0.5743520945318631, 0.3708260974966287, -0.516042519580598, 0.5160501862792607 0.727636353039808, 0.1257227809763328, -0.67078422463534, 0.0691920351337517 0.667994
36 0.29000000000000001 0.5742944723919963, 0.3706382135140771, -0.5160298835676786, 0.5162618840551957 0.7277079078550754, 0.12553775838848493, -0.6708128907405114, 0.06849472857372953 0.66780
37 0.30000000000000001 0.5742421577815828, 0.3704475369260788, -0.5159872362252661, 0.5164995049991478 0.7277152939153756, 0.1253877270845293, -0.6708919608320114, 0.0679142532103868 0.66780
38 0.31000000000000001 0.5741746703784911, 0.370274500535513, -0.5159378380405411, 0.5167478973609665 0.7276756981652386, 0.1252415888320379, -0.6710105929064201, 0.06743446399233918 0.668857
39 0.32000000000000001 0.5740801660731406, 0.3701311667271551, -0.515895863642183, 0.5169986946699069 0.7276021779625425, 0.1250775379658726, -0.6711602053637671, 0.06704221697278916 0.669171
40 0.33000000000000001 0.5739610213530654, 0.3700156973263846, -0.5158624309025769, 0.517245668939938 0.7274955202421663, 0.124893512753902, -0.6713410024417188, 0.06673213075670408 0.669171
41 0.34000000000000001 0.5738184822131405, 0.369919232844466, -0.5158425673249792, 0.5174925664953498 0.727349107479529, 0.124695826536309, -0.671581232175982, 0.06650372388498188 0.669801
42 0.35000000000000001 0.573656459675914, 0.3698263368868715, -0.5158481036611773, 0.51779332082171869 0.7271634998676961, 0.1244854756451108, -0.6718140940863805, 0.06635083863097287 0.670994
43 0.36000000000000002 0.5734807696631662, 0.3697242342793781, -0.515887298466789, 0.5179600523468534 0.7269385569106338, 0.1242643757942027, -0.6721066060612408, 0.06626711064404231 0.671000
```

Figure C.8: *sto.* format file example.

C.10 European Assembly Worksheet

Ergonomic Assessment Worksheet v1.3.5			
Plant	Gender of operator m <input type="checkbox"/> f <input type="checkbox"/>	Body height	
Line	MTM Analysis	Analyst	
Task / Workplace	Task duration [s]	Observation <input type="checkbox"/>	Date
		Planning <input type="checkbox"/>	

Result of overall evaluation: *Calculate the total score of whole body and compare it to the UL score. The overall result is determined by the higher value and the appropriate traffic light is checked. Anyway, interpretation should take into account both values.*

<input type="checkbox"/> Green <input type="checkbox"/> Yellow <input type="checkbox"/> Red	Whole Body	=	Postures	+	Forces	+	Loads	+	Extra	Upper Limbs
		=		+		+		+		

EAWS evaluation	0-25 Points	Green	Low risk: recommended; no action is needed
	>25-50 Points	Yellow	Possible risk: not recommended; redesign if possible, otherwise take other measures to control the risk
	>50 Points	Red	High risk: to be avoided; action to lower the risk is necessary

Extra points "Whole body" (per minute / shift)					Extra points			
0a	Adverse effects by working on moving objects	0	3	8	15	Intensity		
		none	middle	strong	very strong			
0b	Accessibility (e.g. entering motor or passenger compartment)	0	2	5	10	Status		
		good	complicated	poor	very poor			
0c	Countershocks, impulses, vibrations	0	1	2	5	Intensity × frequency		
		light	visible	heavy	very heavy			
		0	1	2,5	4		6	8
[n]	1 - 2	4 - 5	8 - 10	18 - 20	> 20			
0d	Joint position (especially wrist)	0	1	3	5	Intensity × duration or frequency		
		neutral	~ 1/3 max	~ 2/3 max	maximal			
		0	2	2,5	4		6	8
		[s]	3	10	20		40	60
[n]	1	8	11	16	20			
[%]	5	17	33	67	100			
0e	Other physical work load (please describe in detail)	0	5	10	15	Intensity		
		none	middle	strong	very strong			
Extra = ∑ lines 0a – 0e		Attention: Max. score = 40 (line 0c, 0d); Max. score = 15 (line 0a, 0e); Max. score = 10 (line 0b)			Attention: correct evaluation, if duration of evaluation ≠ 60 s		=	
Lines 0a-b mainly relate to the Automotive Industry, for other sectors additional elements may be necessary. For details see the EAWS manual.								

For scoring of repetitive tasks only:			Comments / proposals for improvements
Description	Formula	Result	
Real shift duration [min]			
Lunch break [min]	-		
Other official pauses [min]	-		
Non repetitive tasks (i.e. cleaning, supplies, etc) [min]	-		
Net duration of repetitive task/s (a) [min]	=		
No. of real units (or cycles) (b)			
Net cycle time [s]	(a/b × 60) =		
Idle Time [s]			

C. MATERIALS AND METHODS

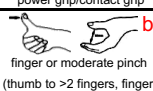
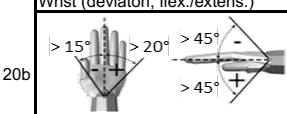
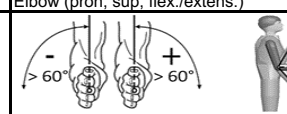
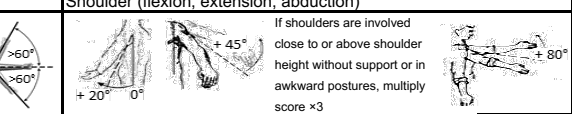
Ergonomic Assessment Worksheet v1.3.5																										
Basic Positions / Postures and movements of trunk and arms (per shift)										Postures																
(incl. loads of <3 kg, forces onto fingers of <30 N and whole body forces of <40 N) Static postures: ≥ 4 s High frequency movements: Trunk bendings (> 60°) ≥ 2/min Kneeling/crouching ≥ 2/min Arm liftings (> 60°) ≥ 10/min										Symmetric					Asymmetric											
										Evaluation of static postures and/or high frequency movements of trunk/arms/legs										Sum of lines	Trunk Rotation 1)	Lateral Bending 1)	Far Reach 2)			
										Duration [s/min] = $\frac{\text{duration of posture [s]} \times 60}{\text{Task duration [s]}}$											int	dur	int	dur	int	dur
										[%]	[s/min]	[min/8h]	5	7,5	10	15	20	27	33		50	67	83	0-5	0-3	0-5
			24	36	48	72	96	130	160	240	320	400	Intensity × Duration	Intensity × Duration	Intensity × Duration											
Standing (and walking)																										
1		Standing & walking in alteration, standing with support	0	0	0	0	0,5	1	1	1	1,5	2														
2		Standing, no body support (for other restrictions see Extra Points)	0,7	1	1,5	2	3	4	6	8	11	13														
3		a Bent forward (20-60°)	2	3	5	7	9,5	12	18	23	32	40														
		b with suitable support	1,3	2	3,5	5	6,5	8	12	15	20	25														
4		a Strongly bent forward (>60°)	3,3	5	8,5	12	17	21	30	38	51	63														
		b with suitable support	2	3	5	7	9,5	12	18	23	31	38														
5		Upright with elbow at / above shoulder level	3,3	5	8,5	12	17	21	30	38	51	63														
6		Upright with hands above head level	5,3	8	14	19	26	33	47	60	80	100														
Sitting																										
7		Upright with back support slightly bent forward or backward	0	0	0	0	0	0,5	1	1,5	2															
8		Upright no back support (for other restriction see Extra Points)	0	0	0,5	1	1,5	2	3	4	5,5	7														
9		Bent forward	0,7	1	1,5	2	3	4	6	8	11	13														
10		Elbow at / above shoulder level	2,7	4	7	10	13	16	23	30	40	50														
11		Hands above head level	4	6	10	14	20	25	35	45	60	75														
Kneeling or crouching																										
12		Upright	3,3	5	7	9	12	15	21	27	36	45														
13		Bent forward	4	6	10	14	20	25	35	45	60	75														
14		Elbow at / above shoulder level	6	9	16	23	33	43	62	80	108	135														
Lying or climbing																										
15		(Lying on back, breast or side) arms above head	6	9	15	21	29	37	53	68	91	113														
16		Climbing	6,7	10	22	33	50	66																		
1) Trunk			int				dur				Σ		Σ		Σ											
			slightly ≤10°				medium 15°				strongly 25°		extreme ≥30°		close		60%		80%		arm stretched					
			0				1,5				2,5		3		0		1		1,5		2					
			never				4 s				10 s		≥ 13 s		never		4 s		10 s		≥ 13 s					
			0%				6%				15%		≥ 20%		0%		6%		15%		≥ 20%					
											(a)		(b)													
Attention: Max. duration of evaluation = duration of task or 100%!												Attention: correct evaluation, if task duration ≠ 60 s														
Postures = Σ lines 1 - 16			(a)				+				(b)		=													

Ergonomic Assessment Worksheet v1.3.5

Action forces (per minute)										Forces				
17		Forces onto fingers (e.g. clips, plugs)	Int	0	7	15	25	50	Intensity × Duration					
				16.7% F _{max}	33.3% F _{max}	50.0% F _{max}	66.7% F _{max}	F _{max}						
18		Forces onto arms / whole body forces	Int	0	6	15	25	50	Intensity × Duration					
				16.7% F _{max}	33.3% F _{max}	50.0% F _{max}	66.7% F _{max}	F _{max}						
Forces F_{max} onto arms / whole body forces (neutral to gender) P15 for planning & P40 for observation			ST Upright	P15	P40	ST Bent	P15	P40	ST Above head	P15	P40	Finger forces F _{max} (neutral to gender)		
											Posture A1 (power grip, pliers)		F _{max}	
			-A 245 315 -B 260 325 -C 170 210 -D 245 315 -E 130 185 -F 110 165		-A 210 285 -B 200 240 -C 205 260 -D 285 390 -E 145 200 -F 90 135		-A 230 280 -B 265 320 -C 160 200 -D 255 310 -E 105 140 -F 100 140		P15 P40 150 205		P15 P40 115 155		P15 P40 55 70	
											Posture B1 (thumb or thumb to 4 fingers)		F _{max}	
			-A 225 280 -B 215 290 -C 240 325 -D 145 195 -E 115 160		-A 180 245 -B 190 225 -C 220 320 -D 140 190 -E 105 135		-A 225 275 -B 210 270 -C 220 275 -D 130 180 -E 130 180		P15 P40 115 155		P15 P40 55 70		P15 P40 40 50	
											Posture B2 (index or wide pinch)		F _{max}	
			-A 205 265 -B 245 285 -C 215 260 -D 205 250 -E 120 165 -F 110 155		-A 190 250 -B 195 245 -C 245 295 -D 215 275 -E 130 175 -F 100 135		-A 215 255 -B 260 295 -C 195 240 -D 210 240 -E 100 130 -F 100 135		P15 P40 40 50		P15 P40 45 55		P15 P40 45 55	
Data based on the "Assembly specific force atlas" (Wakula, Berg, Schaub, Glitsch, Ellegast 2009), adapted neutral to gender Score data are matter to change after the final completion of the force atlas project			Attention: correct evaluation, if task duration ≠ 60s									= <input type="text"/>		
Action forces = ∑ lines 17 - 18										= <input type="text"/>				

Manual Material Handling (per shift)										Loads		
Weights of loads [kg] for repositioning (lifting / lowering), carrying and holding as well as pushing and pulling												
+	Repositioning, carrying & holding	Males	3	10	15	20	25	30	35	40	>40	
		Females	2	5	7	10	12	15	20	25	>25	
+	Pushing and pulling	M1	1	1,5	2	3	4	5,5	7	8,5	25	
		M2										
+	M3	Males	<50	75	100	150	200	250				
		Females	<40	60	80	115	155	195				
Load points: Means of transport			0,5	1	1,5	2	3	4	5	6	8	
Posture, position of load (select characteristic posture)												
+	trunk upright and / or not twisted	little trunk bending or twisting; load at or close to the body	1	2	4	8						
		bending trunk deep or far forward; little trunk bending forward and trunk twisting simultaneously; load far from body or above shoulder level										
+	bending trunk far forward and twisting; load far from the body; limited postural stability while standing; crouching or kneeling	bending trunk far forward and twisting; load far from the body; limited postural stability while standing; crouching or kneeling										
		bending trunk far forward and twisting; load far from the body; limited postural stability while standing; crouching or kneeling										
Working Conditions (pushing and pulling only)												
+	very low rolling resistance	trolley pushing / pulling on (very) slick floor	1	3	5	6	8					
		rough floor and above small gaps / edges into / out of a track										
Frequency of load manipulations (frequency/shift), holding time (min/shift) or travel distance (meter/shift)												
x	Frequency (#) of repositionings / pushing & pulling short	5	25	120	350	750	1000	1500	2000	2500	3000	
		Duration (holding time) [min]	2,5	10	37	90	180	≥240				
x	Distance (carrying, pushing & pulling long) [m]	300	650	2500	6000	12000	≥16000					
		Duration points	1	2	4	6	8	10	11	13	14	15
Manual Material Handling (result)												
19	(Load + posture + condition points) × duration points	Repositioning 1)	()	()	()	()	()	()	()	()	()	
		Holding 1)	()	()	()	()	()	()	()	()	()	
Handling = ∑ line 19		1) Maximal cumulative duration points for all tasks of repositioning, holding, carrying as well as pushing & pulling all together = 15									= <input type="text"/>	

C. MATERIALS AND METHODS

Ergonomic Assessment Worksheet v1.3.5																											
Upper limb load in repetitive tasks																		Upper Limbs									
Force & Frequency & Grip (FFG)																		Basis: number of real actions per minute or percent static actions (analyze only the most loaded limb)									
Legend	 power grip/contact grip	%SA = Percentage of Static Actions										%DA = 100% - %SA															
	 finger or moderate pinch (thumb to >2 fingers, finger)	FDS = Force-Duration Static										FFD = Force-Frequency Dynamic															
	 strong pinch (thumb to 1 or 2, fingers)	GS' = Modified Grip Points Static (Grip x %SA)										GD = Grip Points Dynamic															
	%FLS = Percentage of Static Actions at force level										%FLD = Percentage of Dynamic Actions at force level																
SC = Static Contribution										DC = Dynamic Contribution																	
FDGS = Sum of Static Contributions										FFGD = Sum of Dynamic Contributions																	
Force [N]	Calc Stat				Static actions (s/min)					Grip			Dynamic actions (real actions/min)								Calc Dyn						
	FDS	GS'	%FLS	SC	≥45	30	20	10	5	3	0	2	4	2-5	10	15	20	25	30	35	≥40	FFD	GD	%FLD	DC		
0 – 5					1	1	0	0	0	0	abc			0	0	0	1	2	3	4	7						
> 5 – 20					4	2	1	1	0	0	ab	bc		0	0	1	2	3	4	6	9						
> 20 – 35					7	5	3	2	1	1	ab	b	c	0	1	2	3	4	6	8	12						
> 35 – 90					11	8	5	3	2	1	a	b	b	1	2	3	5	7	9	12	18						
> 90 – 135					16	11	7	4	3	2	a	ab	b	2	3	5	7	9	12	15	24						
> 135 – 225					21	14	10	6	4	3	a	a	b	4	5	6	8	11	14	20	32						
> 225 – 300					28	18	12	8	5	4	a	a	b	5	6	7	9	12	16	26	40						
20a	FDGS = Σ SC _i				FFG = FDGS + FFGD					FFG			%DA = Σ FLD _i								FFGD = Σ DC _i				%DA		
Hand / arm / shoulder postures (use duration for worst case of wrist / elbow / shoulder)																											
20b	Wrist (deviaton, flex./extens.)					Elbow (pron, sup, flex./extens.)					Shoulder (flexion, extension, abduction)					If shoulders are involved close to or above shoulder height without support or in awkward postures, multiply score x3											
																											
Posture points					10% 25% 33%					50% 65% 85%					PP												
Additional factors																											
Gloves inadequate (which interfere with the handling ability required) are used for over half the time																						2		<input type="checkbox"/>			
Working gestures required imply a countershock. Frequency of 2 time per minute or more (i.e.: hammering over hard surface)																						2		<input type="checkbox"/>			
Working gestures imply a countershock (using the hand as a tool) with freq. of 10 time per hour or more																						2		<input type="checkbox"/>			
Exposure to cold or refrigeration (less than 0 degree) for over half the time																						2		<input type="checkbox"/>			
Vibrating tools are used for 1/3 of the time or more																						2		<input type="checkbox"/>			
Tools with a very high level of vibrations																						4		<input type="checkbox"/>			
Tools employed cause compressions of the skin (rednesses, callosities, blebs, etc.)																						2		<input type="checkbox"/>			
Precision tasks are carried out for over half the time (tasks over areas smaller than 2-3 mm)																						2		<input type="checkbox"/>			
More than one additional factor is present at the same time and overall occupy the whole of the time																						3		<input type="checkbox"/>			
Additional points (choose the highest value)																						=		AF			
Repetitive tasks duration																											
20d		Net Duration [min/shift]		< 60		90		180		300		420		≥ 480		+											
		Duration Points		1		1,5		3		5		7		10													
20d		Work Organization		Breaks are possible at every time					Breaks are possible at given conditions					Breaks lead to a stop of the process					+								
				(Cycle time longer than 10 minutes)					(Cycle time between 1 and 10 minutes)					(Cycle time shorter than 1 minute)													
20d		Work Organization Points		0		1		3		4		5		6		+											
		Breaks (≥ 8 min) [#]/shift		0		1		2		3		4		5											6		≥7
20d		Break points		cycle time ≤ 30 s		3		2		1		0		-1		-2		+									
				cycle time > 30 s		0		-0,5		-1		-1,5		-2													
20d		Duration Points		0		-0,5		-1		-1,5		-2		=		DP											
Upper limb load in repetitive tasks																											
20		(a) Force & Frequency & Grip					(b) Postures					(c) Additional factors					(d) Duration					Upper Limbs					
		FFG					PP					AF					DP					=					

RISK ASSESSEMENT GUIDELINES

Introduction

This document provides the guidelines used to assess the ergonomic risk associated to the work-method of the operators in Volkswagen Autoeuropa automotive assembly lines. These are based on and adapted from the **International Organisation for Standardisation (ISO) norm 11226**, used for the evaluation of static working postures, and the pro-forma sheet *European Assembly Worksheet (EAWS)*, used in ergonomic risk rating.

Abbreviations

Henceforth, abbreviations, associated to conditions defined in the ISO norm and in the EAWS pro-forma sheet, are adopted in the ergonomic report.

Table 1: Abbreviations adopted in the ergonomic report with regard to ISO norm and EAWS pro-forma sheet.
Note that bent forward is equivalent to trunk flexion.

Abbreviation	Denotation	Based on
TSymRot	Trunk symmetry - rotation	ISO
TSymBend	Trunk symmetry - bending	ISO
TFlex	Trunk flexion	ISO
AwkUA	Awkward upper arm posture	ISO
UAElev	Upper arm elevation	ISO
ExtElbFE	Extreme elbow flexion	ISO
ExtElbPS	Extreme elbow pronation/supination	ISO
ExtWr	Extreme wrist posture	ISO
U	Standing upright	EAWS
BF	Bent forward - 20°-60°	EAWS
BS	Strongly bent forward - over 60°	EAWS
AbduOS	Arm abduction over shoulder level	EAWS
FlexOS	Arm flexion over shoulder level	EAWS
OH	Hand above head level	EAWS
TR	Trunk rotation	EAWS
TB	Trunk bending	EAWS
FR	Far reach	EAWS
SlNS	Slightly not symmetric	EAWS
MedNS	Medium not symmetric	EAWS
StrNS	Strongly not symmetric	EAWS
ExtNS	Extreme not symmetric	EAWS
S	Symmetric	EAWS
100R	100% reaching	EAWS
80R	80% reaching	EAWS
60R	60% reaching	EAWS
ND	Not described (No reaching)	EAWS
UAAbdu	Upper arm abduction over 60°	
UAFlex	Upper arm flexion over 60°	

ISO Norm 11226 Assessment

The ISO Norm 11226 characterises conditions of the upper body segments, in terms of static postures, as "Acceptable" or "Not recommended". Note that being "Acceptable" or "Not recommended", can depend on the holding time in the static posture, i.e. the duration that it is maintained.

The ISO Norm's criteria was considered to be a safe biomechanical exposure characterisation method. Next, the criteria is outlined for trunk, upper arm, forearm and hand segments.

Trunk

Table 2: Conditions for trunk postures.
Trunk symmetry criteria applies to trunk rotation and bending.

Posture Condition	Characterisation
Trunk Symmetry	
Symmetric < 10°	Acceptable
Slightly Not Symmetric ≥ 10° ∧ < 15°	Acceptable
Medium Not Symmetric ≥ 15° ∧ < 25°	Acceptable
Strongly Not Symmetric ≥ 25° ∧ < 30°	Not Recommended
Extreme Not Symmetric ≥ 30°	Not Recommended
Trunk Flexion	
< 0°	Not Recommended
≥ 0° ∧ > 20°	Acceptable
≥ 20° ∧ ≤ 60°	Depends on holding time
> 60°	Not Recommended

RANGES OF CONDITIONS FOR TRUNK POSTURES

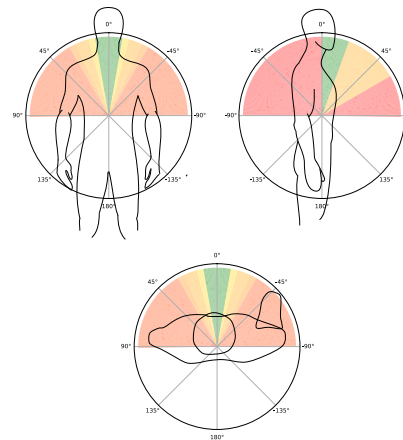


Figure 1: Ranges of conditions for trunk postures: trunk symmetry - bending (top left), trunk flexion (top right) and trunk symmetry - rotation (bottom). Trunk symmetry color scale as symmetric and slightly, medium, strongly and extreme not symmetric. Trunk flexion color scale as Acceptable, Not Recommended and Depends on holding time.

The trunk flexion characterisation for trunk flexion static posture

between 20° and 60° depends on holding time as it follows:

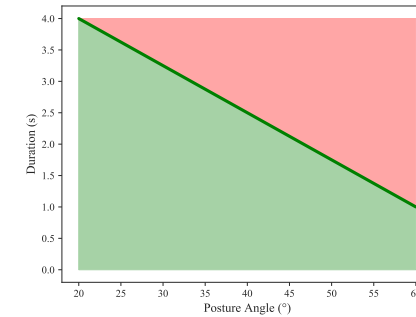


Figure 2: Holding time, and its respective condition that evaluates a static posture. The color scale is as Acceptable and Not Recommended.

Upper Arm

Table 3: Conditions for upper arm postures.

Awkward upper arm posture can be:

- 1) Arm retroflexion, i.e. elbow behind the trunk when viewed from the side of the trunk;
- 2) Upper arm adduction, i.e. elbow not visible when viewed from behind the trunk;
- 3) Extreme upper arm external rotation (90°), i.e. in which "external" refers to an outward rotation around the longitudinal axis of the upper arm with respect to the trunk.

Upper arm elevation refers to upper arm flexion or abduction, which is calculated as the difference between the flexion/abduction angle in the reference posture and the flexion/abduction angle in the static working posture.

Posture Condition	Characterisation
Awkward Upper Arm Posture	
1) Arm retroflexion	Not Recommended
2) Upper arm adduction	Not Recommended
3) Extreme upper arm external rotation	Not Recommended
Upper Arm Elevation	
≥ 0° ∧ > 20°	Acceptable
≥ 20° ∧ ≤ 60°	Depends on holding time
> 60°	Not Recommended

RANGES OF CONDITIONS FOR UPPER ARM POSTURES

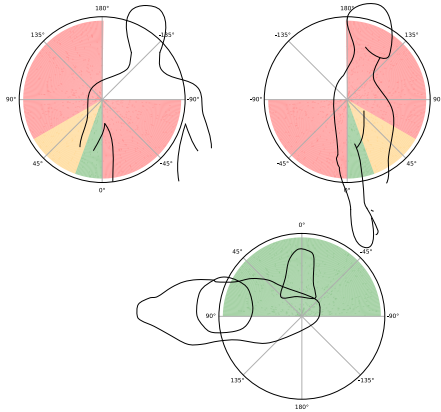


Figure 3: Ranges of conditions for upper arm postures: upper arm abduction/adduction (top left), upper arm extension/flexion (top right) and upper arm inward/outward rotation (bottom). Upper arm rotation color scale as **Acceptable**. Upper arm abduction/adduction and extension/flexion color scale as **Acceptable**, **Not Recommended** and **Depends on holding time**.

The upper arm elevation (abduction/flexion) characterisation for upper arm elevation (abduction/flexion) static posture between 20° and 60° depends on holding time as in Figure 2.

Forearm and Hand

Table 4: Conditions for forearm and hand postures.

Extreme elbow flexion equals to $\geq 150^\circ$, according to the ISO norm 11226, instead it is used the extreme posture defined in the EAWS ($\geq 60^\circ$).

Extreme forearm pronation/supination equals to $\geq 90^\circ / \geq 60^\circ$, according to the ISO norm 11226, instead it is used the extreme posture defined in the EAWS ($\geq 60^\circ$).

Extreme wrist posture is defined in the ISO norm 11226 norm as:

Wrist flexion: $\leq -90^\circ$ (i.e. extension) $\wedge \geq 90^\circ$ (i.e. flexion);

Wrist deviation: $\leq -20^\circ \wedge \geq 30^\circ$;

instead it is used the extreme posture defined in the EAWS as:

Wrist flexion: $\leq -45^\circ$ (i.e. extension) $\wedge \geq 45^\circ$ (i.e. flexion);

Wrist deviation: $\leq -15^\circ \wedge \geq 20^\circ$.

Posture Condition	Characterisation
Extreme Elbow Flexion	
Elbow flexion $< 60^\circ$	Acceptable
Elbow flexion $\geq 60^\circ$	Not Recommended
Extreme Forearm Pronation/Supination	
Forearm pronation/supination $< 60^\circ$	Acceptable
Forearm pronation/supination $\geq 60^\circ$	Not Recommended
Extreme Wrist Posture	
Wrist deviation $> -15^\circ \wedge < 20^\circ$	Acceptable
Wrist deviation $\leq -15^\circ \wedge \geq 20^\circ$	Not Recommended
Wrist flexion $> -45^\circ \wedge < 45^\circ$	Acceptable
Wrist flexion $\leq -45^\circ \wedge \geq 45^\circ$	Not Recommended

RANGES OF CONDITIONS FOR FOREARM POSTURES

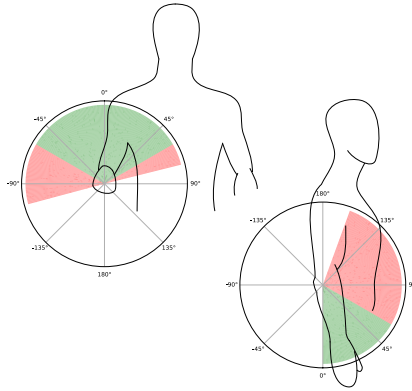


Figure 4: Ranges of conditions for forearm postures: forearm supination/pronation (top left) and elbow flexion (bottom right). Elbow flexion and forearm supination/pronation color scales as **Acceptable** and **Not Recommended**.

RANGES OF CONDITIONS FOR HAND POSTURES

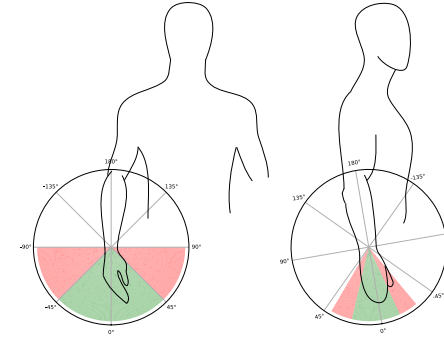


Figure 5: Ranges of conditions for hand postures: wrist extension/flexion (left) and wrist ulnar/radial deviation (right). Wrist flexion and wrist deviation color scales as **Acceptable** and **Not Recommended**.

EAWS Pro-forma Sheet Assessment

The risk score can be computed according to the rating scale proposed in the pro-forma sheet EAWS.

It was implemented an adapted EAWS of the table "Basic Positions / Postures and movements of trunk and arms (per shift)", particularly of its section "Standing (and Walking)".

BASIC POSITIONS / POSTURES AND MOVEMENTS OF TRUNK AND ARMS (PER SHIFT), STANDING (AND WALKING) SECTION

Basic Positions / Postures and movements of trunk and arms (per shift)												Postures													
(incl. loads of <3 kg and action forces of 30-40 N) Static postures: > 4sec High frequency movements: 2 trunk bending or 10 arm lifting > 60° per min												Evaluation of static postures and/or high frequent movements of trunk/arms $Duration [sec/min] = \frac{duration\ of\ posture(s)\ x\ 60}{cycle\ time}$						Asymmetry effects							
																		Trunk Rotation 1)		Lateral Bending 1)		Far Reach 2)		Sum of lines	
												[%]		[sec/min]		[min/8h]		0-5 0-3		0-5 0-3		0-5 0-2			
5	7,5	10	15	20	27	33	50	67	83	int	dur	int	dur	int	dur										
3	4,5	6	9	12	16	20	30	40	50	0-5	0-3	0-5	0-3	0-5	0-2										
24	36	48	72	96	130	160	240	320	400	Intensity x Duration	Intensity x Duration	Intensity x Duration													
Standing (and walking)																									
1		Standing & walking in alteration, standing with support	0	0	0	0	0,5	1	1	1	1,5	2													
2		Standing, no body support (for other restrict. see Extra Points)	0,7	1	1,5	2	3	4	6	8	11	13													
3		Bent forward (20-60°) with suitable support	2	3	5	7	9,5	12	18	23	32	40													
			1,3	2	3,5	5	6,5	8	12	15	20	25													
4		Strongly bent forward (>60°) with suitable support	3,3	5	8,5	12	17	21	30	38	51	63													
			2	3	5	7	9,5	12	18	23	31	38													
5		Upright with elbow at / above shoulder level	3,3	5	8,5	12	17	21	30	38	51	63													
6		Upright with hands above head level	5,3	8	14	19	26	33	47	60	80	100													

Figure 6: Basic positions / postures and movements of trunk and arms - standing (and walking) section. Note that it was not possible to assess conditions of a few postures, such as static postures with support.

The EAWS's section provides the risk score value for each single condition (row) described in it. Single condition score depends of the percentage of values in data that verify the condition.

SINGLE CONDITIONS

Table 5: Single conditions.

Row	Single Condition	
2	Standing upright	Trunk flexion between 0° and 20°
3	Bent forward	Trunk flexion between 20° and 60°
4	Strongly bent forward	Trunk flexion over 60°
5	Arm abduction over shoulder level	Standing upright × Upper arm abduction over 60°
5	Arm flexion over shoulder level	Standing upright × Upper arm flexion over 60°
6	Hand above head level	Standing upright × Upper arm flexion over 60° × Extreme elbow extension

Moreover, on section's right side, there is a part related to combined conditions. Combined condition score depends of the percentage of values in data that verify a condition C, if a single condition is already verified. Besides, the intensity of the condition C is also rated. Combined condition final score is given by the product of both "duration" (i.e. percentage of values in data) and intensity of C, as it can be noticed in Figure 7.

RATING SCALE FOR COMBINED CONDITIONS													
1)	0	0		1		3		5		Σ	Σ (max.=15)	Σ (max.=15)	Σ (max.=10)
		int	slightly	medium	strongly	extreme	Σ (max. = 40)						
	<10°	15°	25°	>30°									
	dur	never	4 sec	10 sec	13 sec	(a)	(b)						
0%	6%	15%	20%										
2)	0	0		1		3		5		Σ	Σ (max.=15)	Σ (max.=15)	Σ (max.=10)
		int	close	60%	80%	arm stretched	Σ (max. = 40)						
	dur	never	4 sec	10 sec	13 sec	(a)		(b)					
	0%	6%	15%	20%									

Figure 7: Rating scale for combined conditions.

COMBINED CONDITIONS

Table 6: Combined conditions entail the evaluation of: trunk symmetry, in terms of rotation and bending, and arm far reaching. Trunk symmetry is assessed as symmetric or slightly, medium, strongly or extreme not symmetric (can be consulted in Figure 1). Far reach is determined through the evaluation of the angle between the upper arm and the forearm, e.g. 100% arm far reaching corresponding to the extreme elbow extension (i.e. elbow flexion of 0°).

Row	Column	Combined Condition
2	1	Standing upright × Trunk rotation
2	2	Standing upright × Trunk bending
2	3	Standing upright × Far reach
3	1	Bent forward × Trunk rotation
3	2	Bent forward × Trunk bending
3	3	Bent forward × Far reach
4	1	Strongly bent forward × Trunk rotation
4	2	Strongly bent forward × Trunk bending
4	3	Strongly bent forward × Far reach
5	1	Arm abduction over shoulder level × Trunk rotation
5	2	Arm abduction over shoulder level × Trunk bending
5	3	Arm abduction over shoulder level × Far reach
5	1	Arm flexion over shoulder level × Trunk rotation
5	2	Arm flexion over shoulder level × Trunk bending
5	3	Arm flexion over shoulder level × Far reach
6	1	Hand above head level × Trunk rotation
6	2	Hand above head level × Trunk bending

Resources

European Assembly Worksheet: [EAWS](#)

C.12 Individual Ergonomic Report Example

Fraunhofer AICOS
 Av. Prof. Gama Pinto 3
 1649-003 Lisboa

Operator: 1
 Workstation: Doors_Left
 Total mean score: 46.0 ± 7.0

ISO Norm 11226 Results

Table 1: ISO Norm 11226 Results. Percentage of values in each cycle, from 0 to N, N being the total number of cycles, in which the condition assessed is within its Not Recommended range.

	TSymRot	TSymBend	TFlex	left AwkUA	right AwkUA	left UAElev	right UAElev	left ExtElbFE	right ExtElbFE	left ExtElbPS	right ExtElbPS	left ExtWr	right ExtWr
0	44.6%	8.3%	26.4%	29.5%	17.1%	14.2%	15.3%	10.1%	28.2%	24.4%	29.8%	88.6%	37.6%
1	36.0%	15.2%	12.9%	36.0%	27.3%	26.9%	14.0%	8.7%	13.6%	47.0%	4.5%	99.6%	47.3%
2	21.5%	20.7%	16.8%	25.0%	33.2%	22.6%	21.2%	8.2%	57.3%	45.7%	7.3%	61.1%	92.7%
mean	34.0%	14.7%	18.7%	30.2%	25.8%	22.6%	16.8%	9.0%	33.1%	39.0%	13.9%	83.1%	59.2%
std	9.5%	5.1%	5.7%	4.5%	6.6%	5.9%	3.1%	0.8%	18.2%	10.4%	11.3%	16.2%	24.0%

EAWS Pro-forma Sheet Results

Table 2: EAWS Pro-forma Sheet Results. Risk score assign to each condition in EAWS section "Basic positions / postures and movements of trunk and arms - standing (and walking)", part a). A risk score is given for each cycle data, from 0 to N, N being the total number of cycles.

	U	BF	BS	left AbduOS	left FlexOS	left OH	right AbduOS	right FlexOS	right OH
0	1.0	11.0	4.0	0.0	0.0	0.0	0.0	0.0	0.0
1	1.0	18.0	8.0	0.0	0.0	0.0	0.0	0.0	0.0
2	0.0	22.0	10.0	0.0	0.0	0.0	0.0	0.0	0.0
mean	0.7	17.0	7.3	0.0	0.0	0.0	0.0	0.0	0.0
std	0.5	4.5	2.5	0.0	0.0	0.0	0.0	0.0	0.0

Table 3: EAWS Pro-forma Sheet Results. Risk score assign to each condition in EAWS section "Basic positions / postures and movements of trunk and arms - standing (and walking)", part b), particularly with regard to trunk rotation symmetry evaluation. A risk score is given for each cycle data, from 0 to N, N being the total number of cycles.

	TR x U	TR x BF	TR x BS	TR x left AbduOS	TR x left FlexOS	TR x left OH	TR x right AbduOS	TR x right FlexOS	TR x right OH
0	10.0	0.0	0.0	0.0	0.0	0.0	0.0	0.0	0.0
1	0.0	0.0	0.0	0.0	0.0	0.0	0.0	0.0	0.0
2	0.0	0.0	0.0	0.0	0.0	0.0	0.0	0.0	0.0
mean	3.3	0.0	0.0	0.0	0.0	0.0	0.0	0.0	0.0
std	4.7	0.0	0.0	0.0	0.0	0.0	0.0	0.0	0.0

Table 4: EAWS Pro-forma Sheet Results. Risk score assign to each condition in EAWS section "Basic positions / postures and movements of trunk and arms - standing (and walking)", part b), particularly with regard to trunk bending symmetry evaluation. A risk score is given for each cycle data, from 0 to N, N being the total number of cycles.

	TB x U	TB x BF	TB x BS	TB x left AbduOS	TB x left FlexOS	TB x left OH	TB x right AbduOS	TB x right FlexOS	TB x right OH
0	0.0	0.0	0.0	0.0	0.0	0.0	0.0	0.0	0.0
1	0.0	0.0	0.0	0.0	0.0	0.0	0.0	0.0	0.0
2	0.0	0.0	0.0	0.0	0.0	0.0	0.0	0.0	0.0
mean	0.0	0.0	0.0	0.0	0.0	0.0	0.0	0.0	0.0
std	0.0	0.0	0.0	0.0	0.0	0.0	0.0	0.0	0.0

Table 5: EAWS Pro-forma Sheet Results. Risk score assign to each condition in EAWS section "Basic positions / postures and movements of trunk and arms - standing (and walking)", part b), particularly with regard to far reach evaluation. A risk score is given for each cycle data, from 0 to N, N being the total number of cycles.

	left FR x U	left FR x BF	left FR x BS	left FR x left AbduOS	left FR x left FlexOS	right FR x U	right FR x BF	right FR x BS	right FR x right AbduOS	right FR x right FlexOS
0	0.0	8.0	0.0	0.0	6.0	0.0	0.0	0.0	0.0	4.0
1	0.0	0.0	8.0	0.0	12.0	0.0	0.0	0.0	0.0	4.0
2	0.0	0.0	1.0	0.0	1.0	1.0	1.0	0.0	0.0	0.0
mean	0.0	2.7	3.0	0.0	6.3	0.3	0.3	0.0	0.0	2.7
std	0.0	3.8	3.6	0.0	4.5	0.5	0.5	0.0	0.0	1.9

Fraunhofer AICOS
 Av. Prof. Gama Pinto 3
 1649-003 Lisboa

Operator: 1
 Workstation: Doors_Left

Appendix

EAWS Pro-forma Sheet Detailed Conditions Percentages

Part a) - Conditions percentages

	U	BF	BS	left AbduOS	left FlexOS	left OH	right AbduOS	right FlexOS	right OH
0	50.5%	23.8%	6.5%	0.5%	2.3%	0.0%	0.0%	4.7%	0.0%
1	48.5%	39.0%	11.7%	1.1%	3.8%	1.1%	0.0%	4.2%	0.4%
2	35.9%	49.2%	13.9%	0.5%	2.2%	0.0%	0.0%	3.0%	0.3%
mean	45.0%	37.3%	10.7%	0.7%	2.8%	0.4%	0.0%	3.9%	0.2%
std	6.5%	10.4%	3.1%	0.3%	0.7%	0.5%	0.0%	0.7%	0.2%

Part b) - Trunk rotation percentages

Table A.1: Trunk Rotation Extreme Not Symmetric. Percentage of values in each cycle, from 0 to N, N being the total number of cycles.

	U x ExtNS	BF x ExtNS	BS x ExtNS	left AbduOS x ExtNS	left FlexOS x ExtNS	left OH x ExtNS	right AbduOS x ExtNS	right FlexOS x ExtNS	right OH x ExtNS
0	22.3%	1.8%	0.0%	0.5%	0.8%	0.5%	0.0%	0.5%	0.0%
1	17.0%	11.0%	0.0%	0.8%	4.5%	1.5%	0.0%	1.9%	0.8%
2	6.2%	6.2%	1.1%	1.9%	1.6%	0.5%	0.0%	2.4%	0.0%
mean	15.2%	6.3%	0.4%	1.1%	2.3%	0.9%	0.0%	1.6%	0.3%
std	6.7%	3.7%	0.5%	0.6%	1.6%	0.5%	0.0%	0.8%	0.4%

Table A.2: Trunk Rotation Strongly Not Symmetric. Percentage of values in each cycle, from 0 to N, N being the total number of cycles.

	U x StrNS	BF x StrNS	BS x StrNS	left AbduOS x StrNS	left FlexOS x StrNS	left OH x StrNS	right AbduOS x StrNS	right FlexOS x StrNS	right OH x StrNS
0	3.6%	0.5%	0.5%	0.0%	0.3%	0.0%	0.0%	0.3%	0.0%
1	3.4%	2.7%	1.1%	0.0%	0.8%	0.0%	0.0%	0.8%	0.0%
2	2.7%	4.3%	0.8%	0.5%	0.8%	0.0%	0.0%	1.4%	0.3%
mean	3.3%	2.5%	0.8%	0.2%	0.6%	0.0%	0.0%	0.8%	0.1%
std	0.4%	1.6%	0.3%	0.3%	0.2%	0.0%	0.0%	0.4%	0.1%

Table A.3: Trunk Rotation Medium Not Symmetric. Percentage of values in each cycle, from 0 to N, N being the total number of cycles.

	U x MedNS	BF x MedNS	BS x MedNS	left AbduOS x MedNS	left FlexOS x MedNS	left OH x MedNS	right AbduOS x MedNS	right FlexOS x MedNS	right OH x MedNS
0	6.0%	4.9%	2.8%	0.0%	3.1%	0.0%	0.0%	4.1%	0.3%
1	11.0%	10.6%	3.4%	0.0%	6.8%	1.5%	0.0%	3.0%	1.5%

2	6.5%	9.5%	3.5%	0.5%	4.9%	0.0%	0.0%	4.3%	0.3%
mean	7.8%	8.3%	3.3%	0.2%	4.9%	0.5%	0.0%	3.8%	0.7%
std	2.2%	2.5%	0.3%	0.3%	1.5%	0.7%	0.0%	0.6%	0.6%

Table A.4: Trunk Rotation Slightly Not Symmetric. Percentage of values in each cycle, from 0 to N, N being the total number of cycles.

	U x SHNS	BF x SHNS	BS x SHNS	left AbduOS x SHNS	left FlexOS x SHNS	left OH x SHNS	right AbduOS x SHNS	right FlexOS x SHNS	right OH x SHNS
0	6.2%	5.7%	1.0%	0.3%	2.1%	0.5%	0.0%	3.4%	1.0%
1	6.4%	4.9%	2.7%	0.4%	5.3%	1.5%	0.0%	3.0%	1.1%
2	4.1%	9.2%	4.3%	0.3%	4.6%	0.3%	0.0%	3.0%	0.3%
mean	5.6%	6.6%	2.7%	0.3%	4.0%	0.7%	0.0%	3.1%	0.8%
std	1.1%	1.9%	1.4%	0.1%	1.4%	0.6%	0.0%	0.2%	0.4%

Table A.5: Trunk Rotation Symmetric. Percentage of values in each cycle, from 0 to N, N being the total number of cycles.

	U x S	BF x S	BS x S	left AbduOS x S	left FlexOS x S	left OH x S	right AbduOS x S	right FlexOS x S	right OH x S
0	12.4%	10.9%	2.1%	0.3%	5.7%	1.8%	0.0%	5.2%	2.6%
1	10.6%	9.8%	4.5%	0.0%	6.8%	0.4%	0.0%	3.4%	0.8%
2	16.3%	19.8%	4.1%	0.0%	9.2%	1.6%	0.0%	6.0%	1.9%
mean	13.1%	13.5%	3.6%	0.1%	7.3%	1.3%	0.0%	4.9%	1.8%
std	2.4%	4.5%	1.1%	0.1%	1.5%	0.6%	0.0%	1.1%	0.8%

Part b) - Trunk bending percentages

Table A.6: Trunk Bending Extreme Not Symmetric. Percentage of values in each cycle, from 0 to N, N being the total number of cycles.

	U x ExtNS	BF x ExtNS	BS x ExtNS	left AbduOS x ExtNS	left FlexOS x ExtNS	left OH x ExtNS	right AbduOS x ExtNS	right FlexOS x ExtNS	right OH x ExtNS
0	0.3%	3.6%	0.5%	0.3%	1.0%	0.3%	0.0%	1.6%	0.0%
1	0.8%	8.7%	1.1%	0.0%	6.4%	0.4%	0.0%	1.5%	0.0%
2	1.6%	8.7%	1.6%	0.8%	4.6%	0.0%	0.0%	3.3%	0.0%
mean	0.9%	7.0%	1.1%	0.4%	4.0%	0.2%	0.0%	2.1%	0.0%
std	0.6%	2.4%	0.5%	0.3%	2.2%	0.2%	0.0%	0.8%	0.0%

Table A.7: Trunk Bending Strongly Not Symmetric. Percentage of values in each cycle, from 0 to N, N being the total number of cycles.

	U x StrNS	BF x StrNS	BS x StrNS	left AbduOS x StrNS	left FlexOS x StrNS	left OH x StrNS	right AbduOS x StrNS	right FlexOS x StrNS	right OH x StrNS
0	1.0%	2.8%	0.0%	0.0%	0.5%	0.0%	0.0%	1.0%	0.0%
1	1.9%	2.3%	0.4%	0.0%	0.4%	0.0%	0.0%	0.0%	0.0%
2	1.1%	6.8%	0.8%	0.0%	2.4%	0.0%	0.0%	0.8%	0.0%
mean	1.3%	4.0%	0.4%	0.0%	1.1%	0.0%	0.0%	0.6%	0.0%
std	0.4%	2.0%	0.3%	0.0%	0.9%	0.0%	0.0%	0.4%	0.0%

Table A.8: Trunk Bending Medium Not Symmetric. Percentage of values in each cycle, from 0 to N, N being the total number of cycles.

	U x MedNS	BF x MedNS	BS x MedNS	left AbduOS x MedNS	left FlexOS level x MedNS	left OH x MedNS	right AbduOS x MedNS	right FlexOS level x MedNS	right OH x MedNS
0	4.7%	3.9%	1.0%	0.0%	0.0%	0.3%	0.0%	0.0%	0.5%
1	4.9%	9.1%	5.3%	0.0%	0.0%	0.0%	0.0%	0.0%	0.4%
2	3.8%	11.4%	1.9%	0.0%	0.0%	0.0%	0.0%	0.0%	0.5%
mean	4.5%	8.1%	2.7%	0.0%	0.0%	0.1%	0.0%	0.0%	0.5%

std	0.5%	3.1%	1.8%	0.0%	0.0%	0.1%	0.0%	0.0%	0.1%
Table A.9: Trunk Bending Slightly Not Symmetric. Percentage of values in each cycle, from 0 to N, N being the total number of cycles.									
	U x SHNS	BF x SHNS	BS x SHNS	left AbduOS x SHNS	left FlexOS level x SHNS	left OH x SHNS	right AbduOS x SHNS	right FlexOS level x SHNS	right OH x SHNS
0	5.4%	3.9%	1.8%	0.0%	0.0%	0.0%	0.0%	0.0%	0.0%
1	4.9%	8.7%	3.0%	0.0%	0.0%	0.0%	0.0%	0.0%	0.0%
2	4.6%	4.9%	1.1%	0.3%	0.0%	0.3%	0.0%	0.0%	0.3%
mean	5.0%	5.8%	2.0%	0.1%	0.0%	0.1%	0.0%	0.0%	0.1%
std	0.3%	2.1%	0.8%	0.1%	0.0%	0.1%	0.0%	0.0%	0.1%

	U x S	BF x S	BS x S	left AbduOS x S	left FlexOS level x S	left OH x S	right AbduOS x S	right FlexOS level x S	right OH x S	left FlexOS x MedNS	left FlexOS x SHNS	left FlexOS x S	right FlexOS x MedNS	right FlexOS x SHNS	right FlexOS x S
Table A.10: Trunk Bending Symmetric. Percentage of values in each cycle, from 0 to N, N being the total number of cycles.															
0	39.1%	9.6%	3.1%	0.8%	0.0%	2.3%	0.0%	0.0%	3.4%	1.8%	2.6%	6.0%	1.8%	1.6%	7.5%
1	36.0%	10.2%	1.9%	1.1%	0.0%	4.5%	0.0%	0.0%	3.8%	6.8%	3.4%	7.2%	3.4%	1.9%	5.3%
2	24.7%	17.4%	8.4%	2.2%	0.0%	1.9%	0.0%	0.0%	1.9%	3.5%	1.4%	9.2%	1.9%	1.4%	9.8%
mean	33.3%	12.4%	4.5%	1.4%	0.0%	2.9%	0.0%	0.0%	3.0%	4.1%	2.5%	7.5%	2.4%	1.6%	7.5%
std	6.2%	3.5%	2.8%	0.6%	0.0%	1.2%	0.0%	0.0%	0.8%	2.1%	0.8%	1.4%	0.7%	0.2%	1.8%

Part b) - Far reach percentages

	U x left FR - ND	U x right FR - ND	BF x left FR - ND	BF x right FR - ND	BS x left FR - ND	BS x right FR - ND	left AbduOS x FR - ND	left FlexOS level x left FR - ND	right AbduOS x right FR - ND	right FlexOS level x right FR - ND
Table A.11: Far Reach Not Described. Percentage of values in each cycle, from 0 to N, N being the total number of cycles.										
0	3.1%	0.0%	0.5%	0.0%	0.0%	0.0%	0.0%	0.3%	0.0%	0.0%
1	4.5%	1.5%	0.8%	0.0%	0.0%	0.0%	0.8%	0.4%	0.0%	0.0%
2	2.2%	1.4%	0.5%	0.3%	0.0%	0.0%	0.0%	0.0%	0.0%	0.0%
mean	3.3%	1.0%	0.6%	0.1%	0.0%	0.0%	0.3%	0.2%	0.0%	0.0%
std	1.0%	0.7%	0.1%	0.1%	0.0%	0.0%	0.4%	0.2%	0.0%	0.0%

	U x left FR - 60R	U x right FR - 60R	BF x left FR - 60R	BF x right FR - 60R	BS x left FR - 60R	BS x right FR - 60R	left AbduOS x FR - 60R	left FlexOS level x left FR - 60R	right AbduOS x right FR - 60R	right FlexOS level x right FR - 60R
Table A.12: Far Reach of 60% Reaching. Percentage of values in each cycle, from 0 to N, N being the total number of cycles.										
0	3.9%	17.6%	3.1%	5.7%	0.0%	1.3%	0.3%	0.0%	0.0%	1.8%
1	6.4%	11.0%	2.3%	10.6%	0.0%	3.0%	0.0%	0.4%	0.0%	1.1%
2	8.7%	14.9%	6.5%	19.6%	1.1%	7.9%	0.0%	2.4%	0.0%	6.8%
mean	6.3%	14.5%	4.0%	12.0%	0.4%	4.1%	0.1%	0.9%	0.0%	3.2%
std	2.0%	2.7%	1.8%	5.7%	0.5%	2.8%	0.1%	1.1%	0.0%	2.5%

	U x left FR - 80R	U x right FR - 80R	BF x left FR - 80R	BF x right FR - 80R	BS x left FR - 80R	BS x right FR - 80R	left AbduOS x FR - 80R	left FlexOS level x left FR - 80R	right AbduOS x right FR - 80R	right FlexOS level x right FR - 80R
Table A.13: Far Reach of 80% Reaching. Percentage of values in each cycle, from 0 to N, N being the total number of cycles.										
0	9.1%	8.3%	4.4%	6.7%	1.3%	2.3%	0.0%	1.8%	0.0%	2.6%
1	9.1%	10.6%	8.0%	9.1%	0.8%	3.8%	0.4%	3.4%	0.0%	2.7%
2	13.3%	10.3%	19.8%	17.4%	6.2%	4.1%	0.0%	9.0%	0.0%	6.0%
mean	10.5%	9.7%	10.7%	11.1%	2.8%	3.4%	0.1%	4.7%	0.0%	3.7%

	std	2.0%	1.0%	6.6%	4.6%	2.5%	0.8%	0.2%	3.1%	0.0%	1.6%	
Table A.14: Far Reach of 100% Reaching. Percentage of values in each cycle, from 0 to N, N being the total number of cycles.												
	U x left FR - 100R	U x right FR - 100R	BF x left FR - 100R	BF x right FR - 100R	BS x left FR - 100R	BS x right FR - 100R	left AbduOS x left FR - 100R	left FlexOS x left FR - 100R	right AbduOS x right FR - 100R	right FlexOS x right FR - 100R	left FlexOS level x left FR - 100R	right FlexOS - level x right FR - 100R
0	34.5%	24.6%	15.8%	11.4%	5.2%	2.8%	0.8%	0.0%	0.0%	0.0%	9.8%	9.1%
1	28.4%	25.4%	28.0%	19.3%	11.0%	4.9%	0.0%	0.0%	0.0%	0.0%	20.1%	8.3%
2	11.7%	9.2%	22.3%	12.0%	6.5%	1.9%	3.3%	0.0%	0.0%	0.0%	9.8%	4.3%
mean	24.8%	19.7%	22.0%	14.2%	7.6%	3.2%	1.3%	0.0%	0.0%	0.0%	13.2%	7.2%
std	9.6%	7.4%	5.0%	3.6%	2.5%	1.3%	1.4%	0.0%	0.0%	0.0%	4.8%	2.1%

D. Results and Discussion

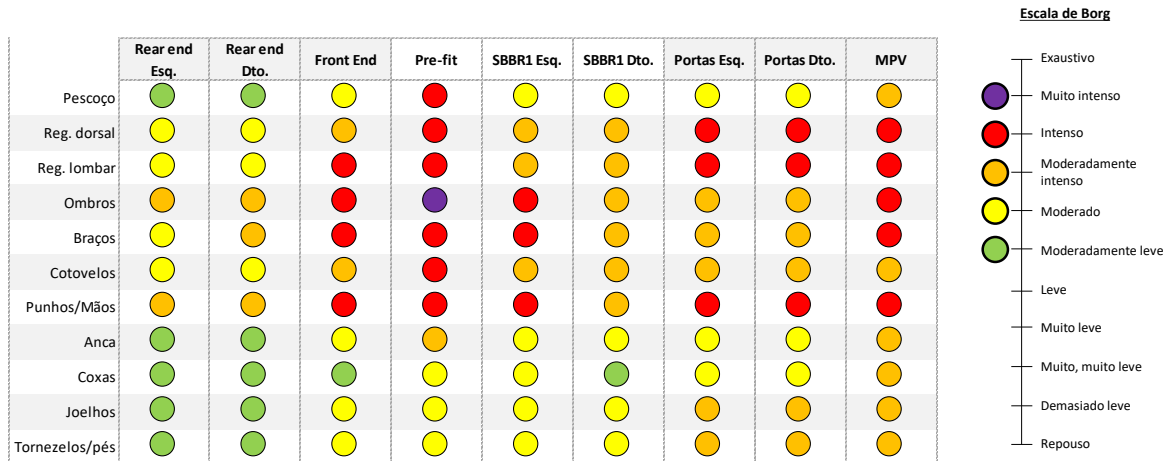
D.1 Self-Report Results



Resultados do Questionário

2. A minha perceção do esforço para cada uma das **regiões corporais**, é:

Resumo



14 Creation date: 07.05.21 | Responsible department for filing: AGIP | CSD-Class: 0.2 – 4 years



Figure D.1: Summary results of a self-reported ergonomic assessment, conducted by Volkswagen Autoeuropa.

D.2 Dataset

Table D.1: Study participants' characteristics values.

Id	Study scenario	Activity	URQ	Gender	Age (years)	Height (cm)	Weight (kg)	Shoe size (cm)	Hip height (cm)	Arm span (cm)	Ankle height (cm)	Knee height (cm)	Shoulder width (cm)
Worker 1	field	Doors	C	M	38	203	95	34,2	113,7	180,2	13,5	55,1	45,5
Worker 2	field	Doors	C	M	39	177	77	30,7	101,2	168,5	11,4	53,2	40,3
Worker 3	field	Doors Right	C	M	30	178	79	30,6	97,6	165,1	11,3	48,3	41,6
Worker 4	field	Prefit SBBR Right Left	B	M	38	184	78	33,3	110,3	173,2	13,1	48,9	45,2
Worker 5	field	Rear and Front End	A	M	36	169	65	26,9	94,8	164,8	9,4	53,6	37,9
Worker 6	field	Rear and Front End	A	M	47	170	76	30,4	98,2	170,4	11,9	53,2	42,6
Worker 7	field	Doors	C	M	40	173	75	29,9	91,1	167,5	11,7	50,9	42,7
Worker 8	field	Prefit SBBR Right Left	B	M	42	170	78	29,1	83,9	166,3	12,5	47,4	44,4
Worker 5	field	Prefit	B	M	36	169	65	26,9	94,8	164,8	9,4	53,6	37,9
Worker 9	field	Rear and Front End	A	M	47	180	92	30,4	98,2	181,8	10,4	55,1	38,1
Participant 1	laboratory	Functional & Simulation	-	M	26	183,5	83	30,4	102,4	185,1	10,8	55,4	39,1
Participant 2	laboratory	Functional & Simulation	-	M	27	187	97	32,1	103,3	192,7	11,1	58,4	42,6
Participant 3	laboratory	Functional & Simulation	-	F	31	171	55	26,1	104,4	170	10,4	54,6	32,1
Participant 4	laboratory	Functional & Simulation	-	M	34	185	72	29,4	105,4	182,8	10,9	53,2	36,9
Participant 5	laboratory	Functional & Simulation	-	M	24	183	75	29,1	104,9	183,1	10,8	56,1	38,1
Participant 6	laboratory	Functional & Simulation	-	F	22	164	48	26,2	93,5	164	10	46,8	34,4
Participant 7	laboratory	Functional & Simulation	-	M	23	162	55	27,1	89,1	171,1	9,4	45,6	33,9
Participant 8	laboratory	Functional & Simulation	-	M	23	162	55	27,1	89,1	171,1	9,4	45,6	33,9

D.2.1 Summary Statistics

Table D.2: Study participants' characteristics values summary statistics.

Characteristic	Study Scenario	Counts	Mean	Std	Min	5%	50%	95%	Max
Male/Female	laboratory	6/2	-	-	-	-	-	-	-
Male/Female	field	9/0	-	-	-	-	-	-	-
Age (years)	laboratory	-	26,6	4,1	22	22,35	26	32,95	34
Age (years)	field	-	39,7	5,3	30	32,4	39	47	47
Height (cm)	laboratory	-	177,6	10,2	162	162,7	183,3	186,3	187
Height (cm)	field	-	178,2	10,6	169	169,4	177	195,4	203
Weight (kg)	laboratory	-	70,9	16,9	48	50,5	73,5	92,1	97
Weight (kg)	field	-	79,4	9	65	69	78	93,8	95
Shoe size (cm)	laboratory	-	29,0	2,4	26,1	26,1	29,3	32	32,1
Shoe size (cm)	field	-	30,6	2,1	26,9	27,8	30,4	33,8	34,2
Hip height (cm)	laboratory	-	100,7	6	89,1	90,6	103,1	105,2	105,4
Hip height (cm)	field	-	98,8	9,1	83,9	86,8	98,2	112,3	113,7
Arm span (cm)	laboratory	-	179,9	10,3	164	166,1	183	191,8	192,7
Arm span (cm)	field	-	170,9	6,3	164,8	164,9	168,5	181,2	181,8
Ankle height (cm)	laboratory	-	10,4	0,6	9,4	9,6	10,6	11,03	11,1
Ankle height (cm)	field	-	11,7	1,3	9,4	9,8	11,7	13,3	13,5
Knee height (cm)	laboratory	-	53,4	4,8	45,6	46	55	58,1	58,4
Knee height (cm)	field	-	51,7	3	47,4	47,8	53,2	55,1	55,1
Shoulder width (cm)	laboratory	-	36,6	3,3	32,1	32,7	36,3	41,4	42,6
Shoulder width (cm)	field	-	42,0	2,8	37,9	38	42,6	45,4	45,5